九州大学学術情報リポジトリ
Kyushu University Institutional Repository

Fabrication of Mesoporous Polymers and Their Application as Adsorbents of Aromatic Compounds in Water

クリスナン, モハンラジ

https://doi.org/10.15017/1500670

出版情報：九州大学, 2014, 博士（工学）, 課程博士
バージョン：
権利関係：全文ファイル公表済

Fabrication of Mesoporous Polymers and Their Application as Adsorbents of Aromatic Compounds in Water

THESIS SUBMITTED FOR THE DEGREE OF
DOCTOR OF PHILOSOPHY

KYUSHU UNIVERSITY
2015

By
MOHANRAJ KRISHNAN

Department of Chemistry and Biochemistry
Faculty of Engineering

Acknowledgements

First and foremost, I extend my sincere acknowledgements to **Prof. Dr. Izumi Ichinose**, for his esteemed guidance for my doctoral studies. It had been a great experience in working with him.

I also want to thank **Dr. Sadaki Samitsu**, for his valuable contribution to my dissertation.

I also thank Dr. **Yoshihisa Fujii**, for his comments and discussions on various scientific topics.

I also thank Kyushu University professors for reviewing my thesis and adding many scientific points.

I thank National Institute for Materials Science (NIMS), Japan for financial support.

Contents

Chapter 2

Fabrication of mesoporous polymers: A nano-crystallization phase separation approach

Chapter 3

Selective surface modification of mesoporous polymers

Chapter 1

Introduction

1.1 Characteristics of porous materials

"With clay, we make a jar. But the empty space inside is what we need."

This old Chinese proverb distinctly explains the significance of porous solids in a few words. Making the materials with empty space (pores) inside to use their cavities is a long standing objective in scientific research. Porous materials are well known for long time and have been used for various applications including filtration and separation. In recent days, the extensive research on porous materials is resulting in the evolution of new porous systems with exceptional properties. A better control of pore size and high free surface are necessary to improve the base properties of porous materials. If the pore dimensions are nano-metric, then they called nanoporous materials. Nanoporous materials exhibit unique surface and structural characteristics better than their bulk counterpart. Therefore, this chapter discusses about their classification, characterization and major applications of porous materials in detail.

Porous materials are defined by IUPAC as solids having cavities, channels or interstices, which are deeper than their width.[1] The presence of pores can render them many useful properties and various applications. The actual importance of porous materials has been recognised when porous charcoal used for several medicinal purposes including treating for poisoning.[2] It absorbs drugs[3] inactivating it and carrying as inert through digestive system whereas charcoal neither adsorbed nor metabolized by the body.[4] The relative performance of porous materials is mainly dependent on their internal porous structure. Therefore it is important to classify these materials based on their pore size and porosity.

1.1.1 IUPAC definitions and classifications

Pore volume (V_p) is volume of the pores, as measured by a given method which must be stated. (Together, for instance, with the nature of the probe-molecule, the wavelength of the radiation used or the ultimate intrusion pressure).

Pore size (or pore width w) is the distance between two opposite walls of the pore (diameter of cylindrical pores, width of slit-shaped pores)

Pore size distribution is represented by the derivatives dV_P/dr_p or dA_p/dr_p as a function of r_p. Where A_p, and r_p are the wall area, and radius of the pores. The size in question is here the radius, which implies that the pores are known to be, or assumed to be, cylindrical. In other cases r_p should be replaced by the width.

Porosity (E) is ratio of the total pore volume V_p to the apparent volume V, of the particle or powder (excluding inter-particle voids). In some cases one may distinguish between open porosity (i.e. the volume of pores accessible to a given probe molecule) and closed porosity. The methods used to measure the pore volume and the apparent volume should be stated.

1.1.1.1 Pore classifications in solids

There are various studies that categorize the pores in solid materials and they have been extensively reviewed in literature.[5] The pores are majorly classified based on their origin, pore width or size and accessibility to the surroundings.

Table 1. Classification of pores based on their origin, pore width (w), and accessibility[5]

Origin and structure	
	(i) Intra particle pore
	(a) Intrinsic intra particle pore
	(b) Extrinsic intra particle pore
	(ii) Inter particle pore
	(a) Rigid inter particle pore (Agglomerated)
	(b) Flexible inter particle pore (Aggregated)
Pore width (w)	
	(i) Macro pore (w > 50 nm)
	(ii) Mesopore (2 nm < w < 50 nm)
	(ii) Micropore (w < 2 nm)
	(iv) Super micropore (0.7 < w < 2 nm)
	(v) Ultra micropore (w < 0.7 nm)
	(vi) Ultra pore (w < 0.35 nm)
Accessibility to surroundings	
	(i) Open pores (Communication with external surface)
	(ii) Closed pores (No communication with surroundings)
	(iii) Latent pores (Ultra pores and closed pores)

1.1.1.2 Origin and structure

The cohesive structures of porous solids are majorly dependent on the interactions between the primary particles constituting them. These primary particles ultimately lead to void space which is not occupied. These voids are highly managed by the inter particle forces which are different from one system to another. They are chemical binding, electrostatic forces, magnetic forces and so on. Therefore pores in solids should be necessarily classified based on their origin i.e. the pores originated either from inter or intra particle.

(i) Intra particle pores

Intrinsic intra particle pore

The pores arising from the inability to occupy the space by their crystalline units are known as intrinsic intra particle pores. Zeolites are the most representative for this type of pores. The tetrahedral units of Al-O and Si-O cannot occupy the space perfectly and hence forming the intrinsic pores. The carbon nanotube found by Ijima A. has also intrinsic crystalline pores.[6]

Extrinsic intra particle pore

When a foreign substance is impregnated in advance with a precursor and finally removing them from the final solid product, the introduced pores in the solids are known as extrinsic intra particle pores. There are various pore forming agents (porogens) available to create this kind of pores in solids. Also when the pore forming agents are introduced into the solid, they produce voids. For example, when K atoms are intercalated in graphite, the interlayer distance increase and act as space for hydrogen gas in storage application whereas the non-intercalated can't host the hydrogen molecule.[7]

(ii) Inter particle pores

When the primary particles are loosely bound with each other in the solids (aggregated), gives flexible pores in the solid matrix. These pores can be readily modified or destroyed by heating or compressing. If the interaction between the primary particles is strong enough in the solid agglomerates, it forms stable and rigid pores. Thus, the inter particle pores have wide varieties in shape, stability and size.

1.1.1.3 Accessibility to surroundings

The pores which are well connected to the external surface of the solid are named as open pores whereas the one having no connections called closed or latent pore. According to Ruike et al. closed pores are the one can't be penetrated by Helium at 303K.[8] When porous solid is deformed by heat or pressure causes the collapse of some part of the solid results in closed pores as shown in Fig.1-1. Insufficient evolution of gaseous substances in a solid is also leads to the

existence of closed pores. The open pores can be easily accessed by molecules, ions from the surroundings but closed pores are not.

The open pores with width less than that of the molecule of interest are considered as closed pores and precisely designated as latent pores. The latent pores in the porous solid vary with respect to the dimension of the molecule of our interest.

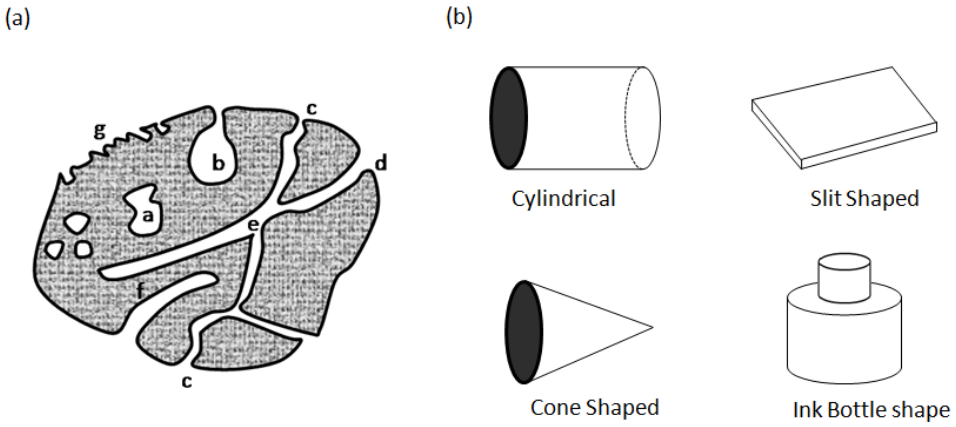

Figure 1-1. (a) Schematic of pores classification based on their accessibility to the surroundings by IUPAC. a- closed pores, b, f- pores open at one end, c, d, g- open pores and e- open at two sides and (b) pores classification based on their geometry.[5]

Another possible pore classification based on their geometry given by Kaneko et al.[5] similar to IUPAC classification.[1] Pores are classified as cylinder, slit-shaped, cone shaped and as ink bottle as shown in Fig.1-1. Due to the irregularity of pore geometry in porous solids, the systems are preferably modelled. The model development is based on several criteria for the complete description of porous materials in terms of geometry, pore location, size and connectivity. The most often modelled porous systems are cylindrical (oxides like alumina), prisms (fibrous zeolites), slits (clays and activated carbon) and spheres or voids left between the spheres that are in contact (silica gel, zirconia, etc).

1.1.1.4 Size of the pores

Porous materials with same porosity, but with different pore size can behave differently under the identical conditions. Considering this fact, classification of porous solids arises based on size of the pores in them. The irregularities in pore size and geometry makes difficult in classifying them more precisely. A summary of the most frequently used classification is given in Table 1. The common classification based on pore size divides the porous materials into three categories. Micro porous materials are the one having pores with less than 2 nm in diameter or width, meso porous materials having between 2 and 50 nm and macro porous materials are with pores greater

than 50 nm. But the microporous materials are in turn further classified into supermicro, ultramicro and ultraporous as shown in Table 1.

1.1.2 Pore analysis of nanoporous materials

1.1.2.1 Molecular porosimetry

Porous solid surfaces are often analyzed by molecular adsorption of probe molecules. The molecular probes are small sized molecule, easy to adsorb on the porous solid surface with the established adsorption theory. Nitrogen molecule adsorption at 77 K is devoted to the physical characterization of porous solid surfaces. The effective size of the N_2 molecule on the solid surface is 0.354 nm in thickness and hence can reveal the sub-nano structure of the porous solids without any destruction. H_2O, CO_2, Ar and He can also be used as molecular probes for the analysis of micro pore system of solids.

Table 2. Probe molecules and adsorption conditions in surface analysis [5(a)]

	He	H_2O	N_2	CO_2
Molecular area (nm^2)	0.117	0.125	0.162	0.142-0.244
Collision diameter (nm)	0.20	0.27	0.41	0.45
Molecular diameter (from van der Waals constant, nm)	0.42	0.46	0.50	0.51
Adsorption temperature (K)	4.2	room temp	77	room temp
Interaction	weak	dipole	quadrupole	quadrupole
Adsorbent	any	hydrophilic	any	any

Table 2 summarizes the most commonly used probe molecules and their adsorption conditions in surface analysis of porous materials. The pore analysis by adsorption with probe molecules is referred as ‘molecular porosimetry’. In this technique multiple probe molecules can also be used to get the detailed surface information. This multiple probe molecule adsorption technique is powerful tool to know the pore size distribution of the porous solids.

1.1.2.2 Molecular adsorption experiment and isotherm

Before discussing the molecular porosimetry in detail, it is important to understand the basic science of probe adsorption on solid surface and the different type of isotherms it generates. An adsorption isotherm is a measurement of amount of probe molecules adsorbed on a solid surface as a function by using equilibrium pressure of the probe (adsorbate) at constant temperature. The amount of adsorbed probes determined either by volumetric or gravimetric analysis after degassing from the solid surface. The total adsorption of probe molecules (W_a) depends on the amount of porous material, temperature and pressure of the probe molecules. The parameters other than pressure of adsorbate (P) are fixed for an isotherm measurement and W_a is expressed as function P to get the resulting isotherm. Physical adsorption is a predominant process for gas adsorption by porous materials below a certain temperature called critical temperature and which has a saturated vapour pressure of P_o. Therefore the pressure is always expressed as relative pressure P/P_o. The IUPAC recommended six type most common isotherms as shown in Fig.1-2.

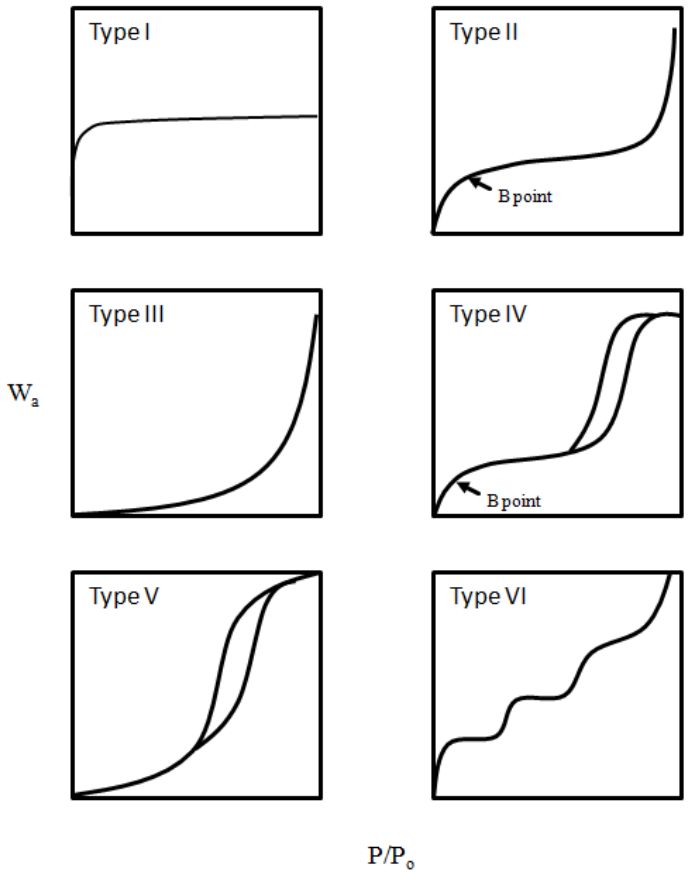

Figure 1-2. IUPAC classification of different types of possible isotherm for gas adsorption of porous materials.[9]

The type I isotherm corresponds to the so-called monolayer or Langmuir adsorption of gas molecules. If the adsorption is physical process, the type I isotherm represents the micro pores where molecules are adsorbed by pore filling phenomenon. The type II isotherm corresponding to multilayer adsorption as proposed by B.E.T adsorption theory. Hence this type of isotherm reveals the pores are weather macro or meso. Type III isotherm arises from the nano or macroporous surfaces which has very high affinity to the probe molecules. The type IV isotherm gives information about mesoporous structure through the hysteresis loop. In mesoporous surfaces, the adsorbate acts as liquids having meniscus that obeys Kelvin equation, and which provides the information of pore distribution. The type V isotherm is very similar to type IV but in which probe and surface have moderate interaction at high affinity range. The type VI is a stepped isotherm and the steps are originated from the phase transition of adsorbed layers or adsorption on different crystalline phases of porous solid. In order to understand the microporous and mesoporous structure Type I and Type IV isotherms respectively are very important.

Comparison plots

The deviation of an isotherm for the sample against the standard is determined by comparison plots. The comparison plots are constructed using the standard data available. Two types of comparison plots are known which are t- and α_s- plots. In t- plot analysis, the adsorbed amount W_a is converted into average film thickness t using the equation 1.1,

Thickness of the adsorbed film t given by,

$$t = (W_a/W_m).\sigma_t \qquad \textbf{1.1}$$

W_a is amount of adsorption; W_m amount of adsorbate required for one monolayer and σ_t is thickness of one single monolayer of adsorbate (For N_2 which is 0.354 nm). The plot of W_a against thickness t, is called as t- plot. The deviation from the linearity in t- plots gives the information on the type of pores, average pore size, surface area and pore volume. However the t- plot analysis has a limited applicability to microporous system due to the absence of monolayer adsorption. Sing et al. proposed a more general comparison plot called α_s- plots as an alternate to t plots.[10] The ratio of total amount of adsorption (W_a) to amount adsorption at P/P_o is 0.4 i.e. $W_a/W_{0.4}$ is plotted against adsorption amount. Such plot is called α_s- plot where the value of α_s is 1 at $P/P_o = 0.4$.[10]

To construct the α_s-plot, it does not require the value of the monolayer capacity. Therefore, it is applicable to microporous system. The straight line passing through the origin represents the multilayer adsorption. Kaneko et al. introduced a high resolution α_s-plot which makes the analysis even below the $\alpha_s = 0.7$.[11]

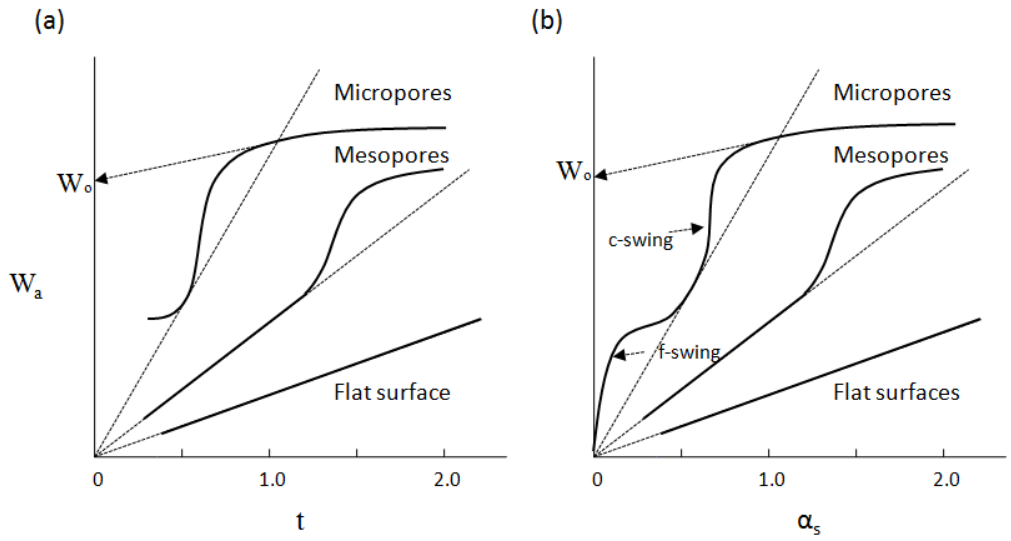

Figure 1-3. (A) t- and (B) α_s - plot for adsorption isotherms of meso and microporous materials.

A typical type of t- and α_s- plots is shown in Fig.1-3. For flat surfaces, the line passes through the origin. But for the system with micropores, there is a hump from 0.7 to 1.0. The slope of the straight line passing through the origin and the line at high α_s value give total and mesoporous surface areas, respectively. The extrapolation at high α_s to y-axis gives mesoporous volume W_o. This high resolution analysis is effective for microporous systems. The α_s has one swing at lower α_s value called f-swing and one at high α_s value called c-swing corresponding to filling and condensation of probe molecules respectively. The type of the α_s-plot suggests the presence of ultra-micropores and super-micropores.

1.1.2.3 Small angle X-ray scattering

Matters scatter X-rays without losing their original phase. The scattered intensity is observed as a function of the spatial distribution of electrons of the scattering body. In X-ray diffraction, the angular region of X-ray scatters below 5^o ($2\theta < 5^o$, where θ is incident angle of X-rays) is known as small angle X-ray scattering (SAXS). In this angle region, two types of scattering phenomenon were observed. One is sharp maxima due to long range periodicity and the other is intensity decrease with increase in scattering angle, which is due to the electronic irregularity or heterogeneity of the irradiated material. The size of heterogeneous entity ranges from 0.5 to 1000 nm. Therefore, SAXS offers much useful information about pore structure, size and distribution from heterogeneous spatial electronic distribution.

The electron radius of gyration $R_{G,}$ about its centre of mass can be obtained from SAXS. From the knowledge of $R_{G,}$ simple geometrical forms of pores can be calculated. If the scattering particle is spherical with radius R, it can be related with R_G as,

$$R_G = (3/5)^{1/2}R \qquad \textbf{1.2}$$

If the scattering particle has slit–shaped pores with width (w), cross-sectional length (*l*) and depth (d), the R_G is given by,

$$R_G = [(w^2+l^2+d^2)/12]^{1/2} \qquad \textbf{1.3}$$

Guinier et al. showed that the scattering curve becomes exponential of $-S^2 R^2_G/3$, as S tends zero (S is scattering parameter, $4\pi\sin\theta/\lambda$). The Guinier equation is given by,[5(a,c)]

$$I(s) = I(0) \exp(-S^2 R^2_G/3) \text{ at (S tends zero)} \qquad \textbf{1.4}$$

Also Guinier approximation is valid, only when $SR_G < 1$. The plot of lnI versus S^2 in low angle region is often found to be linear. From the slope of this linear plot, the electron radius of gyration R_G about its centre of mass can be calculated. If we consider the scattering entities are pores and which are mono disperse (regardless of slight non-linearity) then Guinier approximation holds true for all types of pores in the solid, the Maxwell distribution of scattering intensity with size distribution $M(R_G)$ is assumed as,

$$M(R_G) = 2M_o/r_o^{n+1}\, \Gamma\,[(n+1)/2] \bullet R_G^2 \exp(-R_G^2/r_o^2) \qquad \textbf{1.5}$$

Here n and r_o are pore parameters, M_o the mass of the scattering particles, and Γ is gamma function. The Maxwell approximation gives the expression (equation 1.6) for scattering intensity.

$$\log I(S) = \text{constant} - [(n+4)/2] \log (r_o^2/2) - [(n+4)/2] \log (S^2+3/r_o^2) \qquad \textbf{1.6}$$

The pore size distribution of activated carbon fibers (ACF, pitch based) having a slit type of pores as given in Fig. 1-4.[5(a)] The size distribution in ACF is considerably broad and the mean R_G value is 1.5 nm, which is significantly different from 1.0 nm by simple Guinier analysis. Since the R_G value can be related to the three dimensional parameters of the pores w, *l* and d. The three dimensional pore parameters of ACF can be determined by SAXS analysis.

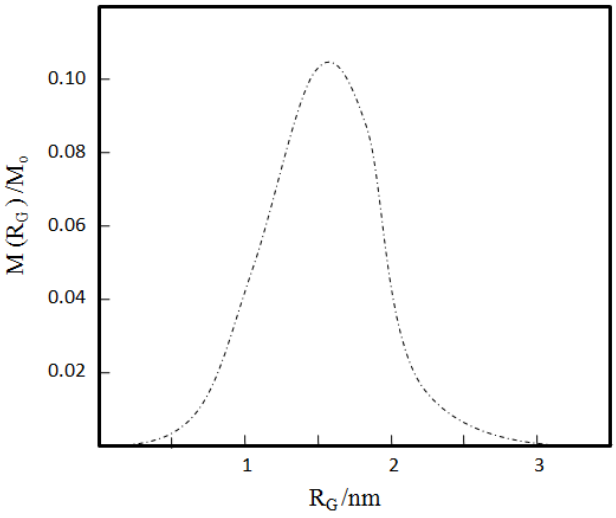

Figure 1-4. Distribution of radius of gyration (R_G) of pitch based ACF.[5(a)]

1.1.2.4 Nuclear magnetic resonance (NMR)

The nuclear magnetic resonance is also an effective technique for surfaces analysis in porous solids. Selective probe molecules are allowed to adsorb on the inner surfaces of porous solids, and by observing the chemical shift on magnetic resonance from their original, the surrounding pore structure can be elucidated. The strength of the actual magnetic field experienced by the given nuclear spin is slightly different from the applied magnetic field because of the electron shielding effect of surrounded nuclei and the difference effectively shifts the magnetic resonance frequency. This phenomenon is called chemical shift. The cause of chemical shift is not necessarily within the molecules, could also be from their surroundings. This serves as the key for NMR technique used for surface analysis of porous solids. Ito et al. introduced the correlation of chemical shift with pore diameter or width of zeolites using xenon probe (^{129}Xe).[12] The atomic size of xenon is 0.44 nm and cross-sectional area is 0.195 nm^2. Xenon at room temperature is a supercritical gas and therefore it is good probe for micropore analysis. A narrow NMR signal has been observed for xenon, if there is uniform pore geometry. The chemical shift increases with decrease in pore size. The NMR technique is successfully applied to mesoporous silica by Conner et al.[13] The observed chemical shift δ_{obs} can be given by,

$$\delta_{obs} = \chi_{ads} \bullet \delta_{ads} + \chi_{pore} \bullet \delta_{pore} \qquad \textbf{1.7}$$

The observed chemical shift is a sum of average contribution from adsorbed Xe into the pore structure (δ_{ads}) and inter-porous Xe (δ_{pore}). χ_{ads} and χ_{pore} are the fractional concentrations of adsorbed and inter-porous Xe, respectively. The chemical shift is average of adsorbed Xe atom into small pores (micropores) and rapid exchange between the Xe in mesopore and Xe adsorbed on surface. NMR signals are different for different pore structured materials of same type. If two

types of mesoporous silica are mixed, the NMR shows two distinct peaks of Xe. Therefore, it is possible to check the heterogeneity of pore structures by using NMR technique.

1.1.2.5 Thermoporosimetry

Thermoporosimetry can only be applied for wet porous materials, in which other molecular porosimetry characterization is not available. The depression of melting points of solids in pores is well known and this can be explained by Kelvin equation. The dependence of solidification temperature of the liquid at pores with pore width is examined by Quinson et al.[14] They assumed that the molecules adsorbed are in liquid phase, when adsorbed by wet porous materials. The depression of the solidification temperature of adsorbed molecules at the pores ΔT, is given by the curvature $2/r_m$. The volume of the pores dW, where the solidification occurs, is proportional to ΔT. For water, the curvature equation given by,

$$r_m = - (64.67/\Delta T + 0.23) \qquad \textbf{1.8}$$

The pore size distribution dV/dr_p is related to the depression in the solidification temperature as,

$$dV/dr_p \propto \Delta T^2 \qquad \textbf{1.9}$$

The solidification temperature can be measured by differential scanning calorimetry (DSC). The determination of depression in solidification temperature makes it possible to know the pore distribution and with the comparison of solidification and fusion thermograms, the information about pore size can be obtained. This thermoporosimetry is available for very small pores of a few nanometers in the wet state.

1.1.2.6 Positron annihilation

Positron annihilation lifetime spectroscopy (PALS) is a powerful tool for the detection and quantification of defects, dislocations, voids or pores in various solids in recent days. Similar to scattering technique, this method allows non destructive detection of inaccessible pores even. This technique predominantly applied to porous polymers and thin porous films. This technique is based on the decay of positron into two γ photons called annihilation and can be found in various literatures.[15]

The decay of radioactive sodium ^{22}Na yields positrons (β^+), accompanied by simultaneous emission of γ of 1.273 MeV. This photon emission is considered as starting signal of positron production. The produced positron has own lifetime in space and decayed into two γ photons of energy 511 keV. The lifetime of the positron coming from the radioactive sodium is highly depending on its surrounding. This surrounding dependence of lifetime of positron decay provides the information about the pores in porous solids. Positron, when enter into the sample, it loses the energy by inelastic collisions with electrons in the sample. These thermalized positrons have energy of a few meV and forms positroniums (electron – positron bound state) that diffuse

through the sample and then annihilate after their specific lifetime in the solid. The lifetimes of positron or positroniums becomes longer, when they are confined or localized at spaces with low electron density (can be considered as voids or pores). Thus positron can be used as probes to investigate the average size of the free volume, and the distribution. PALS has been successfully applied to the investigation of porosity in various types of porous materials such as thin siliceous films,[16] zeolites[17] and mesoporus silica.

1.1.2.7 Mercury porosimetry

Mercury is a non-wetting fluid at room temperature for most of the porous materials. Mercury is allowed to fill in the pores of the solid by applying external pressure and from the volume intruded at each respective pressure, the pore size distribution can be calculated based on Washburn equation.[18] It relates to the pressure required to force a non-wetting liquid into a circular cross-sectional capillary diameter (D) of the pores quantitatively.

$$P = (4\gamma\cos\theta)/D \qquad \textbf{1.10}$$

Where γ is the surface tension of mercury and θ is the contact angle with the porous solid. In mercury porosimetry, the porous sample is firstly degassed at elevated temperature and at low pressure then subsequently immersed in mercury. After immersion in mercury, the pressure gradually increased to force mercury intrusion into the pores and from the volume of the mercury required at any pressure, the pore size distribution can be calculated from Washburn equation. This technique is highly useful to determine the average pore size and pore size distribution between 3 nm to 200 nm. This technique is not applicable for microporous solids.

The total pore volume V_{tot} can be calculated from the highest volume of the mercury intruded into the sample. The total pore surface can be expressed as,[19]

$$S = 1/\gamma\,|\cos\theta| \int_0^{Vtot} p.dV \qquad \textbf{1.11}$$

A good linearity of wide range of pressure and pore radii of the sample in mercury porosimetry technique gives detailed information about the porous structures.

1.1.2.8 Electron microscopy

Recently, this characterization technique became one of the most important tools to study the morphology of nano-scale materials and even at the atomic scale. This method provides the direct image of the porous materials of nanometric dimensions. Some of the limiting points of this technique are, (i) all specimens are viewed at high vacuum and hence it might have different morphology, size and shape at liquid or gel-like surroundings, (ii) the electron microscopic images reveal only a small fragment of the sample and the analysed part may not be the characteristic of the whole sample, and (iii) the samples are treated with high energy electron beam (In the case transmission electron microscope, the sample can be measured at cryogenic condition or frozen state), might have a chance to alter the original structure. Therefore, in general electron microscopic results should always be confirmed by other techniques.

Scanning electron microscopy (SEM)

Scanning electron microscopy produces high-resolution images of the sample surfaces. The highly accelerated electron beam strikes the sample surface and scattered in-elastically by the atoms present at the surface. The scattered electrons were detected and computed as an image. Characteristic X-rays are produced due to the specific interaction of electrons with the surface atoms. By analyzing these characteristic X-ray photons, the elemental composition of the surface can also be mapped. Different detection modes accompanied with this technique give different types of information about the solid surface. The detection of back-scattered electron or electron back scatter diffraction pattern (EBSD) gives the crystallographic information about the solid. The SEM resolution depends on various parameters; most of them are related to the instrument. The resolution generally goes down to 20 nm to 1 nm.

Transmission electron microscopy (TEM)

In TEM, the images are produced by detecting the partially transmitted electrons when a high-energy electron beam is focused on very thin solid specimen. The transmitted electrons by the sample carry the information of inner structures of the specimen. The images are recorded by projecting transmitted electrons from the sample to fluorescent screen, photographic plate or highly sensitive camera. The samples with high organic contents, the images are relatively low contrast, because of the weak interaction of the sample. This can be overcome by staining the sample with heavy metal compounds. The dense electron clouds of heavy metals enhance the electron beam interaction with the sample. But sometimes the organic compounds decomposed on the exposure of electron beam. The decomposition can be avoided by using cryogenic measurement conditions (sample at liquid nitrogen or liquid helium temperature). In addition to imaging the sample structure, other accompanying analytical techniques in TEM give much useful information about the sample. The generated characteristic X-rays due to the interaction of the electron with the surface atoms gives the information on the surface composition of the sample. The diffraction pattern gives information about the crystallinity and the crystal

orientation of the sample. In high resolution TEM (HR-TEM), the resolution goes down to < 100 pm.

Atomic force microscopy

To analyze surface topology of nano-objects, atomic force microscopy is used as an important technique. In this method, a cantilever with a sharp tip at its end (typically silicon or silicon nitride) with the size of a few nanometres is brought into the close proximity of a sample surface. The van der Waals force between the tip and the sample surface leads to tip deflection. The deflection of the cantilever is measured by applying a laser beam. The laser reflected from the top of the cantilever goes into an array of photo diodes. If the tip scanned at constant height, it would have the risk of collision with sample and damage the surface. Therefore, a feedback mechanism is employed to keep the tip-to-sample distance constant by applying external force. The sample will be mounted on the piezoelectric holder in all the three directions (x, y, z). Samples in the direction of x and y is for scanning and in z is to maintain the force between the sample and tip. The resulting map (x, y, z) represents the topology of the sample. The major modes of operation of AFM are contact mode and non-contact mode. In contact mode operation, the force between the tip and the sample is kept constant during scanning by maintaining a constant deflection. In non-contact mode, the cantilever is oscillated at or close to its resonance frequency. The oscillation of the cantilever is modified by the sample–tip interaction forces; the changes with respect to an external reference oscillating cantilever provide the information about the sample. AFM has several advantages over the other microscopic techniques. It is a non-destructive method unlike focusing a high-energy electron beam on samples that can decompose the sample. It does not need any special scanning requirement like cryogenic conditions or high vacuum.

1.2 Properties of nanoporous materials

The nanoporous materials possess unique set of properties that the corresponding bulk materials do not have such as high surface area, gas/liquid permeability, and molecular sieving with shape/size selective effects. The specific surface area, pore size, porosity and pore distribution eventually define the characteristics of nanoporous materials and decide their potential in any given application. The most desirable characteristics of nanoporous materials are,

1.2.1 High adsorption capacity

The specific surface area, surface chemical composition, electronic and geometric factors, pore size and pore accessibility determine the adsorption capacity of nanoporous materials.

1.2.2 High selectivity

The selectivity is highly important for multi-component system to be separated and which is largely dependent on the pore size, shape, porosity and the nature of the adsorbate (the molecule to be adsorbed on porous substrate).

1.2.3 Adsorption kinetics

Adsorption kinetics is majorly determined by the particle size, the porosity and free surface area of the nanoporous materials.

1.2.4 Mechanical properties

The porous material should be mechanically stable and robust for any particular application. The nanoporous materials should be stable against attrition, erosion and crushing, whey they are intended to pack in a column. Attrition resistant, high bulk density and crushing strength are desired properties of nanoporous materials.

1.2.5 Chemical stability and durability

Nanoporous materials are often subjected to the treatment of harsh chemicals, high pressure or thermal environment. The stability in such environments is essential in order to make sure they are durable and available for the long run or repeated use.

1.3 Applications of nanoporous materials

Besides the conventional applications (separation materials, filtration membranes and in catalysis), there are ever expanding applications for nanoporous materials.

1.3.1 Environmental separations

Since the regulatory limits on industrial emissions and effluents becoming more and stringent, industries become more active in developing new materials and technology that can effectively remove the contaminants in air and water stream. Nanoporous adsorbents and filtration membranes are being applied for this purpose increasingly in the industries as they are most promising and cost effective. The nanoporous materials are constantly invented or modified for various environmental preservation applications such as for the removal of SO_x, NO_x and other volatile organic compounds (VOCs). The nanoporous materials like activated carbon, zeolites, silica gels and activated alumina are currently used as adsorbents in various environmental remediation applications.

1.3.2 Clean energy and storage

New adsorbent materials with well-defined pore size and high surface area are being developed and tested for the potential use in energy storage. Future energy might be based on the hydrogen fuel that is so-called clean energy carrier. The hydrogen fuel can be produced from fossil fuels, water electrolysis and biomass. The hydrogen from fossil fuel is accompanied with the emission of the byproduct of carbon dioxide which should be carefully sequestered safely and economically. The carbon dioxide capture from the mixture of H_2/CO_2 will be accomplished with the aid of nanoporous materials. The storage of the hydrogen fuel is also very important for the steady and uninterrupted supply.

For the optimal hydrogen gas storage, the material should meet the following criteria:

1. High storage capacity with appropriate pore size, shape and distribution

2. Low dissociation temperature

3. Low heat of formation in order to minimize the energy required to release hydrogen

4. Low cost

5. Light-weight for the ease of transportation

6. High stability against oxidation and moisture and should have long life.

But the major challenges in the development of hydrogen storage materials are high storage density, storage kinetics and cycle life and all these should be available at reasonable cost. The key for this storage issue of hydrogen fuel will definitely be nano-materials. Molecular organic frameworks (MOFs) are promising candidates for hydrogen storage applications. Carbon nanostructures like carbon nanotube, fullerene and graphene or carbon nano-composites were also found to be very good candidates for hydrogen gas storage. Hydrogen can be stored in porous solids either by physisorption or chemisorption. For physisorption, new nano-scale materials with very high specific surface area are required. MOFs, a new class of crystalline materials with low-density and high surface area attracted great attention in hydrogen storage. Rowsell et al. reported MOFs with hydrogen sorption capacities at 78 K and ambient temperature and pressure up to 20 bar.[20]

1.3.3 Catalysis and photocatalysis

Catalysis by nanoporous materials covers a broad range of processes ranging from crude oil refining to fine chemical productions. These conversions are mainly based on acidic, red-ox and shape-selective properties of nanoporous catalytic materials. The inherent surface acidic functionality of zeolitic materials or the possibility of different surface functionalization and the ability to finely tune the pore size made themselves effective catalysts in organic transformations. The most common acid catalyzed reactions with nanoporous catalysts are fluidized catalytic cracking, hydrocracking, aliphatic alkylation, isomerization and transformation of complex aromatics into simple hydrocarbons like methanol. The red-ox nanoporous catalysts are also increasingly used for a variety of selective oxidations of hydrocarbons, alcohols and amines.

Transition metal modified mesoporous aluminiosilictaes or aluminophosphates are also very good catalyst for acid catalyzed reactions, oxidation, hydroxylation and polymerization reactions. [21] Nanocomposites of highly dispersed transition metal oxide nanoparticles incorporated into crystalline voids of nanoporous silica also exhibit high catalytic activity in CO and CH_3OH oxidation reactions. Hydrophilicity and low metal dispersions in the metal modified nanoporous composite catalyst show reduced catalytic activity and selectivity in organic transformations. The leaching of metal species from the voids of the porous solids also disables the recovery of the catalyst. Therefore, the traditional techniques of impregnation of metal ions in nanoporous materials are not effective in achieving the desired active site dispersion and strong adherence with the support. Incorporation in any one of the synthetic steps of porous solid or intercalation of metal ions after the porous solid synthesized is absolutely necessary.

Semiconducting transition metal oxides exhibit a wide range of physical, chemical and optical properties. The most-studied candidate in this category is titania (TiO_2) semiconductor. Titania in anatase crystal phase exhibits a strong photoctalytic effect upon exposure of UV photons, rendering a strong oxidizing power to decompose organic molecules. Methylene blue dye molecules are degraded by titania supported by nanoporous MCM-4.[22] Nanoporous tungsten

oxide nanotubes exhibit good photocatalytic activity in the visible light region.[23] Y. Li et al. reported template free synthesis of nanoporous $ZnS–In_2S_3–Ag_2S$ which as an active photocatalyst in the visible region to produce hydrogen.[24] Inorganic polynuclear photocatalyst consisting of an oxo-bridged chromophore anchored in mesoporous silica are used for the reduction CO_2 and H_2O.[25]

1.3.4 Biological applications

The self-assembled nanomaterials find very attractive applications in the field of biotechnology. The material topography and spatial distributions of the functional groups are effective in controlling the proteins, cells, and tissue interactions and also in bio-separations. The term bio-nanotechnology is about the development of nanomaterials or biomaterials for biology applications. There are various nanomaterials that are often found to be bio-compatible and mimic the biological activity especially the enzymatic system of living cells. The nanoporous materials have the capability to act as enzymes in biological system and mimic the natural biological reactions. Immobilizing enzymes with nanoporous materials will have the long-lifetime in biological reactors. The possibilities of using these biological reactors for the production of drugs, energy and other complicated synthetic system are limitless.

The nanoporous materials are also used in molecular analysis of various biological systems as the pores are at molecular scale. DNA sequencing is one of the important analyses to understand the biological system and this can be accomplished by forcing the DNA strands (nucleotides) into nanopores and by measuring the change in ionic characteristic current corresponding to the particular unit of the passing strand.[26] The successful use of nanoporous materials towards DNA sequencing demonstrates their potential in bioengineering.

Another exciting biological application of nanoporous material is their use as biosensors. Piezoelectric biosensors utilizing high surface area of the nanoporous materials exhibit increased sensitivity in detection. Immobilized biological molecules on the surface of the nanoporous silica can serve as a potential biological detection system. Biosensors have major potential in health care industry, such as real-time and in-vivo detection of pathogens, drugs, sugar, insulin, and hormonal level in the body under emergency conditions. They are also used to detect the pathogens and amount of preservatives added in the food products and also useful to find the contaminants present.

1.3.5 Sensors

Nanoporous materials with high surface area are highly sensitive to slight changes in the surrounding or environment (temperature, humidity and light). Therefore, nanoporous materials are largely used as sensors. Gas sensors detect the gas by characteristic electric resistivity change with gas molecules adsorbed on the sensors and the sensitivity normally depends on the surface area of the sensor. Nanoporous metal oxides like SnO_2, TiO_2, ZrO_2 and ZnO based gas sensors are applied to detect combustible gases, humidity, ethanol vapors and hydrocarbons. Zirconia is

typically good in oxygen sensing applications. Dickey et al. reported room temperature humidity and ammonia sensors based on nanoporous alumina.[27] Nanoporous silica and ZnO obtained from the anodization process of their respective crystals are capable of hydrogen gas sensing.

1.3.6 Filtration membranes

Membrane technology is an emerging field with a great impact on daily life through water purification, dialysis in medicine, gas separation and solvents recycling. The search for the new membranes that combine good selectivity, permeability and significant stability is a grand challenge. The nanoporous polymer thin films transferred on other porous ceramic membranes exhibits a great potential as highly selective and stable membranes. There are two common strategies to prepare the active nanoporous thin film membranes. One is porous thin films derived from the selective unit removal from the self-assembled block copolymer structures. This method has the difficulty of manual transfer of the thin film to the porous substrate and annealing to remove the specific unit form the self-assembled structure may damage the membrane. Second method is 'phase inversion' involving the solidification of thin cast of polymer film on the substrate by exposing non-solvent. A successful fabrication of the nanoporous membranes from polystyrene-co-polyethylene oxide (PS-co-PEO) diblock copolymer, their pore tunability and chemical stability have been reported.[28] Nanoporous membranes can also be prepared by annealing the filtered polymer nanoparticles on the porous substrate. The free-standing polystyrene membranes prepared by chemical cross-linking of polystyrene nanoparticles reported by Q. Zhang et al.[29]

1.3.7 Other miscellaneous applications

Besides the above applications, nanoporous materials also have tremendous opportunities in the following areas.

1. Composite material reinforcement

2. Porous electrodes in electrochemistry (Fuel cells)

3. High efficient thermal insulators

4. Batteries (Li-ion battery)

5. Porous electronic substrates.

1.4 References

[1] J. Rouquerol, D. Avnir, C. W. Fairbridge, D. H. Everett, J. M. Haynes, N. Pernicone, J. D. F. Ramsay, K. S. W. Sing and K. K. Unger, *Pure & Appl. Chem.*, 66, 1739 (1994).

[2] W. J. Decker and D. G. Corby, *Clinical Toxicology*, 3, 1 (1970).

[3] T. Tsuchiya and G. Levy, *J. Pharm. Sci*., 61, 624 (1972).

[4] J. E. F. Reynolds, *Martingale Extra Pharmacopeia*, 28th edition, 72 (1982).

[5] (a) K. Kaneko, *J. Membr. Sci*., 96, 59 (1994).

(b) B. D. Zdravkov, J. J. Čermák, M. Šefara and J. Janků, *Central European Journal of Chemistry*, 5, 385 (2007).

(c) A. Guiner and G. Fournet, *Small-Angle Scattering of X-Rays*, Wiley, New York, 25 (1955).

[6] S. Ijima, *Nature*, 354, 56 (1991).

[7] T. Enoki, H. Inokuchi and M. Sano, *Phy. Rev. B*, 37, 9163 (1988).

[8] M. Ruike, T. Kasu, N. Setoyama, T. Suzuki and K. Kaneko, *J. Phys. Chem.*, 98, 9594 (1994).

[9] K. S. W. Sing, E. H. Everett, R. A. W. Haul, L. Moscou, R. A. Pierotti, J. Rouquerol and T. Siemienewska, *Pure & Appl. Chem*., 57, 603 (1985).

[10] K. S. W. Sing, *Carbon*, 27, 5 (1989).

[11] K. Kaneko, C. Ishii, M. Ruike and H. kuwabara, *Carbon*, 30, 1075 (1992).

[12] T. Ito and J. Fraissaird, *J. Chem. Soc. Faraday Trans*., 183, 45 (1987).

[13] W. C. Conner, E. L. Weist, T. Ito and J. Fraissard, *J. Phys. Chem.*, 93, 4138 (1989).

[14] J. F. Quinson, J. Dumas and J. Serughetti, *J. Non-Cryst. Solids*, 79, 397 (1986).

[15] (a) O. E. Mogensen, in Positron Annihilation in Chemistry, edited by V. I. Goldanskii, F. P. Schaffer, and J. P. Toennis, Springer-Verlag, Berlin (1995).

(b) D. M. Schrader and Y. C. Jean, *Positron and Positronium Chemistry*, Elsevier, Amsterdam (1988).

(c) V. P. Shantarovich, I. B. Kevdina, Y. P. Yampolskii and A. Y. Alentiev, *Macromolecules,* 33, 7453 (2000).

[16] (a) M. P. Petkov, M. H. Weber, K. G. Lynn and K. P. Rodbell, *Appl. Phys. Lett.*, 79, 3884 (2001).

(b) T. L. Dull, W. E. Frieze, D. W. Gidley, J. N. Sun and A. F. Yee, *J. Phys. Chem. B*, 105, 4657 (2001).

(c) J. N. Sun, D. W. Gidley, T. L. Dull, W. E. Frieze, A. F. Yee, E. T. Ryan, S. Lin and J. Wetzel, *J. Appl. Phys*., 89, 5138 (2001).

(d) . M. P. Petkov, M. H. Weber, K. G. Lynn and K. P. Rodbell, *Appl. Phys. Lett.*, 77, 2470 (2000).

(e) D. W. Gidley, W. E. Frieze, T. L. Dull, J. Sun, A. F. Yee, C. V. Nguyen and D. Y. Yoon, *Appl. Phys. Lett.*, 76, 1282 (2000).

[17] H. Nakanishi and Y. Ujihira, *J. Phys. Chem*., 86, 4446 (1982).

[18] (a) E. W. Washburn, *Proc. Natl. Acad. Sci. USA*, 7, 115 (1921).

(b) J. van Brakel, *Powder Technol.*, 29, 1 (1981).

[19] S. Polarz and B. Smarsly, *J. Nanosci. Nanotech*., 2, 581 (2002).

[20] J. L. C. Rowsell and O. M. Yaghi , *J. Am. Chem. Soc*., 128, 1304 (2006).

[21] (a) J. Y. Ying, C. P. Mehnert and M. S. Wong, *Angew. Chem. Int. Ed*., 38, 56 (1999).

(b) A. Taguchi and F. Schüth, *Micro. Meso. Mater*., 77, 1 (2005).

[22] S. Anandan, *Dyes and Pigments*, 76, 535 (2008).

[23] Z. G. Zhao and M. Miyauchi, *Angew. Chemie*., 120, 7159 (2008).

[24] Y. Li, G. Chen, C. Zhou and J. Sun, *Chem. Commun.*, 2020 (2009).

[25] H. Frei, *CHIMIA International Journal for Chemistry*, 63, 721 (2009).

[26] G. F. Schneider and C. Dekker, *Nat. Biotech.*, 30, 326 (2012).

[27] E. C. Dickey, O. K. Varghese, K. G. Ong, D. Gong, M. Paulose and C. A. Grimes, *Sensors*, 2, 91 (2002).

[28] X. Li, C. A. Fustin, N. Levre, J. F. Gohy, S. D. Feyter, J. D. Baerdemaeker, W. Eggere and F. J. Vankelecom, *J. Mater. Chem*., 20, 4333 (2010).

[29] Q. Zhang, S. Ghosh, S. Samitsu, X. Peng and I. Ichinose, *J. Mater. Chem*., 21, 1684 (2011).

Chapter 2

Fabrication of mesoporous polymers: A nano-crystallization phase separation approach

2.1 Literature overview of fabrication of nanoporous polymer materials

Mesoporous polymers find a broad range of applications in various branches of science and technology. The major applications are separation/filtration including pathogens like virus,[1] sensors,[2] electronics,[3] catalysis[4] and medical applications.[5] Mesoporous polymers can be prepared by a variety of routes including phase separation,[6] self-assembly of block copolymers and selective etching,[7] non-solvent induced microphase separation,[8] carbon dioxide foaming,[9] and so on.

2.1.1. Thermal induced phase separation

Polymer nanofiber matrices can be prepared by lowering the temperature of polymer solution and subsequent phase separation occurs therein, known as thermally induced phase separation (TIPS).[10] This fabrication involves (a) dissolution of the polymer in a suitable solvent, (b) phase separation and polymer gelation at low temperature, (c) solvent exchange by immersing in non-solvent and (d) freeze drying as shown in Fig.2-1. The internal morphology of these matrices can be controlled by the fabrication parameters such as gelation temperature, polymer concentration, solvent, etc. Ma et al. reported successful fabrication of nanofiber network structure of poly-L-lactic acid (PLLA), poly-lactic-co-glycolic acid (PLGA) and poly-DL-lactic acid (PDLLA) with fibrous diameter 50-500 nm and porosity about 98.5 % by TIPS technique.[10] Uyama et al. reported the fabrication of mesoporous polyaniline monoliths by thermal induced phase separation technique.[11]

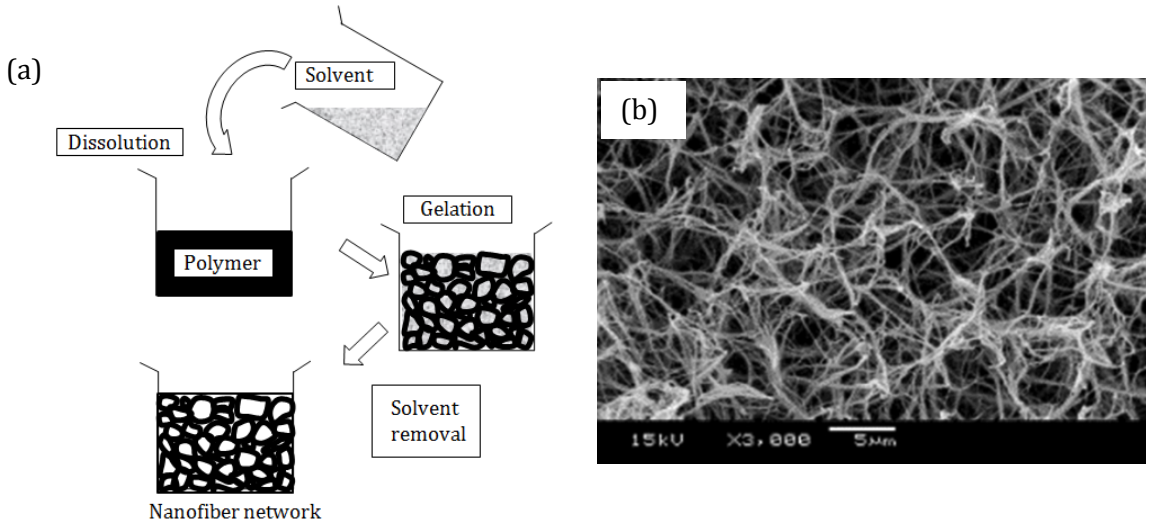

Figure 2-1. (a) Schematic of fabrication of macroporous polymer structure by thermally induced phase separation and (b) SEM image of PLLA nanofiber network structure fabricated by TIPS Adopted with permission from ref 10a. (b) was reproduced with permission from Elsevier. Copyright 2010 Elsevier Limited.

2.1.2. Self-assembly and selective etching of block copolymers

This preparation method of mesoporous polymers involves the self-assembly of block copolymers and selective etching of one of the components. The di- or tri-block copolymers have a specific self-assembling nature under appropriate experimental conditions and removal of any one of the segments leaves behind, a well connected mesoporous polymer as shown in Fig.2-2(a). Mesoporous polystyrene monoliths have been prepared from polystyrene-polylactide (PS-PLA) copolymer.[7] The PS-PLA self-assemblies when placed in aqueous methanol mixture at 65 ^{o}C, which is the temperature below the T_g of PS but above the T_g of PLA. In these conditions, PLA segment undergoes chemical cleavage from PS. After the degradation of PLA from the assembly, mesoporous PS can be obtained. The fabricated mesoporous PS is shown in Fig.2-2(b).

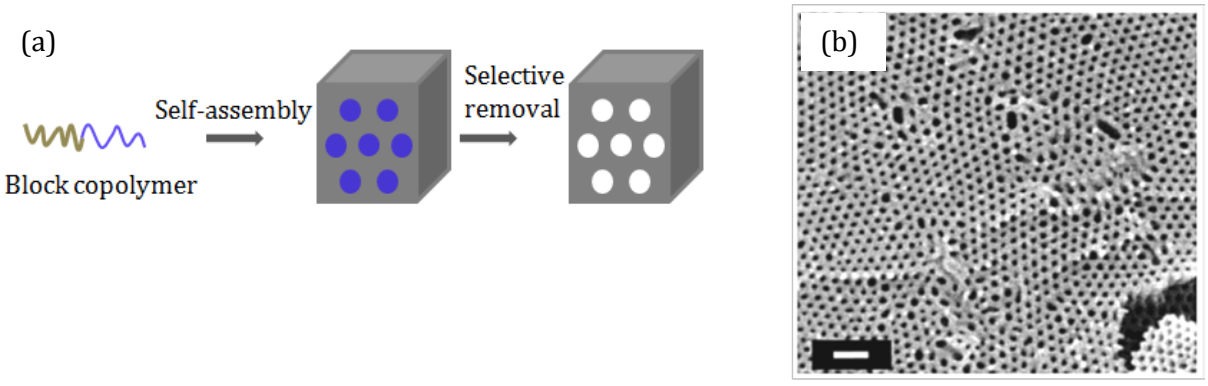

Figure 2-2. (a) Schematic of self assembly of block copolymers and selective etching of any component leaves behind mesoporous polymer and (b) SEM image of mesoporous polystyrene structure fabricated from PS-PLA. The scale bar is 100 nm. Adopted with permission from ref 7. Copyright 2001 American Chemical Society.

2.1.3. Non-Solvent induced phase separation of block copolymers

This fabrication technique involves a combination of non-solvent induced phase separation of block copolymer solution and subsequent self-assembly of copolymer. The block copolymer solution is subjected to controlled microphase separation in the presence of non-solvent and which is miscible with the solvent and eventually exchanged. The resulting integral asymmetric structure has highly connected and regular mesopores.

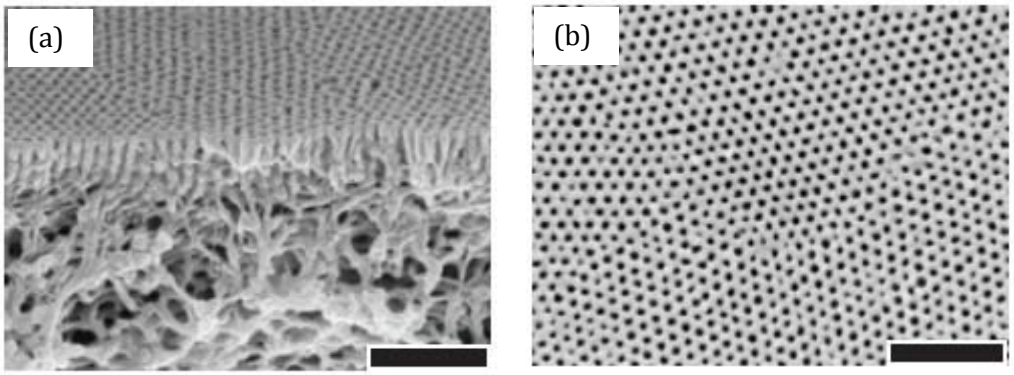

Figure 2-3. SEM images of the surface of the asymmetric PS-b-P4VP diblock-copolymer film fabricated by non-solvent induced microphase separation. (a), view of the edge. (b), view of the top (The scale bars correspond to 500 nm). Adopted with permission from ref 8. Copyright 2007 Nature Publishing Group.

Polystyrene copoly(4-vinyl pyridine) asymmetric mesoporous film was prepared by using a combination of DMF and THF as solvent and water as non-solvent. The preparation process consists of casting of thin polymeric film on a glass substrate, solvent evaporation at room temperature, immersion in a non-solvent bath and drying at ambient conditions.[8] The fabricated PS-P4VP asymmetric membrane with mesoporous structure is shown in Fig.2-3.

2.1.4. Carbon dioxide foaming

Foaming of polymer thin films or fibers with carbon dioxide (CO_2) as a physical blowing agent also yields a bicontinuous mesoporous internal morphology. In this fabrication technique, the polymers will be saturated with CO_2 at elevated pressure at room temperature. The CO_2 saturated polymer is then kept in a glycerol bath at desired foaming temperature allowing the quick release of CO_2 inside. The sudden release of CO_2 from the polymer results in fine nanoporous structure. Then polymer sample is quenched in ethanol/water mixture and washed in ethanol and finally the sample dried in vacuum. The SEM images fabricated polyetherimide (PEI) fiber and film by CO_2 foaming technique is shown in Fig.2-4.

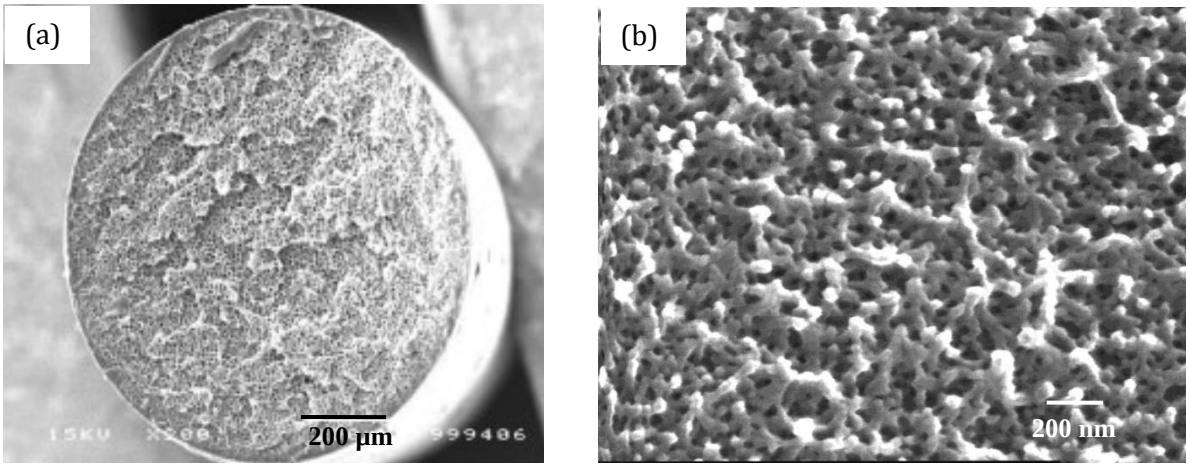

Figure 2-4. (a) SEM micrograph of a PEI fiber saturated at 10 bar of carbon dioxide and foamed at 180 °C for 30 s. The scale bar is 100 µm and (b) SEM micrograph of a PEI film saturated at 50 bar of carbon dioxide and foamed at 180 °C. Adopted with permission from ref 9. Copyright 2001 American Chemical Society.

2.2 Preparation of mesoporous polymers through flash freezing route

Though various fabrication methods have been developed, there are limited mesoporous polymer systems have been well established.[7-10] Also, the processes are multistep and have operational complexity. Moreover, there is no common fabrication strategy available to mesoporous polymers from non-crystalline precursors (polystyrene, polysulfone, polycarbonate, etc). In order to make non-crystalline mesoporous polymers, we have reported a technique based on polymer phase separation at very low temperature and coined the name of the technique as "flash freezing route to mesoporous polymers". Flory-Huggins theory, the basis of the phase separation of polymer solutions was proposed in 1940s.[12] Since then, the phase separation of polymer solutions has been widely studied. The preparation of porous polymer membranes by phase separation technique was intensively focused for the use of sea water desalination. Leob et al. pioneered the fabrication of asymmetric porous membranes by phase separation technique.[13] Solvent induced phase separation technique was also deeply studied in the wet spinning process of polymer fibers. Thermally induced phase separation was invented in 1980s.[14] Though all these techniques were successfully applied in various industrial applications, a subsequent challenge was the precise fabrication of mesoporous polymer materials. Before discussing the flash freezing concept of polymer solutions, the basic understanding of phase separation is important. The following part discusses the definitions and theoretical overview of phase separation of polymer solution.

Definitions

Phase

A Phase is a portion of a thermodynamic system or space which has uniform physical and chemical characteristics. The characteristics include density, chemical composition, refractive index, etc. The distinct phases in a system have distinct physical and/or chemical properties and also separated from each other by definite phase boundaries. An ideal example to understand the concept of phase is melting ice cubes in which the solid ice cubes forms one phase and the liquid water constitutes the other phase.

Homogenous system

A system with single phase

Heterogeneous system

A system with two or more distinct phases

Component

Chemically recognizable species constituting a thermodynamic system (water and sucrose in sugar solution). A binary system contains two components; ternary system contains three and so on.

Equilibrium state

A system at constant temperature and there is no change in pressure and composition with time.

Metastable state

The intermediate stable state of the system along the path to reach the most stable equilibrium state is known as metastable state.

Phase diagram

Phase diagram is a graphical representation of the equilibrium phases of any system as a function of temperature, pressure and composition. In one-component systems, the equilibrium states are defined by the two independent parameters of pressure and temperature, temperature and volume, or pressure and volume. But in the binary component systems, the phase diagram shows what phase exists at equilibrium state and what phase transition possibly occurs with change in any one of the parameter (pressure, temperature, or volume).

It is important to understand the phase behaviour of multi-component system rather one-component system since the real materials are always a mixture. In one-component system, the melting point (phase transition of solid state to liquid state) occurs at well-defined temperature. But in multi-component system the melting occurs over the range of temperatures. The phase diagram of polycrystal solid and polycrystal liquid is shown in Fig.2-5.

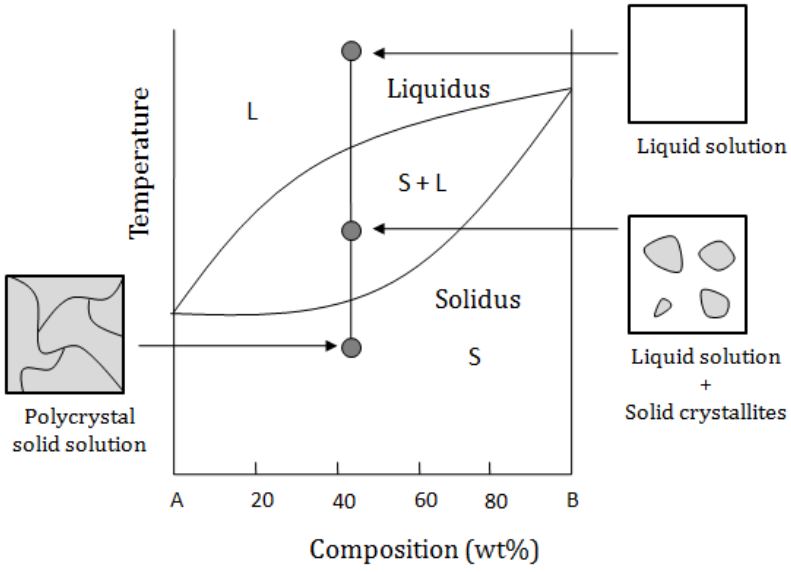

Figure 2-5. Binary phase diagram of A-B solid solution.[15]

'L' in the figure indicates liquid phase region and 'α' indicates solid phase region. 'α+L' indicates the existence of both the phases. The redline in the figure called liquidus line that separates liquid phase from the mixed phase and the line which separates the mixed phase from the pure solid phase is called solidus line.

Interpretation of phase diagram

For a given temperature and composition, the phase diagram determines

(a) The different phases that are present

(b) Compositions of the phases

(c) Relative fractions of the phases

Determining composition in two phase region

To determine the composition of any given phase, the composition point should be located (X_B as shown in Fig.2-6) in composition-temperature phase diagram of a system. Then a tie line connecting the liquidus and solidus lines should be drawn corresponding to the composition point (X_B). The intersections of tie line with the phase boundaries and corresponding values in composition axis (X-axis) in the diagram will tell us the solid and liquid phase composition corresponding to the point the mixed phase. This reading method is depicted in Fig.2-6.

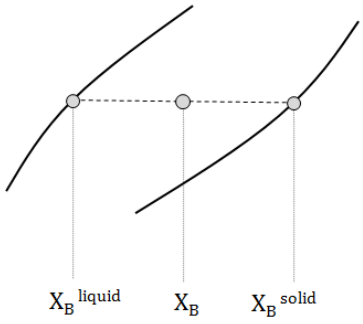

Figure 2-6. Determination of the amount of solid and liquid phases corresponding to the point (X_B) in two-phase region in a binary phase system.[15]

The lever rule

This rule is a mechanical analogy to the mass balance of a fulcrum and the tie-line in the two phase region is analogous to a lever balanced as shown in Fig.2-7.

The lever rule states that,

"The mass fraction of a phase in a given system is determined by the length of the tie-line to the phase boundary for the other phase and dividing by the total length of the tie-line"

$$W_\beta = (C_\alpha - C_O) / (C_\alpha - C_\beta) \quad \textbf{2.1}$$

$$W_\alpha = (C_O - C_\beta) / (C_\alpha - C_\beta) \quad \textbf{2.2}$$

W_α is mass fraction of α (liquid phase)

W_β is mass fraction of β (solid phase)

C_α is concentration of a component in solid phase

C_β is concentration of a component in liquid phase

C_o is total concentration of a component in both the phases

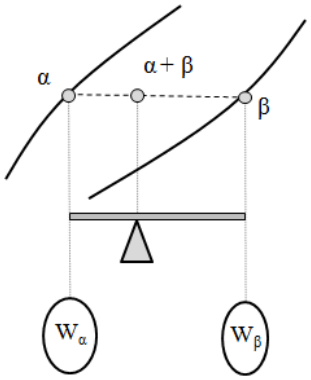

Figure 2-7. Illustration of the lever rule.[15]

Derivation of lever rule

- All the material must be present in either one phase or the other,

$$W_\alpha + W_\beta = 1 \qquad \textbf{2.3}$$

- Mass of a component that is present in the mixed phase is equal to the sum of masses of the component present in the individual phases.

$$W_\alpha C_\alpha + W_\beta C_\beta = C_O \qquad \textbf{2.4}$$

- Solving these two equations,

$$W_\beta = (C_\alpha - C_O) / (C_\alpha - C_\beta)$$
$$W_\alpha = (C_O - C_\beta) / (C_\alpha - C_\beta)$$

With these brief introductions about phase diagram, the following will elaborate the phase behaviour of polymer solutions.

2.2.1 Thermodynamics of polymer solutions

For a mixture of two components involving polymer and solvent, the Gibbs free energy of mixing (ΔG^M) should be negative to form a homogenous mixture. Fig.2-8. shows the schematic of ΔG^M as a function of polymer concentration at different temperatures or pressures in the upper part and the temperature (pressure) – polymer concentration phase diagram is shown in the lower part.[16]

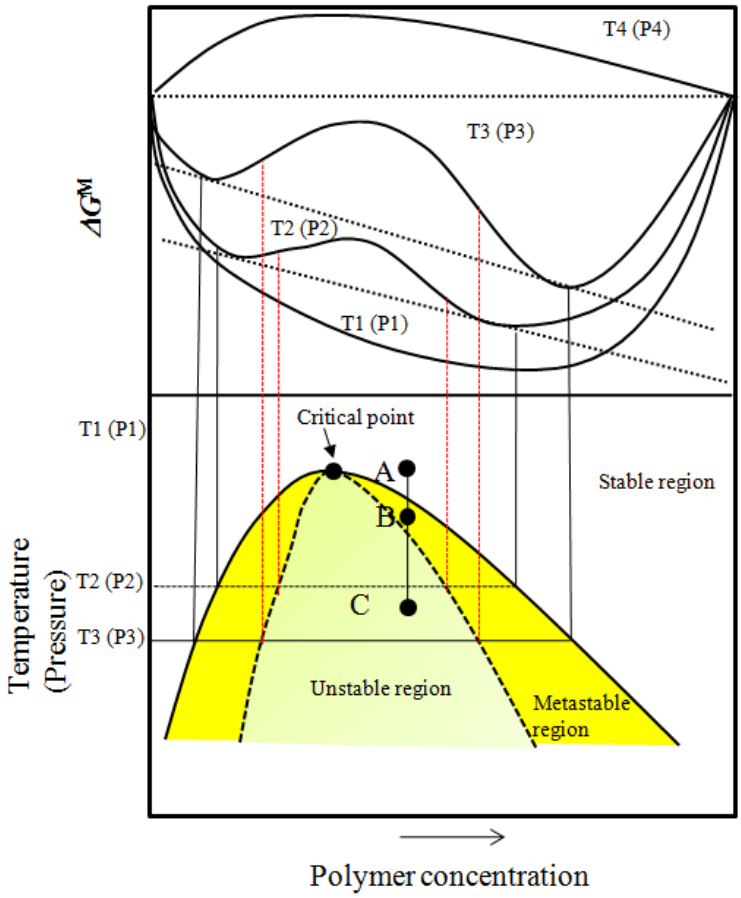

Figure 2-8. Schematic depiction of change of ΔG^M with polymer concentration at different temperature or pressure.[16]

At T1, the ΔG^M shows only one minimum over the whole range of polymer concentration but at T2 and T3 show two minima in Fig.2-8, though the ΔG^M is below zero. The system is only partially miscible at T2 and T3, since the ΔG^M has two local minima in order to have the overall free energy minimum at these temperatures. Therefore, the system will separate into two phases with the different concentrations, which are almost determined by two tangent points of the corresponding ΔG^M curve shown in Fig.2-8.

These two points are called bimodal points and the curve connecting all these points at different temperatures is binodal curve. The curve derived from the inflection points of ΔG^M– concentration curve called spinodal curve, which is also shown in Fig.2-8. The spinodal and binodal curves meet at a point called critical point. In the phase diagram, the region above the binodal curve is stable and homogenous phase. But the region inside the binodal curve is unstable and the system spontaneously phase separates into two phases. Between the binodal and spinodal curves, the system may be at one phase but not stable, which is called metastable region. At T4, the free energy of mixing is larger than zero, and therefore, the system is completely immiscible over the range of polymer concentrations.

The phase behaviour shown in Fig.2-8 is the typical behaviour of system showing an upper critical solution temperature (UCST), where the system enters the one-phase region upon increasing the temperature from C to A. On the contrary, the decrease in temperature brings the system from miscible to immiscible region referred as lower critical solution temperature (LCST). Various combinations of these phase behaviours are shown in Fig.2-9. In addition to the case with only UCST (Fig.2-9b) or LCST (Fig.2-9c), the system can be the combinations of these two behaviours. These are illustrated in Fig.2-9d – Fig.2-9f. A typical example for Fig.2-9d is polystyrene-acetone system.[17]

The phase behaviour is more complex, when a third component is introduced to the system. It can either improve or reduce the miscibility of the system. In some cases, two non-solvent to the polymer can act as a good solvent in some proportion and subsequently dissolve the polymer. This effect is called ‘co-solvency’. Another important phase transition is solid-liquid phase separation. This type of phase behaviour is also important for the polymer solution because the polymer can exist in solid phase in the solution. In the presence of a solvent, the crystallization (or glass transition) temperature and melting temperature of polymers are highly reduced. In the semi-crystalline polymers, the solid-liquid phase behaviour is involved when the solution are under cooled below the crystallization temperature (or glass transition temperature).

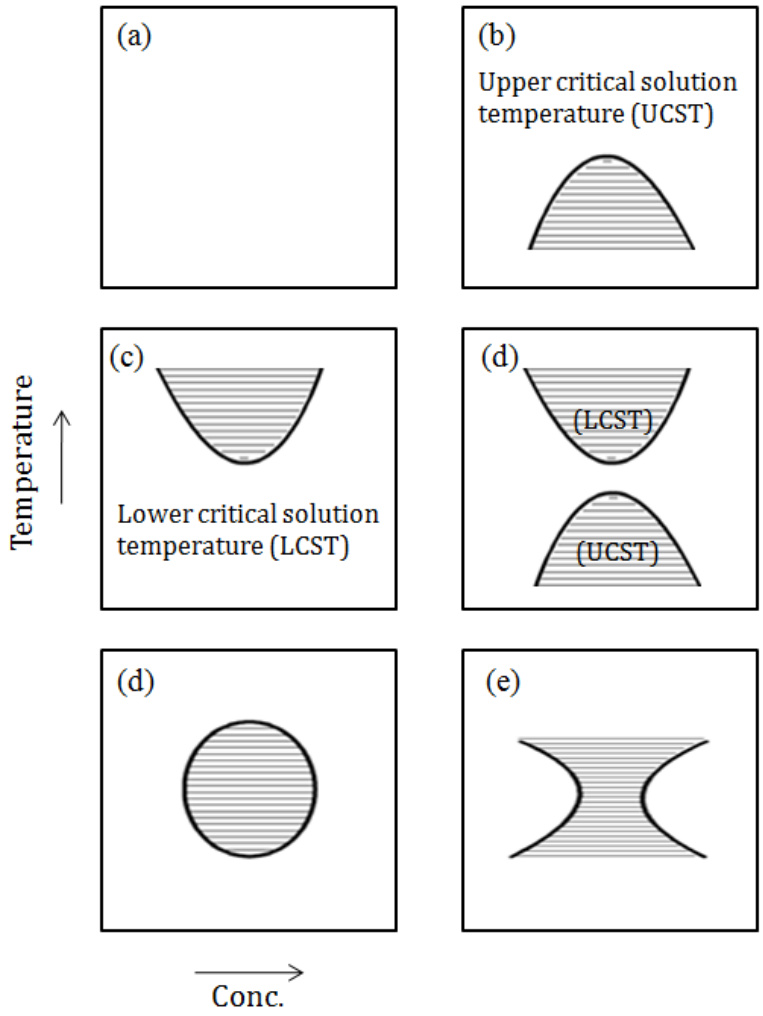

Figure 2-9. Schematic representation of phase behaviours of polymer solution. The shaded areas indicate two-phase region and un-shaded areas indicate one-phase region.[16]

Schematic of T-x (Temperature - Concentration) phase diagrams of semi-crystalline polymers in solution are shown in Fig.2-10.

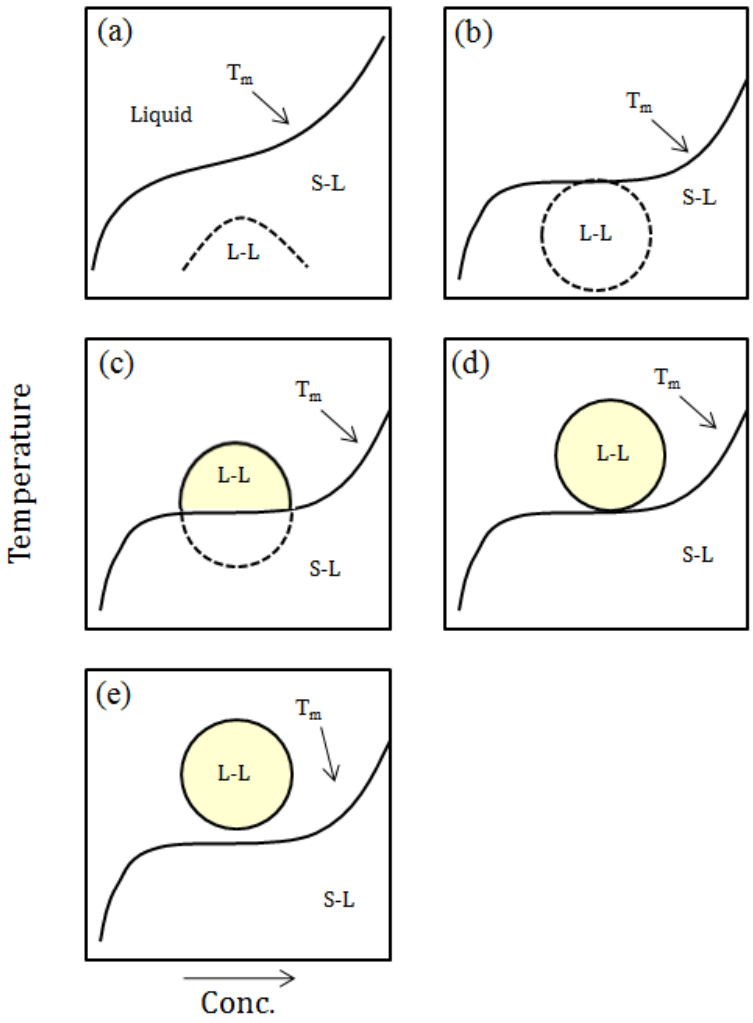

Figure 2-10. Phase diagrams showing the interference of liquid-liquid with solid-liquid phase equilibria (A-E). T_{m2} is the melting temperature of a semi-crystalline polymer and S_2 is crystalline phase.[16,18]

In Fig.2-10a, the liquid-liquid phase boundary is submerged under the solid-liquid phase boundary. As the melting temperature (T_{m2}) of the polymer decreases, the liquid-liquid critical point meets the solid-liquid line (Fig.2-10b). As T_{m2} moves further down to lower temperatures, the liquid-liquid phase boundary is exposed with UCST type as in Fig.2-10c or with UCST and LCST boundaries as in Fig.2-10d and Fig.2-10e.

2.2.2 Kinetics of phase separation

It is very important to understand both dynamic and thermodynamic aspects of phase separation phenomena. The polymer solution is brought from the stable to metastable region by quenching it and depending on the location where the system brought from in the phase diagram, the phase separation occurs via two different mechanisms: nucleation and growth, or spinodal decomposition.

2.2.2.1 Nucleation and growth mechanism

When a polymer solution is brought from the stable region to metastable region, the system can exist in single phase and that is thermodynamically unstable and undergoes phase separation. Since the free energy change is a local minimum for the above mentioned change, the system is stable to the small concentration, temperature or pressure fluctuations. However, the fluctuation is large enough; the system immediately separates into two-coexisting phases, a polymer-rich and a solvent rich phases. For a system with the overall concentration located on the left side of the phase diagram in Fig.2-9, a polymer rich cluster surrounded by polymer lean region is formed from the bulk phase. This is typical for a liquid-liquid phase separation process. A similar kind of behaviour is also observed in solid-liquid phase separation and the only difference is that, the polymer phase is solidified polymer chains with small portion of solvent molecules. This process is favoured by a decrease in free energy, but between these polymer-rich, polymer-lean and bulk phase surrounded each other and subsequent raise in interfacial energy contributes to the overall free energy change.

The classical nucleation theory assumes for the formation of a spherical cluster with radius R, the free energy change ΔF is given by,

$$\Delta F = - (4\pi/3) R^3 \Delta G + 4\pi R^2 \sigma \qquad \textbf{2.5}$$

Where ΔG is the change in Gibbs free energy and σ is the interfacial energy between polymer-rich phase and their surroundings.[16]

The first term in the equation is proportional to the volume of the new polymer phase while the second term is proportional to its surface area. The classical nucleation theory, which uses the bulk properties of the new phase, solution properties for their surrounding regions and assumes a sharp interface in between. This is illustrated in Fig.2-11, where the newly formed polymer phase with diameter 2R reaches its coexisting concentration c_α with a sharp interface. [16,19]

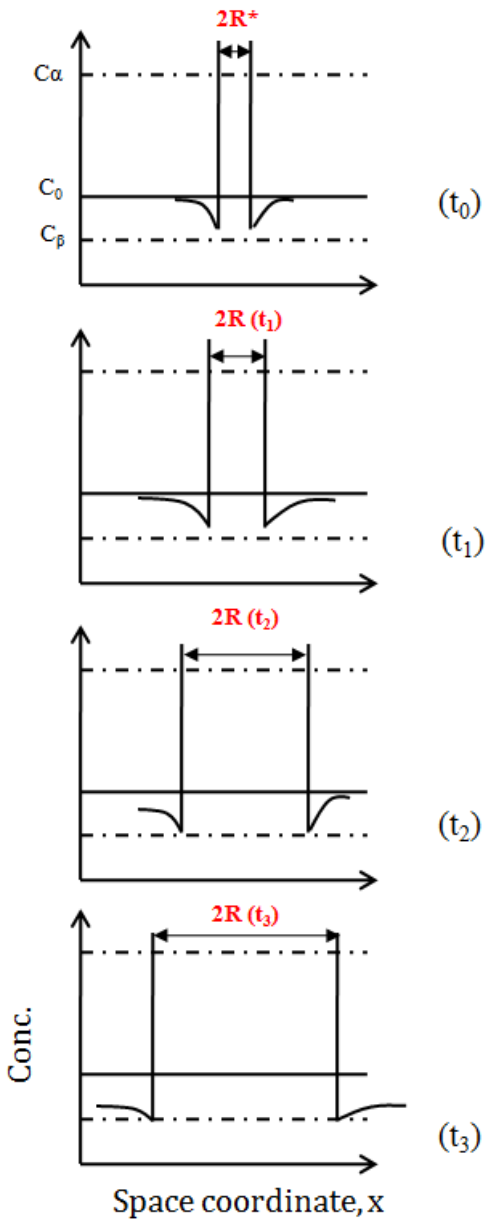

Figure 2-11. Schematic of concentration profile after the system is quenched into unstable region and phase separation occurs via nucleation and growth mechanism. The concentration c(x) is plotted against the spatial coordinate x at time t_0, t_1, t_2 and t_3. The diameter of the critical droplet is shown as 2R*. C_0 is concentration of polymer solution before phase separation while C_α and /C_β are the coexisting concentrations.[16]

The free energy change is sketched in Fig.2-12, as a function of R of the spherical cluster. Here ΔF shows a maximum (ΔF*) at the critical radius R* of the new phase. The clusters that are smaller than R*, re-dissolve back into the solution and larger than R* grow spontaneously. The value of ΔF* and R* can be given by the following expressions,[16]

$$\Delta F^* = (16\pi\sigma^3) / 3\Delta G^2 \qquad \textbf{2.6}$$

$$R^* = 2\sigma / \Delta G \qquad \textbf{2.7}$$

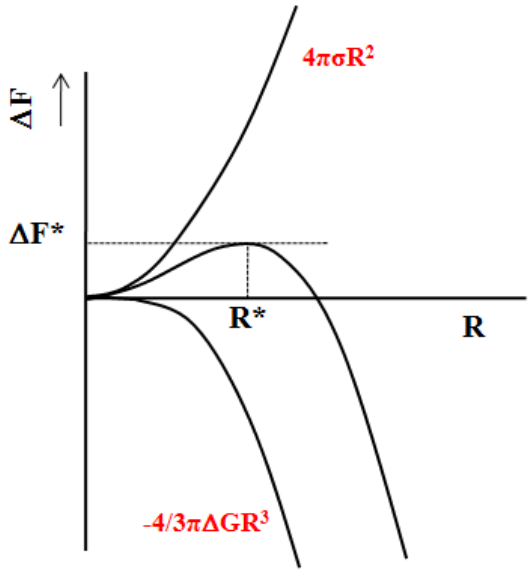

Figure 2-12. Free energy change (ΔF) for the formation of a cluster as a function of cluster radius.[20]

Assuming a steady state and assuming the growth rate is slower than the rate of critical cluster formation, the nucleation rate J is given by,

$$J = J_o \exp(-W^* / kT) \qquad \textbf{2.8}$$

The pre-exponential factor J_o can be related to the mobility of the molecules, surface area of the critical cluster and the total number of the clusters. W* is the work function.

2.2.2.2 Spinodal decomposition

When the system is brought from the stable region to unstable region, the phase separation may proceed by spinodal decomposition mechanism since the energy barrier to form a new phase disappears, and the phase separation takes place spontaneously. In the earlier stage of the spinodal decomposition, the fluctuation wavelength does not change, but the amplitude increases with time. This stage is described by the Cahn-Hilliard theory.[21] The spinodal decomposition mechanism along with concentration profile with time can be depicted as in Fig.2-13.

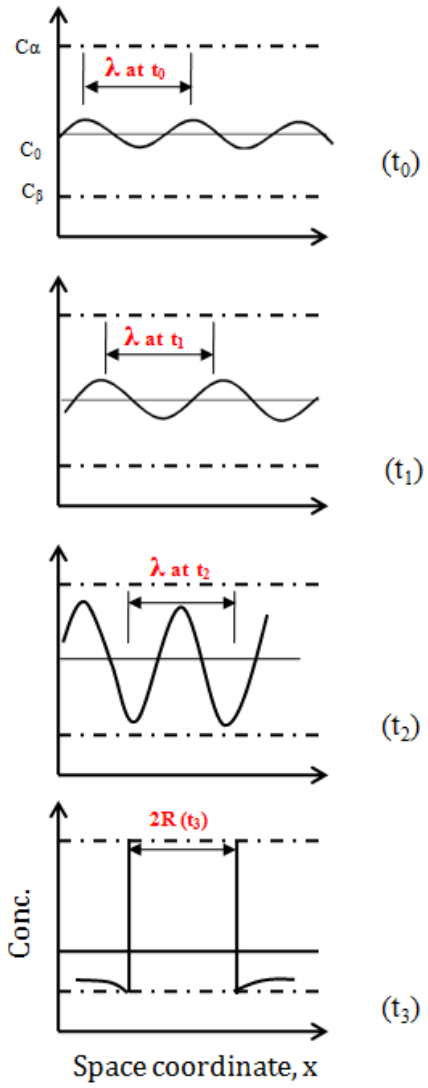

Figure 2-13. Schematic of concentration profile after the system is quenched into the metastable region and phase separation occurs via spinodal decomposition mechanism. The concentration is plotted against the space coordinate x at time t_0, t_1, t_2 and t_3. C_0 is the concentration of polymer solution before phase separation, while C_α and C_β are the coexisting concentrations.[20]

The linearized Cahn-Hilliard theory only works for the very initial stage of the spinodal decomposition. This is because the linearization process neglects short-range interactions and the relationships between the concentration field and other variables. During the intermediate stage of the spinodal decomposition, non-linear effects play even larger roles and in the late stage of the spinodal decomposition, self-similar growth in morphology is observed.[22]

2.2.2.3 Determination of phase boundaries

There are two types of methods used to determine or to map out the phase diagram of a system: analytic method or synthetic method. The first method involves loading of the vessel with the components to be studied, and brings the system to a phase separated state and in equilibrium. A pair of binodal points is determined by measuring the concentration of each phase. This measurement can be done either by sampling and measurement or *in-situ* measurement. The sampling might affect the measurement if the sample is too large compared to the total amount. *In-situ* measurement with spectroscopy can avoid this sampling but it has to be calibrated before the measurement. After the pair of binodal points, the experiment is repeated by changing the external parameters (temperature or pressure) with the concentration, and finally phase diagram can be obtained. The synthetic method is more straightforward, load a vessel with the components with known composition. The phase separation is observed by changing the external conditions. The phase diagram is mapped out with many loadings at different concentrations.

2.2.2.4 Determination of critical and spinodal points

Two approaches are used to determine the critical and spinodal points in phase separation system. One is the extrapolation method based on Debye's scattering theory. Scattered light intensity is recorded as a function of temperature or pressure as the system is brought to the vicinity of the critical point or spinodal line. Then the reciprocal of the scattered light intensity is plotted as a function temperature or pressure and the spinodal temperature or pressure is determined by extrapolation to zero. Then the temperature or pressure at the intercept is determined as critical or the spinodal points.

As a system approaches its critical point, the long-range interactions rise and cause critical opalescence. According to Debye's theory, the scattered light intensity is given by the following equation,

$$I_\theta/I_o = C_\theta [T/(T-T_c)] \qquad \textbf{2.9}$$

Where T_c is the critical temperature and T is the temperature at which the scattering light is measured, C_θ is the instrument constant, I_θ and I_o are the scattered and incident light intensity respectively.

The equation **2.9** suggests that as the temperature approaches critical temperature, the scattered light intensity goes to infinity. The same equation **2.10** can also be applicable spinodal points T_s.[23]

$$I_\theta / I_o = C_\theta [T/(T-T_s)] \quad \textbf{2.10}$$

T_s is the spinodal temperature.

The equation **2.10**, further modified for the systems using pressure as the independent parameter.[24] By replacing the spinodal temperature Ts with spinodal pressure Ps, the equation **2.10** can be rewritten as,

$$I_\theta^{-1} = C''_\theta [(P-Ps/P)] \quad \textbf{2.11}$$

C''_θ is also a constant. From the equations **(2.10)** and **(2.11)**, the spinodal temperature or pressure can be determined from the plot of the inverse of the scattered light intensity as a function of temperature and pressure, when the inverse of the scattered light intensity goes zero.

The other method for the determination of the critical and spinodal points is the quench-induced phase separation method. It utilizes the time evolution of the scattered light intensity after the system is quenched into two-phase region. In the determination of spinodal pressures, a series of fast pressure quenches is applied to the system to bring it from the homogenous region into two phase region. The scattered light intensity evolution with time is then plotted as a function of the end pressure. This method is called multiple rapid pressure drop techniques.

2.2.2.5 Types of polymer phase separation

Phase separation of the polymer solutions can be induced in several different routes.

Thermally induced phase separation (TIPS)

This method is based on the phenomenon that the solubility of the polymer usually decreases when the temperature of the polymer solution is decreased. After the demixing is induced in the polymer solution, the solvent is removed by extraction, evaporation or by freeze drying. The liquid-liquid demixing processes play an important role in most of the TIPS process. In addition, crystallization (or glass transition) of the polymer, gelation, and organization of the components in the system can also occur.

Liquid-Liquid demixing (L-L demixing)

A phase diagram of binary polymer-solvent system is schematically represented in Fig.2-14. At high temperature, the polymer solution is still homogenous and by lowering the temperature, the miscibility gap is induced and phase separation of polymer-rich and lean phase takes place. These systems are characterized by UCST. For entropic reasons, many polymer-solvent systems also phase separate at temperatures close to (or at elevated pressures even higher than) the boiling point of the solvent. These systems are characterized by LCST. Liquid-Liquid demixing is also sometimes induced by heating the polymer solution to make the porous structures.

The boundary of the L-L demixing gap is usually called binodal, but for polydisperse polymers, it is called 'cloud point curve'.

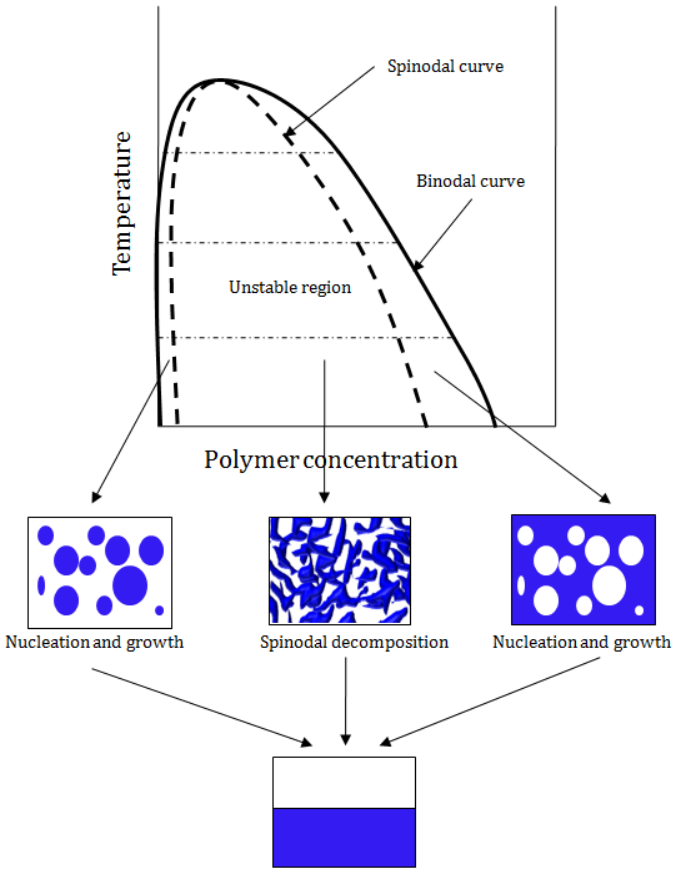

Figure 2-14. Schematic of binary phase diagram of a polymer solution exhibiting a liquid-liquid demixing and the possible structure formation in the different parts of the demixing. Nucleation and growth of polymer-rich phase (left), spinodal decomposition (middle) and nucleation and growth of polymer lean phase (right).[25]

The L-L demixing gap is subdivided into the region of spinodal demixing and the two regions of nucleation and growth. The compositions that are in equilibrium are located on the binodal and are connected by horizontal tie lines. The ratio of the equilibrium phases after the demixing of a polymer solution with a specific composition is described by 'lever rule'. The point where binodal and spinodal point meet called critical point and at the vicinity of this point, the compositions of polymer rich phase and poor phase become more similar. For the monodisperse polymer, this point located at the maximum of the binodal. Depending on the polymer concentration of the solution, the L-L demixing proceeds according to different mechanisms. Composition located between the binodal and spinodal are metastable. This means that the solutions are stable for small fluctuations in the composition. However, L-L demixing occurs when the fluctuation is large enough.[26] The degree of undercooling is necessary to induce the rapid binodal decomposition.[27]

L-L demixing takes place by nucleation and growth of droplets of a polymer lean phase when the composition of the solution is located at the polymer concentrations higher than that of critical point. The demixing also occurs by nucleation and growth of polymer rich phase when the polymer concentration is lower than that of the critical point. Once the droplet has formed and it grows because of the presence of a concentration gradient towards the droplet. Solutions quenched into the area enclosed by spinodal are unstable. All fluctuations in the composition result in decrease in free energy and trigger a wave fluctuation. The spinodal decomposition proceeds via the formation of bicontinous structures. Both polymer rich and lean phase are completely interconnected. As shown in Fig.2-14, the spinodal area can be only entered by critical point. In all other cases, the metastable area must be passed through. High cooling rates can be used to prevent demixing in the metastable area.[28]

The structures shown in Fig.2-14, will eventually coarsen in time and become two separated layers obtained. The driving force behind the coarsening is minimization of the interfacial energy. Two types of coarsening process are known: coalescence and Ostwald ripening. Coalescence results in a decrease in the number of droplets and Ostwald ripening involves the growth of larger droplets at the expense of smaller ones. Ostwald ripening originates from the size dependence of the formed droplets with the local concentration gradient of the solution. In Ostwald ripening, the droplets larger than a certain size only grow further. The coalescence is the dominant coarsening process in L-L demixing. In nucleation and growth, the radius of the polymer poor droplets increases exponentially with time or proportional to time raised to certain power. The growth rate decreases with increasing concentration and decreasing quench temperature. While cooling, the phase separation can occur repeatedly in polymer rich and poor phase that were formed in earlier stages. Structures formed by spinodal decomposition can also coarsen, by the growth of some of polymer domains. The structure formation by spinodal decomposition of polymer solution was elaborately discussed by Caneba et al.[29]

Solid-Liquid phase separation: Crystallization of the polymer

If the polymers consist of the molecular units with sufficient regularity in the chain, then the polymers will be likely to crystallize during phase separation. Depending on the initial concentration of the polymer, the polymer crystallization may result in different morphologies. The final morphology could be precipitates, or various types of interconnecting network structures known as gels. Many factors influence the crystallization of the polymers from the solution.[30] The polymer concentration particularly plays a crucial role in polymer crystallization. The schematic of solid-liquid phase separation of polymer solution is shown in Fig.2-15.

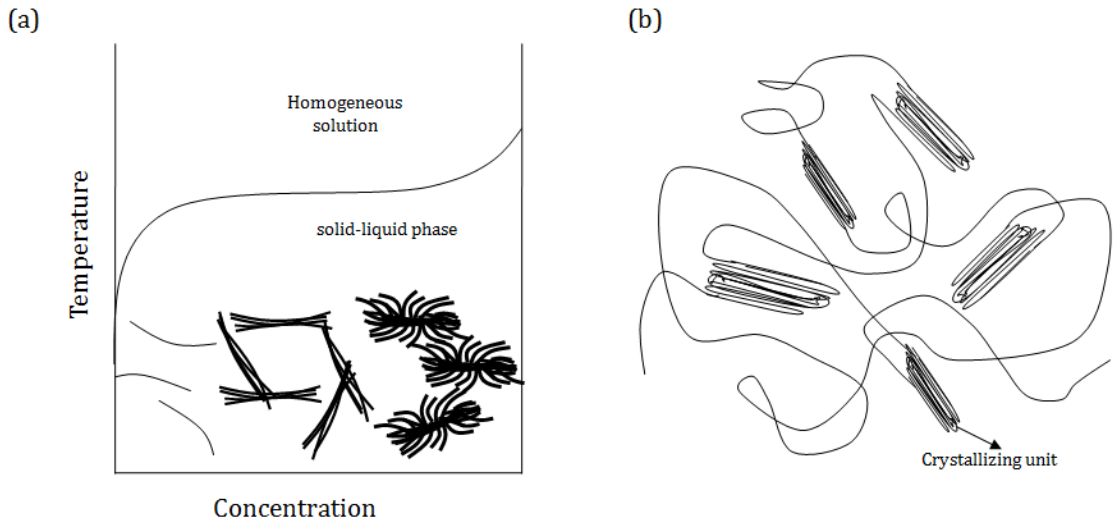

Figure 2-15. Schematic equilibrium phase diagram for solid-liquid phase transition (a) morphologies of polymer obtained by crystallization from the solution. Very low concentrations: single crystals, low concentrations: lamellar stacks, high concentrations: spherulites. (b) Gel structure formed by crystallization.[25]

Crystallization of polymers from much diluted solution results in single crystals whereas from the dilute solution results in lamellae. The morphology of lamellae strongly depends on the characteristics of the polymer and on the conditions of the crystallization. At higher concentrations, suspensions of supra-molecular architectures of the lamellae were obtained.[31]

Kinetic aspects play very important role in the supramolecular organization of the polymer crystals. At sufficiently high concentration, interpenetration and interlocking of these agglomerates of the crystals give raise to highly brittle crystalline gels. Most of the crystalline polymers can form this kind of gels. The size of the polymer crystallites determines whether the gels are transparent or turbid. Highly crystalline polymers will usually give relatively large crystallites and turbid gel. But polymers with low crystalline form transparent gels. The extent of supramoelcular organization decreases with decreasing crystallinity.

It should also be noted that the ultimate morphology of the crystallites also depends on the kinetics of nucleation and growth of the crystallites. Due to the large activation energy barrier for the formation of crystalline nuclei and the limited growth rate, the crystallization curve is situated at much lower temperature than the melting curve obtained by reheating a crystallized solution. But it is difficult to describe when polymers can crystallize into different crystalline morphologies.

2.3 Experimental schemes of fabrication of mesoporous polymers

Materials

Polymers

Polystyrene (M_w 208,000) was purchased from Wako Pure Chemical. Polysulfone (M_w 60,000), polycarbonate (M_w 36,000), polyethersulfone (Melt flow index: 3.98 g/10 min at 320°C), and poly(*p*-phenylene oxide) (M_w 50,000) were purchased from Scientific Polymer Products. Polyetherimide (M_w 30,000) was purchased from Polysciences.

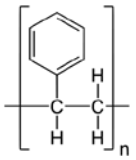

Polystyrene (PS)

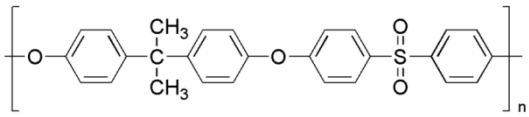

Polysulfone (PSF)

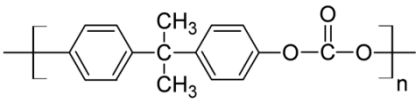

Polycarbonate (PC)

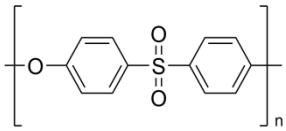

Polyethersulfone (PES)

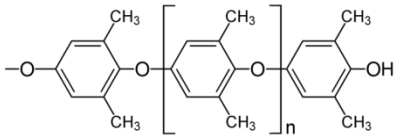

Poly(*p*-phenylene oxide) (PPO)

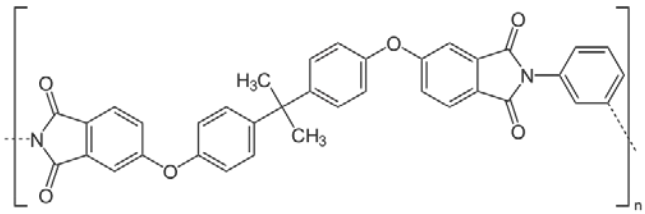

Polyetherimide (PEI)

Solvents

N,N-dimethylformamide (DMF, M_w 73.09, GC purity 99.7%), *o*-dichlorobenzene (DCB, M_w 147.0, GC purity 99%), chloroform (M_w 119.4.09, purity 99%), cyclohexanone (M_w 98.14, GC purity 99%), nitrobenzene (M_w 123.11, GC purity 99.5%), N-methyl-2-pyrrolidone (NMP, M_w 99.13, GC purity 99%), and methanol (M_w 32.04, GC purity 99.8%) were obtained from Kanto Chemical and used without further purification.

2.3.1 Mesoporous polymers as sheet shaped structures

Mesoporous polymers were prepared by using a newly developed nano-crystallization technique in a frozen polymer solution.[32] When the temperature of the polymer solution is rapidly decreased from room temperature to that of liquid N_2, the solvent molecules are frozen among polymer chains. The glassy polymer solution is then slowly heated to a temperature slightly lower than the melting point of the solvent in order to initiate nano-crystallization of the solvent molecules. By extracting the nano-crystallized solvent molecules with a poor solvent (usually methanol), a mesoporous polymer is obtained.

Polymer solutions

PS was dissolved in N,N-dimethylformamide (DMF). PSF solution was prepared by dissolving in *o*-dichlorobenzene (DCB). PC and PPO solutions were prepared with chloroform. PES was dissolved in cyclohexanone, and PEI was dissolved in a 1:1 w/w mixture of nitrobenzene and N-methyl-2-pyrrolidone (NMP). When the dissolution rate of the polymer was not high at room temperature, the solution temperature was gradually elevated to 70 °C, if required. The typical concentration of these polymer solutions was 20 wt%.

Rapid freezing of polymer solution

The prepared polymer solution (10 mL) was applied as a coating to the inner surface of a 100 mL cylindrical glass bottle by rotating horizontally to make a thin layer of the polymer solution. The glass bottle was then immediately immersed into liq. N_2 and allowed to stand for 15 min to make the deep-frozen polymer solution.

Solvent exchange and drying

90 mL of methanol (non-solvent) pre-cooled at −80 °C was added to the above frozen polymer solution, and subsequently transferred to the refrigerator pre-cooled at −80 °C and kept for five days to substitute the solvent with methanol. Then the polymer was brought to room temperature and the methanol was decanted off. The polymer was washed with methanol many times for two days at room temperature. Finally, the methanol was removed completely and dried in a vacuum chamber for 12 h. The experimental scheme of fabrication procedures of mesoporous polymers is shown in Fig.2-16.

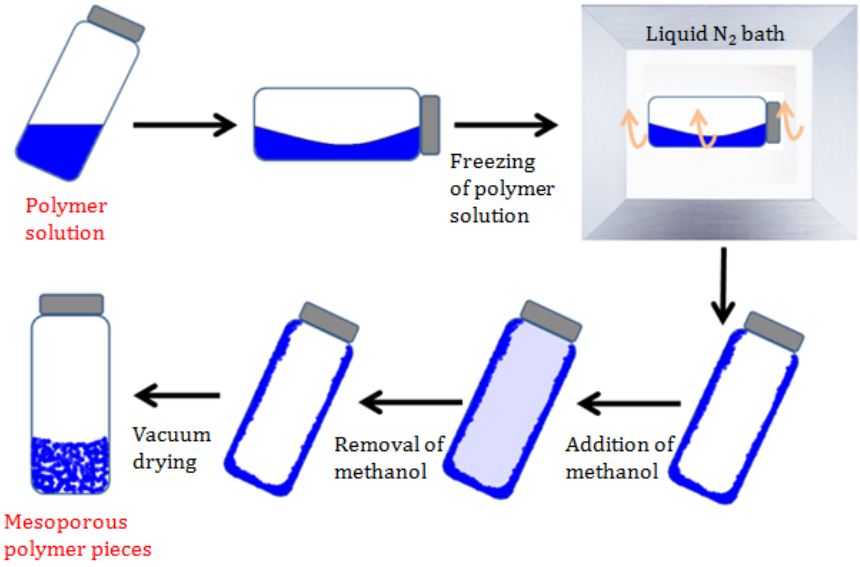

Figure 2-16. Schematic of fabrication of mesoporous polymer.

2.3.2 Mesoporous polymer as macrofibers

The control of material shape in the fabrication of mesoporous polymer is very important in processing the materials in their potential applications. Specific application of mesoporous polymer such as adsorbents highly demands the control of macro geometry in the fabrication processes. Therefore, we fabricated the mesoporous polymers with various shapes.

The fiber fabrication setup of mesoporous polymer is shown in Fig.2-17. The instrument consists of a compressor attached with spinneret, from which the polymer solution is extruded. The overhead motor compress the polymer solution and polymer jet is introduced by spinneret and eventually solidified in the non-solvent bath which is kept in a liq N_2 dewar. The solidified polymer fibers are kept at -80 ^{o}C for solvent exchange for several hours, and then the fibers are vacuum dried.

(a) (b)

Figure 2-17. Optical image of (a) polymer fiber spinning setup and (b) the fabricated mesoporous polymer.[32]

2.3.3 Mesoporous polymer as free-standing membranes

To fabricate mesoporous polymer as a free standing membrane, the polymer solution is firstly spin coated on a silicon substrate and then subjected to low temperature freezing with liq. N_2. The non-solvent exchange is carried out at -80 ^{o}C and the resulting mesoporous polymer membrane is vacuum dried. The experimental scheme and the fabricated mesoporous polysulfone membrane are shown in Fig.2-18.

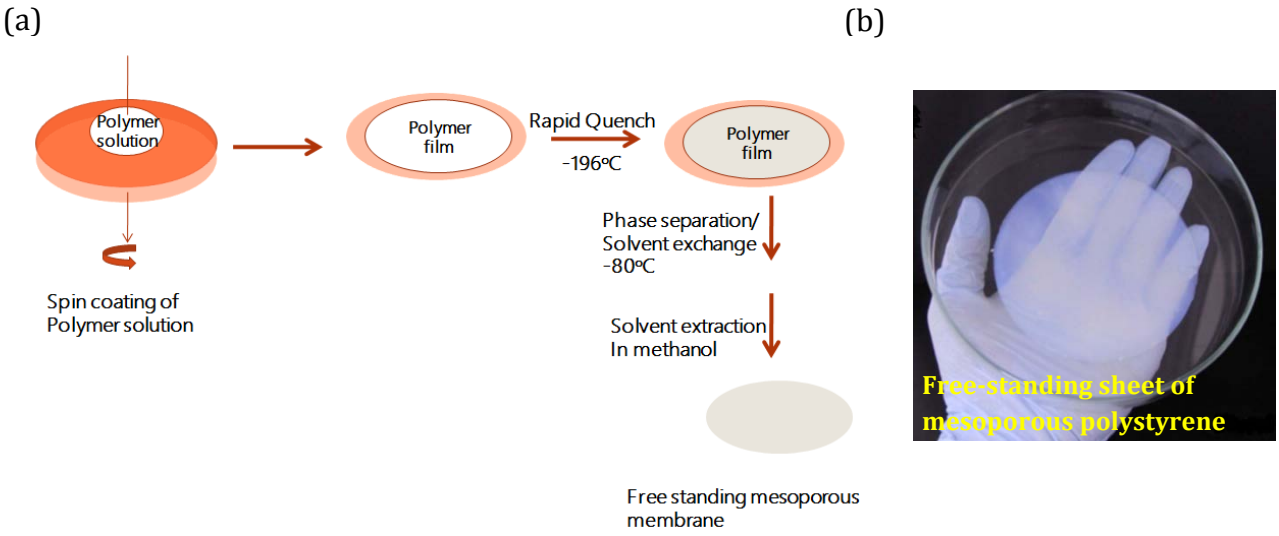

Figure 2-18. (a) Schematic representation of preparation of free-standing mesoporous polymer membrane and (b) photo image of fabricated mesoporous polysulfone.[32]

2.4 Characterization mesoporous polymers

The fabricated mesoporous polymers were characterized by BET isotherm and SEM observation. The isotherm indicated the large increase in the surface area of the fabricated structures than that of reported macroporous polymers and SEM images revealed the interconnected mesoporous structures.

2.4.1. Scanning electron microscopy

Scanning electron microscopy (SEM) images of the mesoporous polymers were obtained using a Hitachi S-4800 (Fig.2-19a). To prepare the specimens, the vacuum-dried sample was immersed into ethanol to remove air inside the mesopores. Then the sample was broken in liquid N_2 to analyze the cross-section. This freeze-fracturing was essential to prevent the elongation of the mesoporous structure. The specimen was attached to an SEM sample holder and a 2 nm thick platinum layer was deposited using a Hitachi E-1030 ion sputter (Fig. 2-19b), in order to prevent electric charging of the specimen. The deposition was conducted at room temperature under an argon atmosphere of 10 Pa or lower and at a current density of 10 mA. All images were obtained at accelerating voltages of 5 kV or 10 kV.

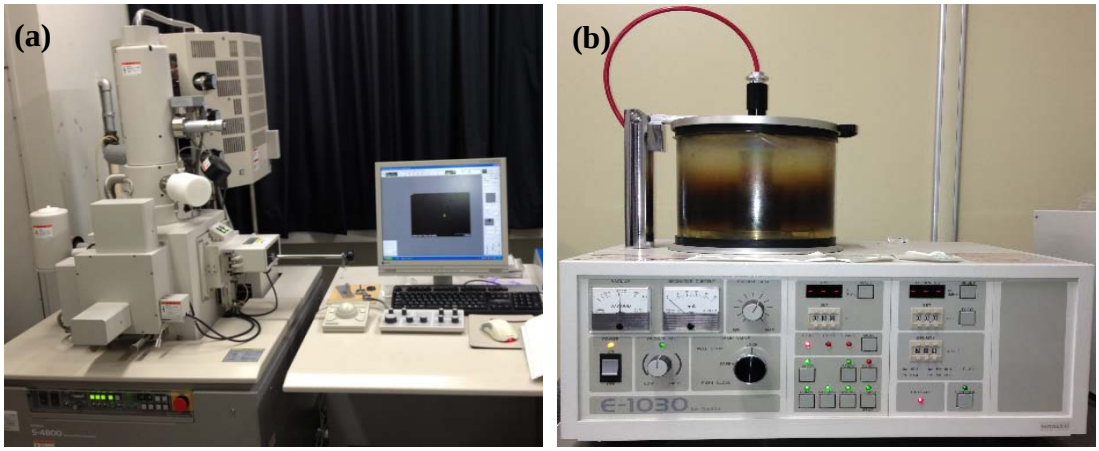

Figure 2-19. Appearance of (a) Hitachi S-4800 scanning electron microscope and (b) Hitachi E-1030 ion sputterer.

2.4.2 BET isotherm and BJH analysis

The specific surface area of the mesoporous polymers were analyzed based on N_2 gas adsorption isotherms. The measurements were conducted using a BEL Japan Belsorp max instrument. The mesoporous polymers were thoroughly degassed under high vacuum and injected into the sample port. The specific surface area was determined by means of the BET model from the low-pressure regions ($p/p_0 < 0.3$) of the N_2 adsorption isotherms. The photo image of the BELSORP-HP instrument is shown in Fig.2-20.

Figure 2-20. Appereance of BELSOR-HP pore analyzer instrument

The Barrett–Joyner–Halenda (BJH) model, which employs the Young–Laplace equation for the capillary condensation of N_2, was used to determine the pore size distribution from the isotherm at higher pressures ($p/p_0 > 0.3$).

2.5 Results and discussion

2.5.1 Concept of flash freezing of polymer solutions

During fabrication of the mesoporous polymer, a concentrated polymer solution (10–40 wt%) is first frozen using liq. N_2 (−196 °C). The solvent molecules are subsequently converted to a glassy state between the entangled polymer chains. In the second step, the temperature is slowly increased to induce the cold crystallization of the frozen solvent molecules. During this crystallization process, the polymer chains are expelled from solvent nano-crystals, producing a polymer network structure, which effectively suppresses further growth of the solvent nano-crystals. Finally, extracting the nano-crystallized solvent using a non-solvent at low temperature, mesoporous polymers were obtained. The concept of flash freezing of polymer solution in a typical polymer-solvent phase diagram is shown in Fig.2-21.

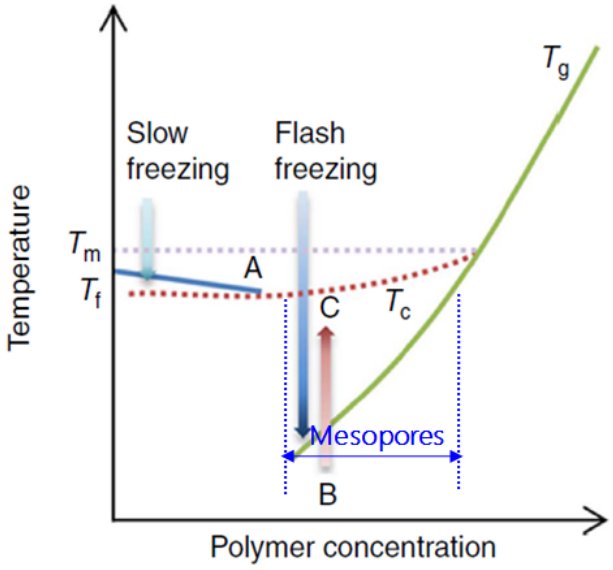

Figure 2-21. Schematic phase diagram of flash freezing phase separation and the range to the formation of mesoporous polymer.[32]

Macroporous polymers can be prepared by crystallizing solvents in the liquid state, in which the growth of macro solvent crystals causes the frozen solution to take on a white, opaque appearance.[33] In contrast, the rapid freezing in liq. N_2, used in our process generates transparent frozen solutions, indicating that macrocrystals are not formed over the entire sample. The stepwise phase transition of polymer solution in fabricating mesoporous mesoporous polymer is schematically represented in Fig.2-22.

Differential scanning calorimetry (DSC) additionally revealed that the solvent molecules were glassified during cooling (Fig.2-23). To quantitatively evaluate the nano-crystallization of solvents, we performed DSC measurements at elevated temperatures. As the temperature was increased, the DSC curve of a frozen dimethylformamide (DMF) solution of 20 wt% polystyrene (PS) showed a baseline shift at −136 °C, followed by an exothermic peak (T_c) at −105 °C and an endothermic peak (T_m) at−61 °C. The baseline shift indicates a transition of the solvent molecules from the glassy state to an extremely super-cooled liquid (or a more liquid-like glass) state, while the two peaks demonstrate that nano-crystallization of DMF and melting of the nano-crystals occur. The enthalpy associated with nano-crystallization (H_c, 57.0 J/g) was similar to that of melting (H_m, 56.0 J/g), indicating that all the solvent molecules crystallized at the elevated temperature. The observed enthalpy of melting (H_m) of DMF nano-crystals in a PS nanofiber network was 83 % that of pure DMF crystals reported in the database.

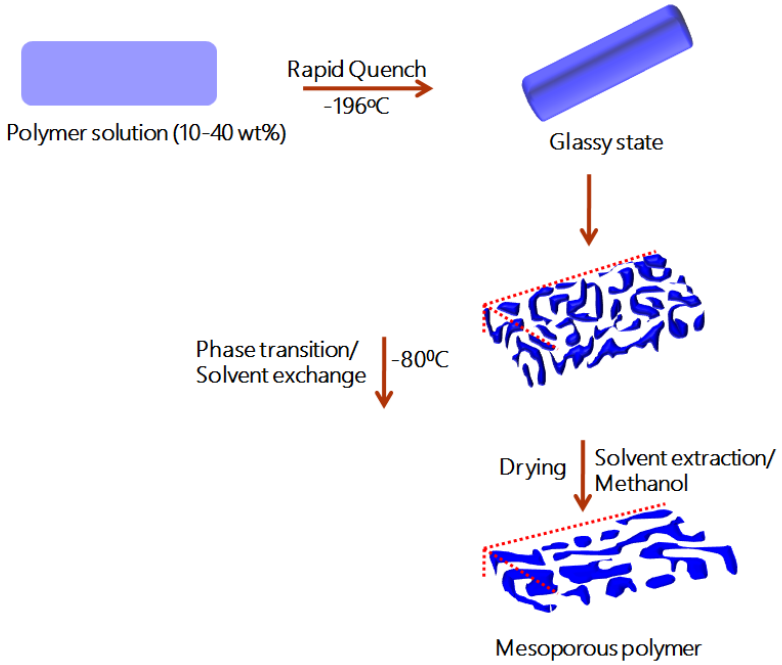

Figure 2-22. Schematic representation of the fabrication of the mesoporous polymer by flash freezing technique.

Mesoporous polystyrene was obtained after extracting the nano-crystallized solvent with methanol at –80 °C. Scanning electron microscopy (SEM) cross sections revealed uniform mesoporous morphology free of macrovoids (Fig.2-24). As seen in the high magnification image, the specimens consist of highly branched fibers connected with one another forming mesopores. The diameter distribution of these nanofibers was analyzed based on more than 1000 points in SEM images and then Gaussian fitting gave an average diameter of 17.6 ± 5.6 nm, assuming that the nanofibers have circular cross sections. Mesoporous structure was much finer when polystyrene concentration was 40 %wt. The Brunauer–Emmett–Teller (BET) model was

used for the analysis of N_2 adsorption isotherms at low pressures ($p/p0 < 0.3$). The BET surface areas of the fabricated mesoporous polymers are also shown in Fig.2-24.

2.5.2 Control over mesoporous structure. A key factor in achieving a mesoporous structure is attaining cold crystallization near T_g. When the temperature of the polymer solution is slowly decreased, the solvent crystallizes at a temperature slightly below its melting point (T_m). But flash freezing of polymer solution results in vitrification without allowing solvent crystallization. When the temperature is then slowly increased, cold crystallization (essentially phase separation in the frozen state) is induced. This crystallization process, however, results in an increase of the polymer concentration forming a glassy polymer-rich phase and further solvent crystallization is then restricted. Regardless the types of solvent, solvent crystallization always results in the formation of several micrometer-sized pores and thus, to ensure the selective formation of mesopores, the polymer solution should be rapidly quenched to below the T_g line.

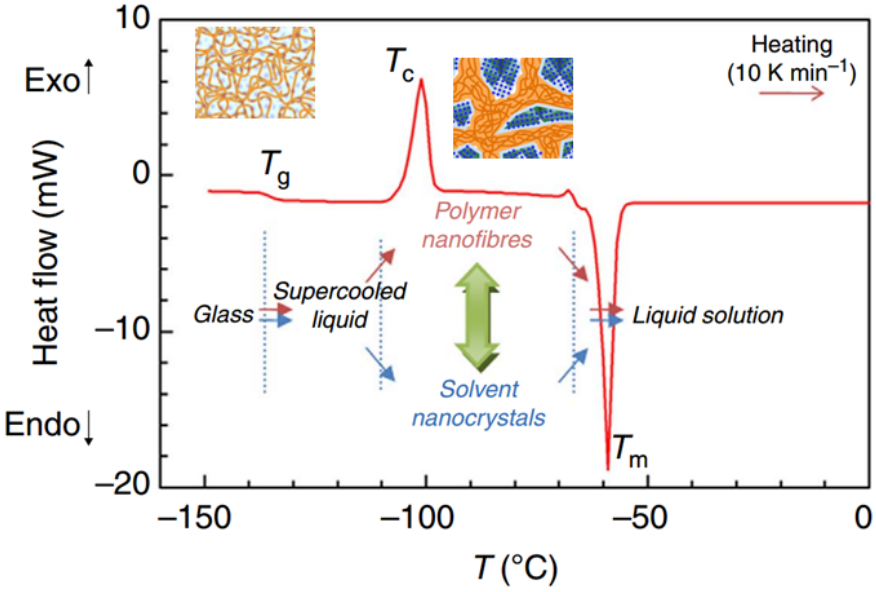

Figure 2-23. Differential scanning calorimetry (DSC) of polystyrene/DMF describing the nano-crystallization of DMF and eventual phase separation polystyrene.[32]

Nano crystallization of solvent molecules in the frozen state is very slow, and so the solution temperature must be maintained below the melting point of the solvent for several hours. We also found that, over certain ranges of concentration and temperature, a bi-continuous mesoporous structures composed of polymer nanofibers form. This finding may be the most important extension of the basic principles of thermally-induced phase separation since Castro A. proposed the process in the late 1970s.[14]

The mesopores decrease in size with increasing concentrations of the polymer solution likely due to the strong steric hindrance of the polymer network. In general, mesopores smaller than 5 nm in radius readily extinguished under the effects of the strong Laplace force and therefore we believe that pores prepared by flash freezing route is the smallest which polystyrene, with a T_g of approximately 100 °C, can achieve. The cross-sectional SEM images and their corresponding surface area of mesoporous polymers fabricated by flash freezing route are given in Fig.2-24.

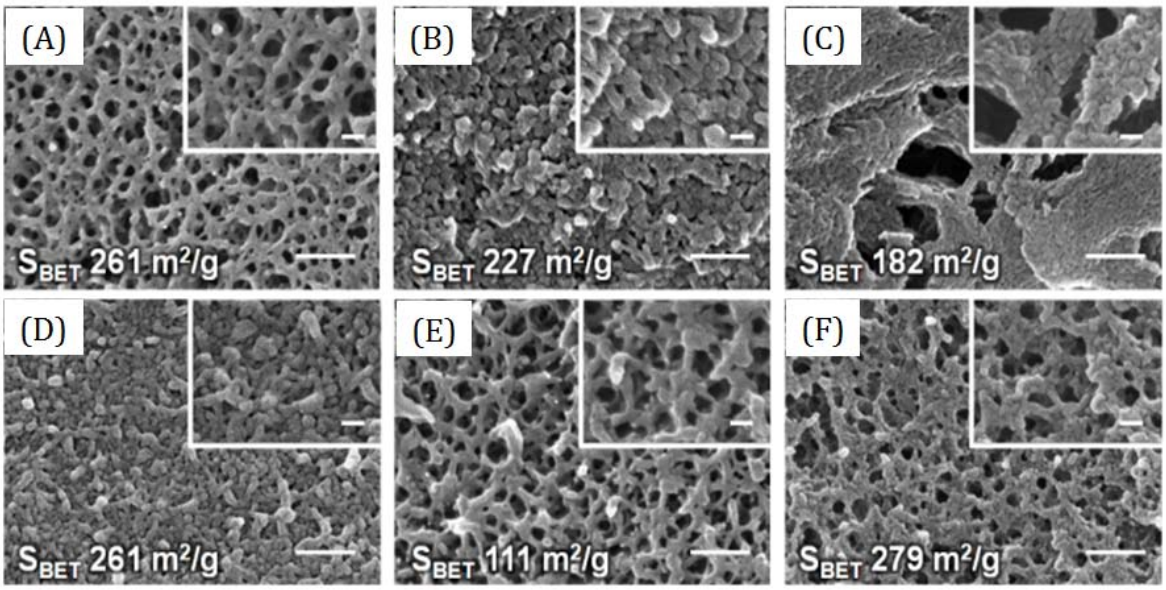

Figure 2-24. SEM images of mesoporous polymers. (A) Polystyrene, (B) polysulfone, (C) polycarbonate, (D) polyethersulfone, (E) poly(*p*-phenylene oxide) and (F) polyetherimide. The scale bars are 200 nm (inset: 50 nm). The corresponding specific surface area of the mesoporous polymers was given therein.

The BET specific surface area of the mesoporous polymers can be calculated from their N_2 adsorption/desorption isotherms. The N_2 isotherms of mesoporous polystyrene are given in Fig.2-25(a). The pore size distributions of the mesoporous polystyrene by BJH analysis is shown in Fig.2-25(b). The average pore radii of the mesoporous polymers were not exceeding 10 nm in both analyses of adsorption (red) and desorption (blue) curves. The polymer nanofiber diameter were statically analysed in SEM images (Fig.2-25(c)) and the diameter distribution is given in Fig.2-25(d). The average nanofiber diameter was found to be 18 nm. The initial concentration of the polymer in the solution plays a key role in controlling the size of the solvent crystals during the phase separation process in nano-crystallization phase separation technique. The effect of polymer concentration on pore size distribution and average pore size of the final mesoporous polystyrene is given in Fig.2-26. With increase in the polymer concentration (10 wt% to 40 wt %), the pore size distribution becoming narrower and the average pore size is observed to be much smaller.

This serves as the clear evidence of increased control over the size of the solvent crystals during the phase separation in case of the high concentrated polymer solution in comparison with relatively lower concentration.

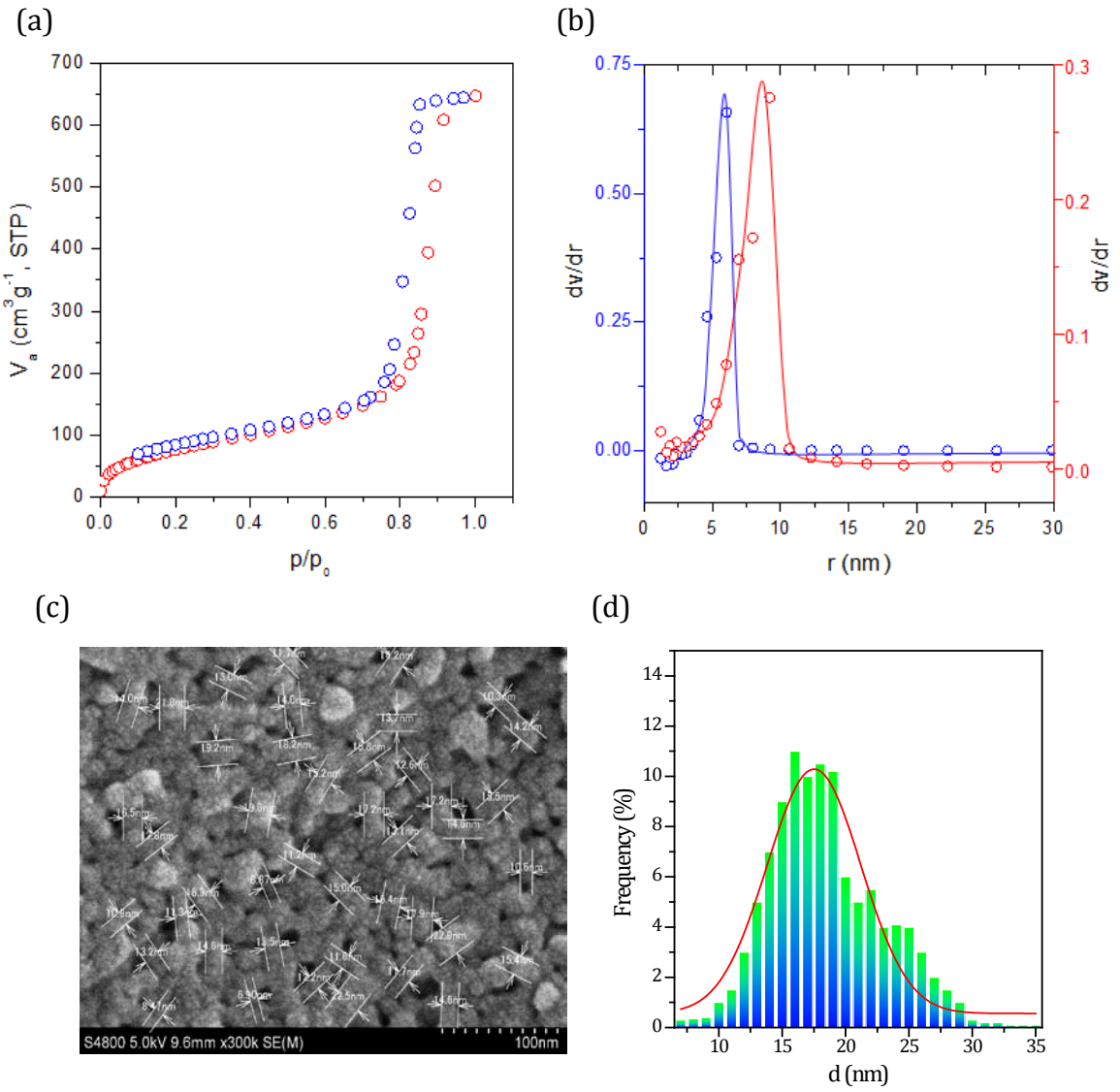

Figure 2-25. (a) N_2 adsorption/desorption isotherms of mesoporous polystyrene, (b) pore size distribution calculated from the isotherms by using BJH analysis, (c) SEM image of mesoporous polystyrene nanofiber network, and (d) its nanofiber diameter histogram.

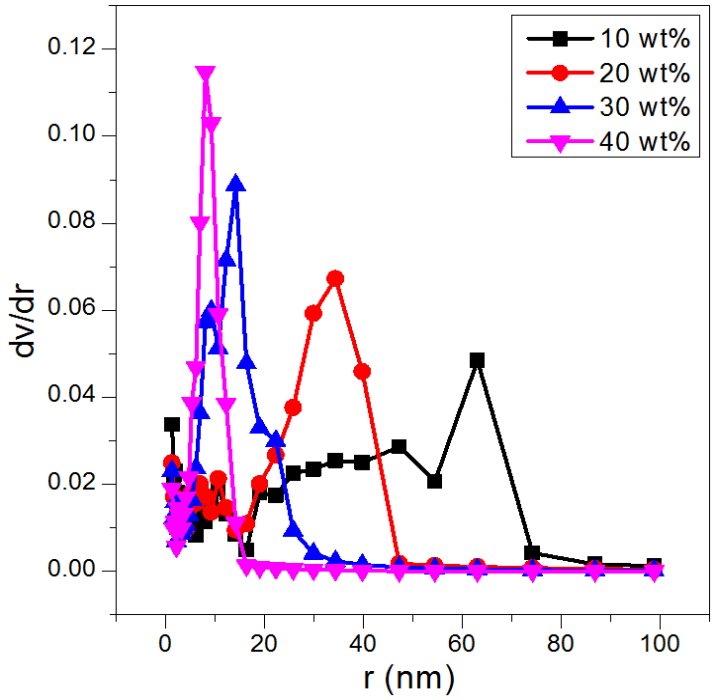

Figure 2-26. Effect of polymer concentration on pore size distribution and average pore size of the mesoporous polystyrene fabricated by nano-crystallization phase separation technique.

The different types of polymers can also be fabricated as macrofibers having cross sectional morphology of mesoporous structure. Polystyrene, polysulfone and polycarbonate are the polymers successfully fabricated as macrofibers with the mesoporous morphology. The prepared polystyrene macrofibers and their corresponding cross-sectional morphology are shown in Fig.2-27. The diameter of the macrofiber can be controlled by using pore diameter of the spinneret of the fiber spinning instrument (Fig.2-17). The fabricated polystyrene macrofiber has highly interconnected nanofiber internal structure and the diameter of the nanofiber of polystyrene was about 20,000 times smaller than that of the macrofiber. Owing to its small diameter of interconnected nanofiber structure, the specific surface area of the mesoporous polystyrene has been largely increased to 280 m^2/g. This low temperature freezing of polymer along with its solvent molecules and by consequent solvent exchange will be the easy and convenient technique to prepare nanofiber network materials with controlled macrofiber geometry. The polymers can also be fabricated as free standing membranes or thin films with internal nanofiber network structure. The polymer solution is firstly spin-coated as a thin film and then subjected to flash freezing fabrication technique. The free-standing polysulfone nanofibre network membrane has been shown in Fig.2-18.

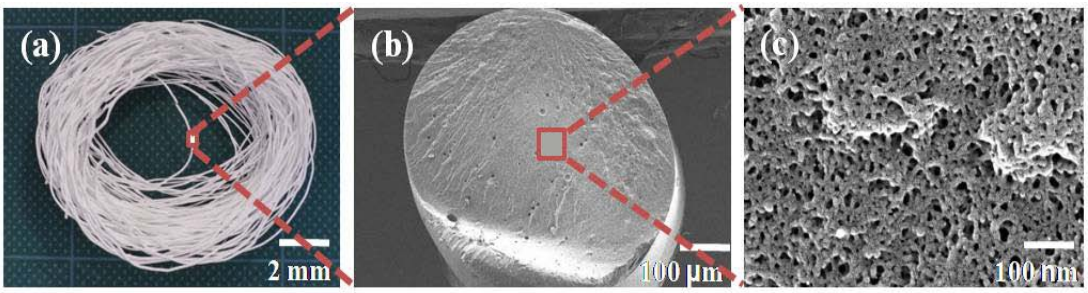

Figure 2-27. (a) Photo image of polystyrene macrofiber, (b) SEM image of cross section of polystyrene macrofiber, and (c) its high magnified image.

Flash freezing route appears to be very close to the freeze-drying method that is commonly used to prepare the tissue engineering scaffolds.[34] However, these conventional preparatory methods have some practical difficulties. To form solvent nano-crystals, the solvent needs to have crystallization temperature near T_g of polymer solution, which usually appears at low temperature. However, the nano-crystals formed at low temperature are very hard to be removed by vacuum techniques. On the other hand, the solvents with relatively high crystallization temperature can be readily removed by vacuum process. Note that sublimation rate becomes high with increasing melting temperature of the solvent. But such solvents cannot form the nano-crystals at experimentally achievable cooling rate. The advantage of solvent extraction in flash freezing route is that the extraction rate is high even at the temperature of –80 °C. Because of the high specific surface area and percolating pores, these materials exhibited a variety of interesting separation properties (Chapter 4).

2.6 References

[1] (a) V. Thavasi, G. Singh and S. Ramakrishna, *Energy. Environ. Sci.*, 1, 205 (2008).

(b) H.Y. Chung , *US patent,* 6743243B2, (2004).

(c) R. S. Barhate and S. Ramakrishna, *J. Membr. Sci.*, 296, 1 (2007).

(d) J. O'Grady, A. Losikoff, J. Poiley, D. Fickett and C. Oliver, *Dev. Biol. Stand*., 88, 319 (1996).

[2] (a) J. Huang , S. Virji , B. H. Weiller and R. B. Kaner, *J. Am. Chem. Soc*., 125, 314 (2003).

(b) J. Huang, S. Virji, B. H Weiller and R. B. Kaner, *Chem. Eur. J,* 10, 1314 (2004).

[3] (a) A. N. Aleshin, *Adv. Mater*., 18, 17 (2006).

(b) Y. Z. Longa, M. M. Li, C. Gub, M. Wanc, J. L. Duvaild, Z. Liue and Z. Fan, *Prog. Polym. Sci*., 36, 1415 (2011).

[4] (a) B. C. Kim, S. Nair, J. Kim, J. H. Wak, J. W. Grate, S. H. Kim and M. B. Gu1, *Nanotechnology*, 16, 382 (2005).

(b) F. Xu, M. Hui, X. Shili, S. Mingwu, G. Rui, C. Xueyan and S. Xiangyang, *J. Mater. Chem*., 21, 4493 (2001).

[5] (a) Z. M. Huanga, Y. Z. Zhang, M. Kotaki and S. Ramakrishna, *Comp. Sci. Technol.*, 63, 2223 (2003).

(b) Q. P. Pham, U. Sharma and A. G. Mikos, *Tissue Engineering*, 12, 1196 (2006).

(c) J. Venugopal and S. Ramakrishna, *Appl. Biochem. Biotech.*, 125, 147 (2005).

(d) Y. Z. Zhang C. T. Limi, S. Ramakrishna and Z. M. Huang, *J. Mater. Sci: Mater. Med.*, 16, 933 (2005).

(e) L. J. Lee, *Ann .Biomed. Eng.*, 34, 75 (2006).

[6] (a) P. X. Ma, *Adv. Drug. Deli. Rev.*, 60, 184 (2008).

(b) L. A. Smith and P. X. Ma, *Colloids and Surfaces B: Biointerfaces*, 39, 125 (2004).

(c) P. X. Ma, *Materials Today*, 7, 30 (2004).

[7] A. S. Zalusky, R. Olayo-Valles, C. J. Taylor and M. A. Hillmyer, *J. Am. Chem. Soc*., 123, 1519 (2001).

[8] K-V. Pinemann, V. Abetz and P. F. W. Simon, *Nature Materials*, 6, 992 (2007).

[9] B. Krause, H. J. P. Sijbesma, P. Münüklü, N. F. A. van der Vegt and M. Wessling, *Macromolecules*, 34, 8792 (2001).

[10] (a) V. Beachely and X. Wen, *Progress in Polymer Science,* 35, 868 (2010).

(b) P. X. Ma and R. Zhang, *J. Biomed.Mater.Res.part A*, 46, 60 (1999).

[11] K. Okada, M. Nandi, J. Maruyama, T. Oka, T. Tsujimoto, K. Kondoh and H. Uyama, *Chem. Commun*., 47, 7422 (2011).

[12] (a) P. J. Flory, Thermodynamics of high polymer solutions, *J. Chem. Phy*., 9, 660 (1941).

(b) M. L. Huggins, Solution of long-chain compounds, *J. Chem. Phy*., 9, 440 (1941).

[13] S. Leob and S. Sourirajan, Sea water demineralization by means of an osmatic membrane, *Adv. Chem*., 38, 117 (1963).

[14] A. Castro, *U.S. Patent*, 4247498 (1981).

[15] L. V. Zhigilei, Introduction to materials science, Chapter 9, Univeristy of Virginia (Course material).

[16] (a) L. A. Utracki, in Interpenetrating polymer networks by L. H. Klempner and L. A. Utracki. (Eds.) Chapter 3, 239, 77.

(b) W. Zhang, Phase behavior and phase separation kinetics in polymer solutions under high pressure, Chapter 2 (Thesis submitted to Virginia Polytechnic Institute and State University).

[17] M. Luszczyk, L. P. N. Rebelo and W. A. Van Hook, *Macromolecules*, 28, 745 (1995).

[18] R. Koningsveld, W. H Stockmayer and E. Nies, Polymer Phase Diagrams: A Textbook, Oxford Press (2001).

[19] (a) T. Hashimoto, M. Itakura and N. Shimidzu, *J. Chem. Phys*., 85, 6773 (1986).

(b) K. Binder, P. Fratzl, Spinodal Decomposition. In G. Kostorz. (Eds), Phase Transformations in Materials, Weinheim: Wiley-VCH, 410 (2001).

[20] R. Wagner, R. Kampmann and P. W. Voorhees, Homogeneous Second-Phase Precipitation. G. Kostorz. (Eds.), Phase Transformations in Materials,Weinheim: Wiley-VCH. 309 (2002).

[21] (a) J. D. Gunton, M. S. Miguel and P. S. Sahni, The Dynamics of First Order Phase Transitions. In C. Domb, J. L. Lebowitz (Eds), Phase Transitions and Critical Phenomena, London, San Diego, New York: Academic Press, 8, 267 (1987).

(b) J. D. Gunton, *J. Stat. Phys.*, 95, 903 (1999).

[22] J. Maguey, T. Van Nuland and P. Navard, *Polymer*, 42, 4353 (2001).

[23] T. G Scholte, *J. Polym. Sci:Part C*, 39, 281(1972).

[24] F. Kiepen and W. Borchard, *Macromolecules*, 21, 1784 (1988).

[25] P. van de Witte, P. J. Dijkstra, J. W. A. van den Berg and J. Feijen, *J. Membr. Sci*., 117, 1 (1996).

[26] (a) K. Binder, Systems Far from Equilibrium Lecture Notes in Physics, 132, 76 (1980).

(b) K. Binder, Spinodal decomposition, in P.Hassen (Eds), *Materials Science Technology*, A comprehensive treatment, VCH, New York, 5, 405 (1991).

(c) J. W. Cahn, Spinodal decomposition, *Trans. Metall.Soc*. AIME, 242, 166 (1968).

[27] A. Ronner, S. G Wassink and C. A Smolders, *J. Membr. Sci.*, 42, 27 (1989).

[28] (a) F. J. Tsait and J. M Torkelson, *Macromolecules*, 23, 4983 (1990).

(b) F. J. Tsait and J. M. Torkelson, *Macromolecules*, 23, 775 (1990).

[29] G. T Caneba and T. S Soong, *Macromolecules*, 18, 2545 (1985).

[30] L. Mandelkern, C. Booth and C. Price (Eds), *Comprehensive Polymer Science*, 2, 363 (1989).

[31] A. Prasad, H. Marand and L. Mandelkern, *J. Poly. Sci., Part B: Poly. Phy. Ed.*, 32, 1819 (1993).

[32] S. Samitsu, R. Zhang, X. Peng, M. R. Krishnan, Y. Fujii and I. Ichinose, *Nature Communications*, 4, 2653 (2013).

[33] H. Zhang et al. *Nature Materials*, 4, 787 (2005).

[34] M. C. Gutiérrez, M. L. Ferrer and F. del Monte, *Chem. Mater.*, 20, 634 (2008).

Chapter 3

Selective surface modification of mesoporous polymers

3.1 Sulfonation of mesoporous polymers

The polymers which are most commonly used in several industrial applications are inherently hydrophobic. The surface modification generally performed to the polymer if the surface properties of the polymer do not suit the desired application. The selective introduction of hydrophilic functionality to the surface extends the application of hydrophobic polymers to aqueous solutions. After the modification, the surface should carry the new functionalities while the bulk properties and the original morphology remain unchanged. In this chapter, we mainly focus on the surface modification of mesoporous polystyrene because this is the polymer quite frequently used in industries due to its low cost and easy processing. The surface modification of polystyrene by high-energy irradiation is well known in the literature. For instance, UV and γ irradiation,[1] plasma treatment,[2] and glow discharge are the mostly used dry methodologies for surface modifications. The major disadvantage of this high-energy irradiation methodology is that the degradation of polymer surfaces occurs therein. Wet surface modification processes of polystyrene surface have also been extensively reported in literature.[3]

The polystyrene was, probably first sulfonated in a homogenous phase by a method developed by Turbak.[4] This method involves the reaction of polystyrene with triethyl phosphate complexes and sulfur trioxide in dichloroethane. The lightly sulfonated polystyrene is prepared by reacting with acetyl sulphate complexes in dichloroethane.[5] In the following years, various preparatory methods for the sulfonation of polystyrene have been reported with different sulfonating agents includes silver sulphate,[6] acyl sulphate,[7] and sulfur trioxide complexes. Heterogeneous sulfonation, i.e solid-liquid or solid-gas sulfonation, is a yet another advantageous technology for selective surface modification of polymers. The successful heterogeneous phase sulfonation of porous polystyrene and polystyrene beads with SO_3 was conducted by Kucera et al.[8] Various sulfonation conditions and different sulfonating agents to polymers are also reviewed by Kucera et al.[9]

We studied the sulfonation of mesoporous polystyrene surfaces with two distinct sulfonating agents which are chlorosulfonic acid and conc. sulfuric acid. The sulfonated polystyrene has been characterized for limited solubility in water and its original morphology is kept.

3.2 Experimental procedures

Materials and Methods

Mesoporous polymers, chlorosulfonic acid (Wako, 97% + Ti), sulfuric acid (Kanto chemical 96% GC purity), ethanol (Wako, 99.5% GC purity) and anhydrous methanol (Wako) were used without any further purification.

1 g of the mesoporous polystyrene was cut into pieces and added to 10 ml of ethanol to remove air inside the pores. After decanting ethanol, 3 ml of chlorosulfonic acid (Scheme 1) or 5 ml of conc. H_2SO_4 (Scheme 2) was added to the polymer. In all the sulfonation experiments, the sulfonating agents are kept in large excess to avoid any heterogeneity in sulfonation procedure.

3.2.1 Sulfonation with chlorosulfonic acid (scheme 1)

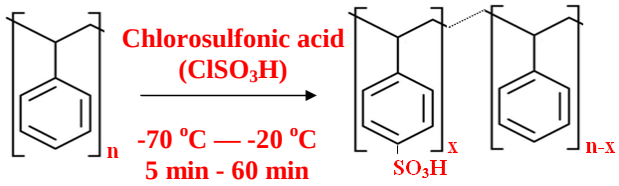

The mesoporous polystyrene samples were treated with excess chlorosulfonic acid in 9 cc closed glass bottles. The sulfonation time was varied from 5 to 60 min and the reaction temperatures varied from -70 °C to -20 °C. After the reaction of mesoporous polystyrene with chlorosulfonic acid at desired temperature, the samples were removed from the acid and subsequently washed in anhydrous methanol several times followed by DI water until the pH of the washed water was around 6. This washing process involves removing the excess chlorosulfonic acid adhered on the surface of the polystyrene. After several cycles of anhydrous methanol washing, the samples were vacuum dried. The experimental scheme is shown in Scheme 1.

3.2.2 Sulfonation with conc. sulfuric acid (scheme 2)

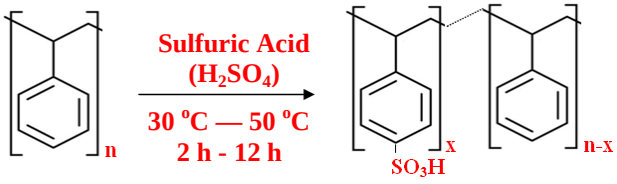

The mesoporous polystyrene samples were also treated with excess conc. H_2SO_4 in 9 cc closed glass bottles. The sulfonation time was varied from 2 h to 12 h and the temperatures were from 30 °C to 50 °C. After the reaction of mesoporous polystyrene with sulfuric acid at desired reaction time and temperature, the samples were removed from the acid and subsequently

washed in anhydrous methanol several times followed by DI water until the pH of the washed water was around 6. This ensures the complete removal of excess sulfuric acid from the polymer samples. After several cycles of anhydrous methanol and DI water washing, the samples were vacuum dried. This experimental procedure is given in scheme 2.

Sulfonation of the other mesoporous polymers

Sulfonation of mesoporous polycarbonate (PC) was carried out using sulfuric acid acetyl ester produced from acetic anhydride (3 mL) and conc. H_2SO_4 (1 mL) in methanol (16 mL). But the sulfonation of polysulfone (PSF) was not achieved with either conc. H_2SO_4 or sulfuric acid acetyl ester. Therefore, mesoporous polysulfone was sulfonated using 0.3 mL of chlorosulfuric acid (Wako, 97% grade) in *n*-hexane (7 mL). Caution: The chlorosulfonic acid reacts violently with water to yield sulfuric acid and HCl. Mesoporous polyphenyleneoxide (PPO) was sulfonated with freshly prepared sulfuric acid acetyl ester, whereas mesoporous polyethersulfone (PES) was sulfonated with chlorosulfonic acid using similar procedures. Through this controlled sulfonation of mesoporous polymers were made the polymers sufficiently hydrophilic to quickly absorb water.[10]

3.3 Ion exchange capacity of sulfonated mesoporous polystyrene

Back titration method

The ion exchange capacity (IEC) of a sulfonated polymer is defined as the number of replaceable H^+ ions. This IEC value of the sulfonated polymer is directly related to the extent of substitution of sulfonic acid groups. When the sulfonated polymer was added to dilute NaCl solution, Na^+ ion replaces the H^+ ion from the introduced sulfonic acid group (SO_3H) onto the polymer surface. If the replaced H^+ ion is back titrated with diluted NaOH solution, we can estimate the ion exchange capacity (IEC) of the sulfonated polymer.

100 mg of sulfonated polystyrene was treated with 10 ml of 1M NaCl solution in 50 cc glass bottle and the solution stirred for 24 h. Then polymer is removed from the NaCl solution and the solution was titrated with 0.1M NaOH solution by using a pH meter. From the required titration volume, the IEC can be determined. The scheme of IEC determination by back titration is represented as follows:

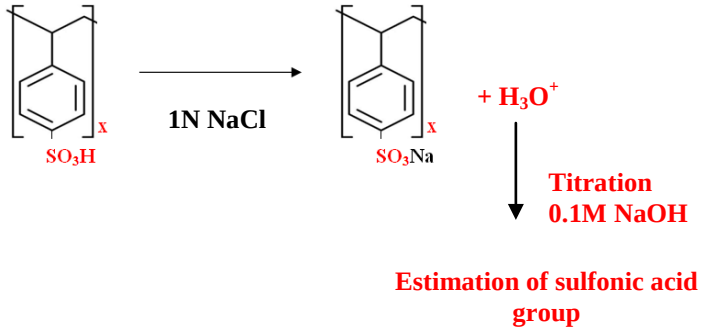

From the back titration, the ion exchange capacity value can be calculated from the following expression,

$$IEC = \frac{[Vol\ of\ NaOH\ (ml) \times Con\ of\ NaOH\ (M)]}{Weight\ of\ dried\ polymer\ \ (g)} \qquad \textbf{3.1}$$

From the IEC value, other characteristic parameters can also be determined by following mathematical expressions (3.2 – 3.4),

Degree of substitution (DS) is the average number of substituted sulfonic acid group per monomer. In the case of sulfonated polystyrene,

$$DS = \frac{104 \times IEC}{1000 + (104 \times IEC) - (184 \times IEC)} \qquad \textbf{3.2}$$

The number of substituted SO_3^-,

$$N_{SO_3^-} = \text{IEC (mmol/g)} \times N_A \text{ (mol}^{-1}\text{)} \qquad \textbf{3.3}$$

The equivalent weight of R-SO_3H is the equivalent weight of polymer per mole of SO_3H substitution,

$$E_w = 1 / (\text{IEC} \times 10^{-3}) \qquad \textbf{3.4}$$

Scanning electron microscopy

The structure of sulfonated mesoporous polystyrene was characterized by SEM observations. The SEM images revealed the changes in interconnected mesoporous polystyrene structure from the original morphology. All SEM images of the original mesoporous polymer were recorded using a Hitachi S-4800. The vacuum dried sulfonated mesoporous polystyrene was firstly added with excess of ethanol for the removal of air inside the pores. Then the samples are broken in liquid N_2 and the cross-section of the samples analyzed with a scanning electron microscope. The samples were broken in liquid N_2 to avoid any surface plasticization or elongation frequently caused at room temperature.

SEM observations were conducted after depositing about 2 nm thick platinum layer (deposition time 20-30 s) by using a Hitachi E-1030 ion sputter in order to prevent charging of the specimens. The deposition was conducted at room temperature under an Ar atmosphere of 10 Pa or lower. The current density for the deposition was 10 mA. The deposition did not have any effect on the film morphology. All images were captured at the accelerating voltages of 5 kV or 10 kV.

Dye adsorption

The positively charged dyes were allowed to adsorb on the sulfonated mesoporous polystyrene to understand the homogeneity of the sulfonation of the mesoporous polymer. Methylene Blue (MB) was used as characterizing dye for the sulfonated mesoporous polystyrene. The positively

charged (cationic) segment of this dye chemically forms an ionic complex with an anionic sulfonic acid group of partially sulfonated mesoporous polystyrene and eventually the sulfonated polystyrene surface carries the characteristic colour of the corresponding dye. The colour contrast was carefully observed by high resolution optical microscope to understand the homogenous sulfonation.

In a typical dye adsorption experiment, 100 mg of sulfonated mesoporous polystyrene was taken in a 10 cc glass bottle. 5 ml of 0.01 mM MB solution was added to the sulfonated polystyrene sample at ambient conditions. The dye solution was treated about 60 min approximately. Then the sample was removed from the solution and washed, dried and analysed.

3.4 Results and discussion

The treatment of sulfonating agents like chlorosulfonic acid or conc. sulfuric acid with mesoporous polystyrene, specifically introduces sulfonic acid (SO_3H) groups to surface phenyl ring of the polymer. The introduction of these sulfonic acid groups on the polymer surface brings hydrophilic nature to the originally hydrophobic polymers. Higher the surface functionality, higher the degree of swelling in water. The degree of sulfonation is directly related to the swelling of individual polymer nanofibers and subsequently the porosity of the mesoporous polystyrene decreased largely at high degree of sulfonation. If the degree of sulfonation is high enough, firstly the polymer swells with water and finally dissolves in water.

The effect of degree of sulfonation on the mesoporous polymer swelling in water is schematically presented in Fig.3-1.

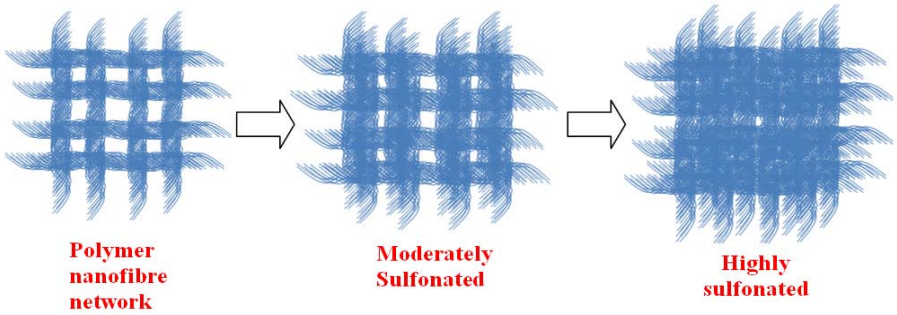

Figure 3-1. Scheme of the effect of degree of sulfonation and resulting mesoporous polystyrene swelling in water.

Sulfonation of mesoporous polystyrene by chlorosulfonic acid

The mesoporous polystyrene has been successfully sulfonated with chlorosulfonic acid at different temperatures. In this synthetic approach, a mild sulfonation conditions by controlling the reaction temperatures were applied. The sulfonic acid groups were introduced in the surface phenyl groups of polystyrene by electrophilic substitution of aromatic group of the polymer. Since mild sulfonation conditions are desired, the reaction was carried out at very low temperatures ranging from -70 ^{o}C to -20 ^{o}C. The mesoporous polystyrene was predominantly homogenously sulfonated on the surface by this sulfonation methodology. In addition to the reaction temperature, the reaction time also plays a crucial role in retaining the mesoporous polystyrene morphology. The reaction kinetics at different temperatures, their corresponding IEC values and the other characteristic sulfonation parameters (DS, Nso_3^- and E_w) are presented in Table 3. The morphology of the sulfonated mesoporous polystyrene has been carefully analyzed by SEM. The cross-sectional SEM images of sulfonated mesoporous polystyrene by chlorosulfonic acid at different temperatures are given in Fig.3-2. The SEM images revealed the retention of sulfonated mesoporous polystyrene morphology by comparing that of original mesoporous polystyrene. At higher temperature, the rate of sulfonation reaction was rapid and it was a large impact on the original mesoporous morphology.

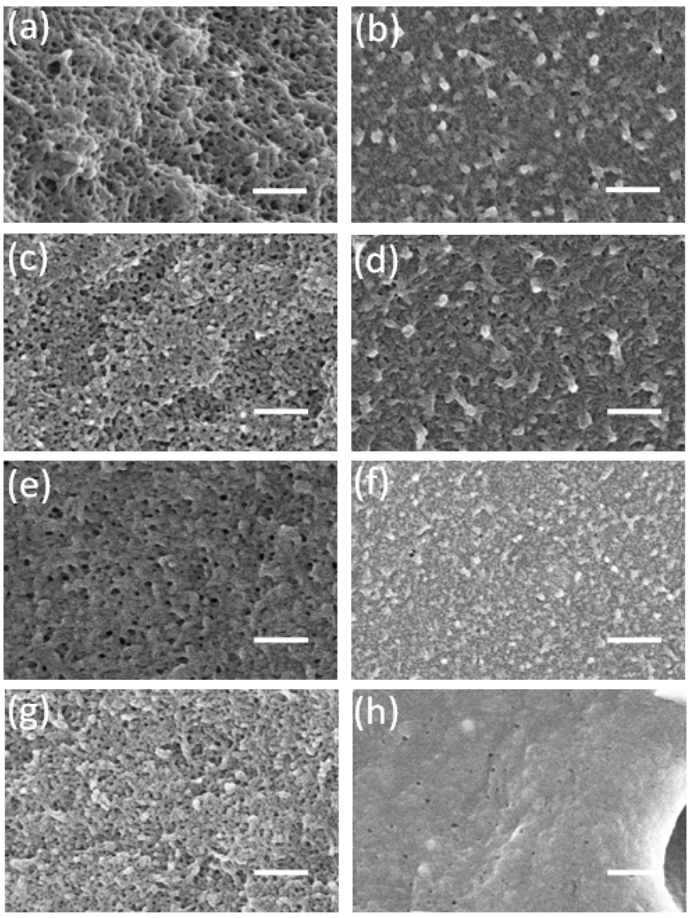

Figure 3-2. Cross-sectional SEM images of sulfonated polystyrene by chlorosulfonic acid at different conditions of (a) at -70 ^{o}C, 5 min; (b) at -70 ^{o}C, 60 min; (c) at -60 ^{o}C, 5 min; (d) at -60 ^{o}C, 60 min; (e) at -40 ^{o}C, 5 min; (f) at -40 ^{o}C, 60 min; (g) at -20 ^{o}C, 5 min; and (f) at -20 ^{o}C, 60 min. The scale bars are 200 nm.

Table 3. Kinetics of sulfonation of mesoporous polystyrene by chlorosulfonic acid at different conditions

Temp (^oC)	Time (min)	IEC (meq/g)	DS	Nso_3^- (10^{18}/g)	E_w (g/meq)
	5	0.09	0.011	0.54	10.9
	10	0.10	0.012	0.62	9.61
-70	15	0.11	0.013	0.65	9.17
	30	0.14	0.017	0.85	7.04
	45	0.17	0.021	1.04	5.74
	60	0.21	0.214	1.28	4.67
	5	0.24	0.029	1.44	4.10
-60	10	0.29	0.035	1.74	3.4
	15	0.33	0.040	1.98	3.0
	30	0.38	0.047	2.28	2.63
	45	0.40	0.049	2.40	2.50
	60	0.48	0.059	2.89	2.0
	5	0.29	0.035	1.74	3.44
	10	0.31	0.038	1.86	3.22
-40	15	0.34	0.041	2.04	2.94
	30	0.50	0.060	3.01	2.00
	45	0.66	0.080	3.97	1.51
	60	0.83	0.100	4.99	1.20
	5	0.97	0.120	5.84	1.03
	10	1.00	0.130	6.02	1.00
-20	15	1.07	0.131	6.06	0.99
	30	1.10	0.145	6.64	0.90
	45	1.20	0.159	7.22	0.83
	60	1.31	0.175	7.90	0.76

Sulfonation of mesoporous polystyrene by conc. H_2SO_4

Controlled sulfonation of mesoporous polystyrene can also be achieved by treating with sulfuric acid at different temperatures and reaction times. The sulfonic acid groups were introduced in the surface phenyl group of mesoporous polystyrene by electrophilic substitution. This sulfonation reaction with conc. sulfuric acid is kinetically very slow at room temperature. Therefore, the reaction was carried out at relatively higher temperatures from 30 ^{o}C to 50 ^{o}C. In this methodology, the polystyrene will predominantly be homogenously sulfonated on the surface.

The sulfonation kinetics at different temperatures with their corresponding IEC values along with other characteristic sulfonation parameters (DS, Nso_3^- and E_w) is presented in Table 4. The morphology of the sulfonated mesoporous polystyrene has been carefully analyzed by SEM technique. The cross-sectional SEM images of sulfonated polystyrene by sulfuric acid at different temperatures are given in Fig.3-3. The SEM images revealed the retention of sulfonated mesoporous polystyrene morphology by comparing that of original mesoporous polystyrene, except the sulfonation at 50 ^{o}C for 8 h. When increase the reaction temperature, the rate of sulfonation reaction was found to be relatively higher and still kept the original morphology. Prolonged treatments with sulfuric acid will eventually result in either partial or complete loss of nanofibre morphology. Fabricated polystyrene completely lost its mesoporous polystyrene morphology when it is treated with sulfuric acid at 50 ^{o}C and for about 8 h. In all other experimental conditions we carried out, the mesoporous polystyrene morphology is kept. All the sulfonated sample surfaces by sulfuric acid were completely wettable in water and had good contact to the water whereas the original polystyrene has no contact to water.

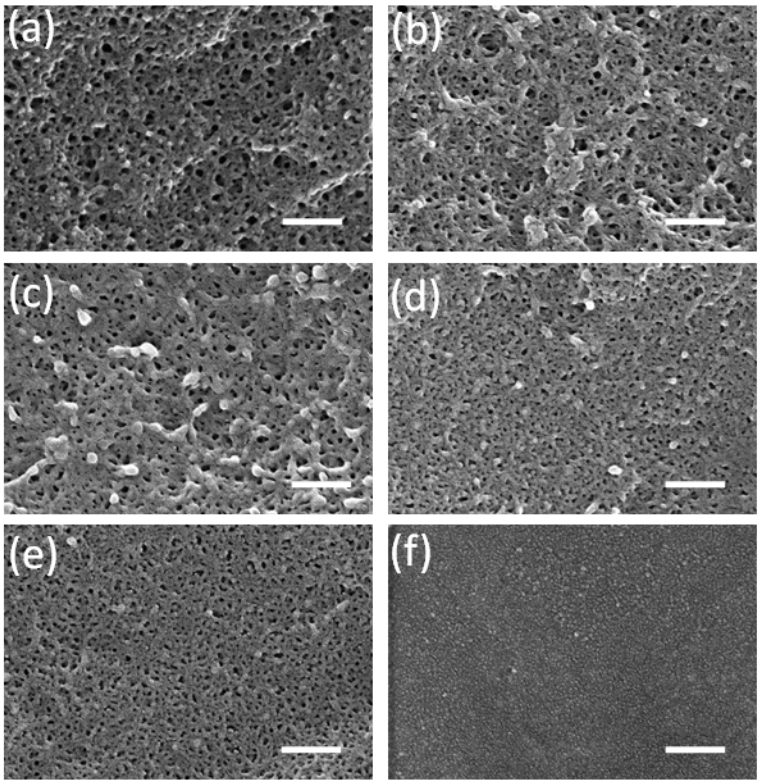

Figure 3-3. Cross-sectional SEM images of sulfonated polystyrene by conc. H_2SO_4 acid at different conditions (a) at 30 ^oC, 2 h; (b) at 30 ^oC, 12 h; and (c) at 40 ^oC, 2 h; (d) at 40 ^oC, 12 h; (e) at 50 ^oC, 2 h and (f) at 50 ^oC, 8 h. The scale bars are 200 nm.

Table 4. Kinetics of sulfonation of mesoporous polystyrene by conc. H_2SO_4 at different conditions

Temp (^oC)	Time (h)	IEC (meq/g)	DS (10^{-3})	Nso_3^- (10^{18}/g)	E_w (g/meq)
30	2	0.011	1.15	6.63	90.9
	4	0.013	1.35	7.83	76.9
	6	0.016	1.67	9.64	62.5
	8	0.020	2.08	12.0	50.0
	12	0.024	2.50	14.5	41.7
40	2	0.019	1.98	11.4	52.6
	4	0.023	2.40	13.9	43.5
	6	0.027	2.81	16.3	37.0
	8	0.030	3.13	18.1	33.3
	12	0.040	4.17	24.1	25.0
50	2	0.034	3.55	20.5	29.4
	4	0.040	4.17	24.1	25.0
	6	0.046	4.80	27.7	21.7
	8	0.053	5.54	31.9	18.9
	12	0.063	6.59	37.9	15.8

3.4.1 FT-IR characterization of sulfonation reactions

The surface sulfonated mesoporous polystyrene was characterized by FT-IR measurements. The initial sulfonation reaction was successfully monitored based on the increase of the FT-IR peak at 1010 cm^{-1} which is attributed to in plane deformation of the sulfonated benzene ring (*v2* in Fig.3-4c).

3.4.2 Dye adsorption of sulfonated mesoporous polystyrene

The sulfonated mesoporous polystyrene was characterized by positively charged dye adsorption technique. Some typical dyes have strong absorption of visible light and have characteristic colours. The positively charged dyes are allowed to adsorb to the sulfonated mesoporous polystyrene to understand the homogeneity of sulfonation on the polymer surface. The positively charged (cationic) segment of the dyes chemically forms an ionic complex with the sulfonic anion of partially sulfonated mesoporous polystyrene and eventually the sulfonated polystyrene surface carries the characteristic colour of the corresponding dyes. Methylene blue (MB) was used as characterizing dyes for the sulfonated mesoporous polystyrene. The colour contrast on

the surface of the polymer has been carefully observed by high resolution optical microscope to understand the homogenous sulfonation.

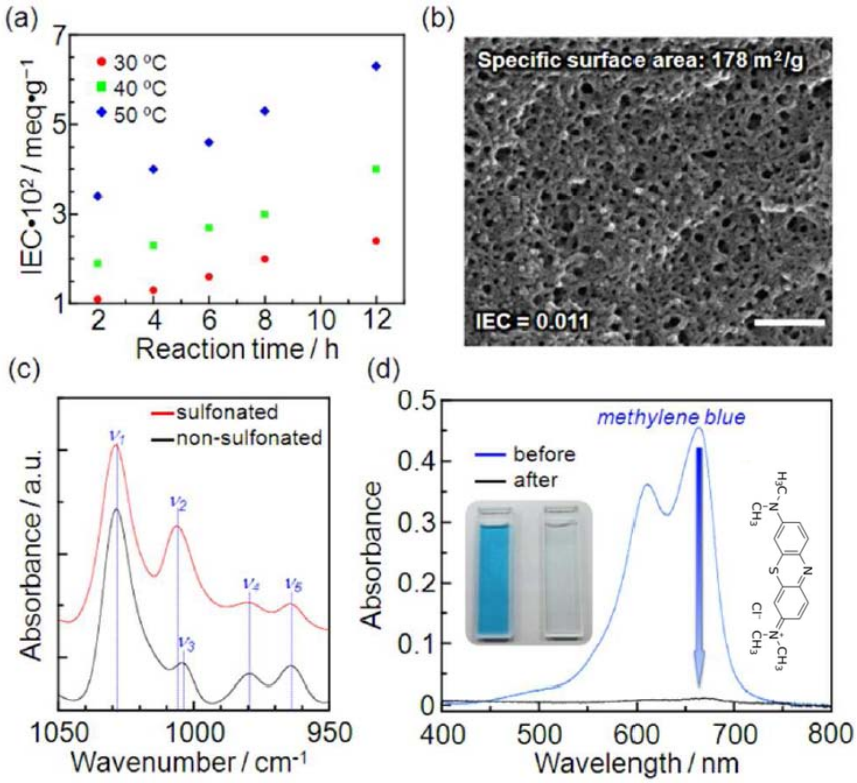

Figure 3-4. (a) Increase in ion exchange capacity (ICE) with reaction time. (b) Cross-sectional SEM image of sulfonated mesoporous PS. The scale bar is 200 nm. (c) FT-IR spectra of mesoporous PS and sulfonated mesoporous PS (30 °C, 2 h). (d) UV-vis absorption spectra of methylene blue (MB) solution (5 mL) before and after treatment with the sulfonated mesoporous PS. Initial concentration: 0.01 mM (pH 7.0). The inset shows a photographic image of the dye solutions and structure of MB dye.

The dye adsorption scheme of mesoporous sulfonated polymer is given as follows,

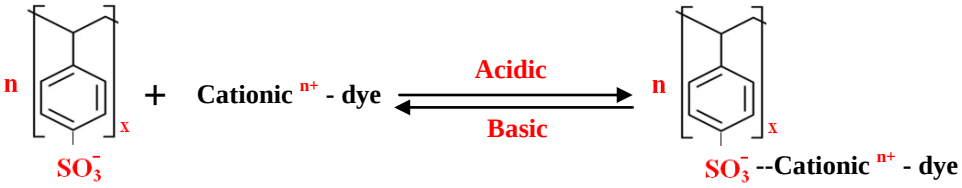

The stronger electrostatic interaction of cationic segment of dye and anionic segment of the sulfonated polymer facilitates rapid dye adsorption from aqueous solution. When the sulfonated mesoporous polystyrene is added to a typical dye solution, it adsorbs the dye equivalent to the degree of substitution during sulfonation of that polymer and leaves behind the excess dye in the solution. The measurement of initial and final visible spectra of dye solution signifies the amount of sulfonation (surface modification) on mesoporous polystyrene surfaces. The rate of dye adsorption was highly dependent on the initial concentration of the dye solution, amount of the sulfonated mesoporous polystyrene used and the degree of sulfonation in the typical sulfonated sample used. The Methylene Blue (MB) dye adsorption behaviour of sulfonated mesoporous polystyrene is shown in Fig.3-4d as an example.

3.5 References

[1]E. C. Onyiriuka, *J. Appl. Poly. Sci.*, 47, 2187 (1993).

[2] (a) E. C. Onyiriuka, L. S. Hersh and W. Hertal, *J. Colloid. Interface. Sci.*, 144, 98 (1991).

(b) S. B. Idage and S. Badrinarayanan, *Langmuir*, 14, 2780 (1998).

[3] (a) B. S. Rao, J. B. Puschett and K. Matiyjaszeski, *J. Appl. Poly. Sci.*, 43, 925 (1997).

(b) Y. Feng, A. Karim, R. A. Weiss J. F. Douglas and C. C. Han, *Macromolecules*, 31, 484 (1998).

(c) H. W. Gibson and F. C. Baily, *Macromolecules*, 13, 34 (1980).

[4] A. F. Turbak, *Ind. Eng. Chem, Prod. Res. Rev.*, 1, 275 (1962).

[5] H. S. Makowski, *U.S patent application* 3,870,841 (1975).

[6] H. Wink, *Macromol. Chem.*, 182, 279 (1981).

[7] W. A. Thaler, *Macromolecules*, 16, 623 (1983).

[8] F. Kucera and J. Jancar, *Chem. Papers*, 50, 224 (1996).

[9] F. Kucera and J. Jancar, *Poly. Engg. Sci*., 38, 783 (1998).

[10] B. Smitha, S. Sridhar and A. A. Khan, *J. Membr. Sci.*, 225, 63 (2003).

Chapter 4

Solid phase extraction of organic compounds from aqueous solutions

Solid phase extraction (SPE) is an efficient purification technique for the removal of highly toxic organic compounds dissolved in water. The presence of organic compounds in waste water causes severe environmental problems. It originates from sewage, urban run-off, industrial effluent and agricultural waste. The *in-situ* decomposition of such organic compounds is quite often used in order to purify the contaminated water. But it could cause a severe depletion of dissolved oxygen in the treated water and eventually replenished. A number of alternative methods such as coagulation, filtration with coagulation, precipitation ozonation, ion exchange and reverse osmosis techniques are employed for the purification of water. These methods have often been found to be highly limited, since they involve high capital and operational costs.

Among the possible techniques for water treatment, adsorption by suitable solid adsorbents is prominent as it is one of the most efficient ways to treat the organic compounds that contaminate water. Adsorption has the advantage over the other methods because of the simple design and also low investment. In recent days, the search for low-cost adsorbents with high binding capacities has been intensified. The solid phase extraction technique dates back to 1960s, and it is very popular for sample preparation followed by chromatographic analysis.[1] But since then there has been a constant demand of SPE adsorbent with improved analyte recoveries, sorptive capacity, selectivity and stability. The search for the new material seems to be a never-ending task as the current efforts are at finding an optimum adsorbent for specific applications.

The major criteria in the search of effective adsorbents are,

- Developing high capacity adsorbent even for the trace analysis of organic compounds
- Specificity and selectivity
- Considerable adsorption

Over the years, considerable progress has been made in the development of new materials for SPE.[2] But the development of SPE materials in the optimized configuration has been very slow. Therefore, research on alternative adsorbent fabrication technique is also equally important in the complete development of SPE technique. The SPE adsorbent fabrication technique should offer a structure which can be chemically and/or morphologically modified. And also an optimal SPE sorbent material combines the benefits of,

(i) High surface area

(ii) Simplified fabrication

(iii) Ability to be modified to carry desired functionalities

In order to understand the SPE technique, it is highly necessary to understand the fundamentals of adsorption phenomenon.

4.1 Fundamentals of adsorption

4.1.1 General definition of adsorption

Adsorption is a process in which a substance (in gas or liquid phase) excessively accumulates on a solid surface. The porous solids in which the adsorbates are retained are known as adsorbents. This adsorption phenomenon is based on the capability of the porous material with large surface area to retain the compound. Adsorptions are of two types; physical and chemical adsorptions.

4.1.1.1 Physical adsorption

The adsorption achieved by van der Waals forces, dipole interactions and hydrogen bonding is termed as physical adsorption. This process involves no electron exchange between adsorbent and adsorbate, and hence there is no activation energy required. The physical adsorption is reversible and non-specific.

4.1.1.2 Chemical adsorption

This adsorption process involves the strong interaction between adsorbate and adsorbent and hence it is highly specific and irreversible. Since it occurs with electron exchange, the chemical properties of adsorbate and adsorbent are more likely to change. Adsorption by covalent binding is weak compared to that of ionic.

4.1.2 Adsorption phenomenon

Adsorption is a surface phenomenon and occurs when adsorbable molecule comes into contact with a solid of highly porous structure. Adsorption is basically a mass transfer process of a material either from gas or liquid phase to the surface of a solid and eventually bounded by physical and/or chemical interactions. In general, the surface atoms of a solid are not saturated with their chemical bonds (ionic, covalent, metallic, etc.) as those in bulk of the solid. This chemical bonding unsaturation of the surface atoms in any solid is termed as 'coordinative unsaturation' and which strongly lead to the adsorption of molecules (adsorbates) on the surface. But the exact nature of the bonding between the surface of adsorbent and adsorbate depends on the details of the species involved.

As the adsorption progresses, the system finally attains an equilibrium condition where the transfer of the solute from the bulk to the adsorbent stops. The equilibrium adsorption amount (amount of solute adsorbed per gram of adsorbent at the equilibrium condition, q_e (mg/g) is determined by the following equation (4.1),

$$q_e = (C_o - C_e)V/W \qquad \textbf{4.1}$$

C_o is initial concentration of the adsorbate (mg/*l*)

C_e is equilibrium concentration of the adsorbate (mg/*l*)

V is volume of the adsorbate solution (*l*)

W is weight of the adsorbent used (g)

4.1.3 Adsorption dynamics in solid-liquid system

The adsorption phenomenon in water is essentially a dynamic process in a heterogeneous system in which transport of molecules (organic or ionic) from one phase to another occurs. This adsorption process led by decrease in free energy until it reaches a minimum value. The organic solute dissolved in water is partitioned to the solid phase according to their distribution coefficients (K_d). This distribution is governed by "law of mass action"

$$K_d = \frac{Conc.\ of\ organic\ \ solute\ \ in\ solid\ \ phase\ (C1)}{Conc.\ of\ \ organic\ \ \ solute\ \ \ in\ water\ \ (C2)} \qquad \textbf{4.2}$$

In thermodynamic point of view, the adsorption occurs via two mechanisms.

(i) Strong chemical affinity between adsorbate and solid phase (adsorbent)

(ii) Very poor interaction of the adsorbate in the liquid phase (water)

The former mechanism is majorly governed by the nature of solid phase and organic solute which determine their mutual interactions. Different interactions with their corresponding energies are listed below.[3]

Interaction	Energy (kJ/mol)
Dispersive	5-20
Dipole-induced dipole	8-25
Dipole-dipole	25-40
Hydrogen bonding	25-40
Ionic	250-1050
Covalent	670-3360

It might be concluded from the above table that the most suitable interaction is covalent binding of the adsorbate to active sites of the adsorbents. However, the higher the energy released in adsorption step, the elution (desorption) is more difficult.

The nature of the later mechanism depends on the type of the organic solute and their polarity (degree of hydrophobicity). Frank et al. reported that the hydrophobic molecules can be dissolved in water and the adjacent layer of water molecules to the organic solute are more ordered in a partial crystalline form.[4] When the organic molecules are adsorbed on the adsorbent, the oriented molecules are dispersed again and the order of the water decreases. This process is accompanied with increase in entropy and decrease in free energy which makes the whole process is highly favourable and spontaneous.

4.1.4 Adsorption isotherms

Adsorption isotherm is a plot of equilibrium adsorption (q_e, mg/g), against the equilibrium concentration of the adsorbate (C_e, mg/*l*) at constant temperature. The different types of gas phase adsorption isotherms by porous solids have been discussed already (See in chapter 1.1.2.2). A number of isotherm models have been developed to represent the actual adsorption/desorption phenomenon of various organic molecules on solid surfaces.[5]

Freundlich Model

This basic adsorption isotherm model assumes that the energy of adsorption may vary since the solid surfaces are energetically heterogeneous. Freundlich derived an adsorption isotherm equation as (4.2),[6]

$$q_e = K_f \ C_e^{1/n} \qquad \textbf{4.3}$$

Where C_e is equilibrium concentration in solution, K_f is the Freundlich equilibrium constant and n is degree of non-linearity (adsorption intensity).

The linearization of the above equation gives,

$$\ln q_e = \ln K_f + 1/n \ln C_e \qquad \textbf{4.4}$$

The plot of ln q_e as a function of ln C_e, is a straight line with intercept of ln K_f and slope n. This plot is known as linear form Freundlich adsorption isotherm. This isotherm equation brings the value of adsorption intensity and capacity at any given temperature. These values are very important in designing the adsorption setup and deriving the best adsorption conditions.

4.1.5 Adsorption kinetics

Adsorption kinetic study provides valuable insight into the reaction pathways and their corresponding mechanism. Kinetics also describes the rate at which reaction takes place and in turn the residence time of the adsorbate at solid-solution interface. Therefore, it is very important to predict the rate of any organic compound adsorption by adsorbents in order to design an efficient removal system. For a solid-liquid adsorption process, the solute transfer is usually determined by either external mass transfer or intra-particle diffusion or both.[7] The adsorption of solute on the interior surface of the pores or capillary spaces of the adsorbent is an equilibrium reaction whereas the solute diffusion into the pore of the adsorbent is assumed to be rapid and hence negligible in kinetic calculation. The overall rate of adsorption will be controlled by the slowest step, which is either film diffusion or pore diffusion. Various kinetic models have been reported for adsorption of porous solids including Lagergren pseudo-first order kinetics,[8] pseudo second order kinetics,[7] external diffusion model,[9] and intra-particle diffusion model.[9]

4.1.5.1 Lagergren pseudo-first order kinetic equation

Lagergren derived a kinetic equation assuming that any adsorption process is a simple reversible chemical phenomenon and the overall rate of the reaction will be controlled by the diffusion of solute on the surface boundary film.[8] The Lagergren kinetic equation is not included the available active sites of the adsorbent. The linearized pseudo first order equation (Lagergren equation) is given as,

$$\log(q_e - q_t) = \log q_e - \frac{k_1}{2.303} t \qquad \textbf{4.5}$$

q_e is amount of solute adsorbed (mg/g) at equilibrium

q_t is amount of solute adsorbed (mg/g) at any time 't'

k_1 is pseudo first order rate constant

4.1.5.2 Pseudo second order kinetic equation

The pseudo second order kinetic model has been developed by considering the available active sites of any given adsorbent. The details of pseudo second order kinetic model can be found elsewhere.[7, 9]

The second order kinetic model can be expressed as,

$$\frac{dq}{dt} = k_2(q_e - q_t)^2 \qquad \textbf{4.6}$$

On integration with limits of 0 to t, and q_t = 0 to q_t = q_t, the above second order equation becomes,

$$\frac{1}{(q_e - q_t)} = \frac{1}{q_t} + k_2 t \qquad \textbf{4.7}$$

This equation can be rearranged to get the linear form as,

$$\frac{t}{q_t} = \frac{1}{k_2 q_e^2} + \frac{1}{q_e} t \qquad \textbf{4.8}$$

Where k_2 (g/mg·min) is the second order rate constant and q_e is the equilibrium adsorption (mg/g). If the second order kinetics is applicable, the plot of t/q_t against t should give a linear relationship.

4.1.5.3 External film diffusion model

If in a solid-liquid dynamic system, the rate of solute accumulation in solid surface is equal to that of solute transfer across the film boundary, then the rate equation can be represented as,[9]

$$\frac{dq_t}{dt} = -k_s S(C_t - C_s) \qquad \textbf{4.9}$$

C_s is solute concentration at the surface

C_t is solute concentration in solution

k_s is mass transfer coefficient

S is specific surface area of the adsorbent

Eq. (4.9) is called as 'linear driving force' rate law, which is generally applied to describe the mass transfer across the external liquid film.

4.1.5.4 Intra-particle diffusion model

If the solute adsorption varies proportionally with $t^{1/2}$ rather that the contact time 't', then the rate equation can be given by,[9]

$$q_t = k_i t^{1/2} \qquad \textbf{4.10}$$

k_i is the rate parameter at intra-particle diffusion model.

According to Eq. (4.10), the plot of q_t against $t^{1/2}$ should be a straight line and go through the origin, if the intra-particle diffusion is the sole rate limiting step.

4.1.6 Thermodynamics of adsorption

Enthalpy of adsorption (ΔH)

The enthalpy of the adsorption (ΔH) can be calculated by van't Hoff equation which is given below,

$$\ln C_e = \left(\frac{\Delta H}{RT}\right) + \ln K_f \qquad \textbf{4.11}$$

K_f is Freundlich constant.

4.2 Removal methods of dissolved organic compounds from water

4.2.1 Adsorption of phenol

Phenol has been in production with initial use as an antiseptic since 1860. During the late 19th century the use of phenol was extended to the synthesis of various dyes, plastics, pharmaceuticals, pesticides and petrochemical products. In the year of 2000, the global phenol production reached about 7.8 million tons.[10] Among the various organic pollutants present in waste water, phenols are considered to be the major since they are harmful to plants, animals and human even at trace level. The major sources of phenol and phenolic derivatives are coke plants, petroleum refineries, pharmaceutical industries and huge resin and plastic production. The coke processing plants typically discharge phenol with the highest concentration of 1000 mg/L whereas the resin industries discharge about 10-300 mg/L. The Environmental Protection Agency (EPA) has set a limit of 0.1 mg/L of phenol in water before discharged from industries. The World Health Organization (WHO) has set a limit of 0.001 mg/L of phenol in drinking water. Therefore, it is very important to find out the ways to effectively remove the phenol from the industrial effluents before discharge into environment or to be recycled.

Removal of phenols and their derivatives from aqueous solutions was largely investigated so far using activated carbon.[11] Activated carbons are the most widely used adsorbent for phenolic compounds dissolved in water due to their excellent adsorption properties of organic pollutants. However, the costly regeneration process makes it economically less viable as an adsorbent. Therefore the search for low cost adsorbent with excellent adsorption capacity to remove organic pollutants from water is endless. Because of their availability and low cost, natural organics and minerals such as chitosan, zeolites are also used as adsorbents. Clays and clay minerals also exhibit very good adsorption behaviour of phenol dissolved in water.[12] Polymeric adsorbents also show a great potential to remove dissolved organic pollutants from aqueous solutions.[13] We studied the adsorption potential of sulfonated mesoporous polystyrene in the removal of phenol dissolved in water at various concentrations.

4.2.2 Adsorption of *m*-cresol

Cresols are positional isomers of methyl phenols and are majorly derived from petroleum, coal and wood tar. Cresols are highly stable organic compounds and soluble in water. Cresol finds a great variety of applications in chemical, paints, resins, preservatives, paper and textile industries. This increased application of cresols in many industries enhances the increase in concentration of cresols in water or soil. The soil adsorption or water contamination of cresols tends to bioaccumulate and has a huge impact to both environment and human. Therefore, the United States Environmental Protection Agency (US-EPA) classified cresols as priority toxic chemicals.[14] EPA has also classified cresols as potential carcinogens and tumour promoters evidencing dermal animal studies.[15] World Health Organization (WHO) has set a limit of cresol concentration in drinking water should not exceed 10 ppb. Therefore, numerous studies have been done to remove cresol contamination in both soil and water including the photo-catalytic degradation by titania,[16] by thermal plasma degradation[17] and adsorption by activated carbon.[18] In this thesis, we demonstrate the adsorption potential of sulfonated mesoporous polystyrene for the removal of dissolved *m*-cresol in water.

4.2.3 Adsorption of pyridine

Pyridine and its derivatives are extensively used as solvent(s) in paint industries, rubber preparation, as an intermediate in the synthesis of insecticides and many other fine chemicals. They also used considerably in making medicines, vitamins, food flavours and dyes. Pyridine is a volatile, toxic and highly inflammable colourless liquid with empyreumatic odor. It is very easily mixes with water and soluble in alcohol, ether and benzene. The pyridine vapour is a fire and explosion hazard. On decomposition by heating, it emits highly toxic vapours of NO_x. It has very a high half life and mildly toxic upon inhalation. Pyridine vapour is skin and eye irritant and its exposure causes depression, liver and kidney damage, headache, dizziness, and so on. Pyridine bearing waste water originates from several fine chemical manufacturing industries including pharmaceutical and pyridine synthetic units. The typical concentration of pyridine in wastewater produced in a multidrug intermediates production plant is in the range of 20-300 mg/L.

Adsorption by activated carbon,[19] spent rundle oil shale,[20] sepiolite,[21] zeolites,[22] biodegradation using free and immobilized cells, [23] ozonation with biodegradation, [24] and photocatalytic degradation [25] are general practical methods to treat pyridine containing waste water. The adsorption of pyridine from waste water is attractive, if it is cost effective. We examined the adsorption of pyridine from aqueous solutions onto to the sulfonated mesoporous polystyrene. Adsorption kinetics and equilibrium isotherms were also studied. Thermodynamic parameters were derived from the equilibrium data to understand the feasibility and effect of pyridine concentration on heat of adsorption.

4.2.4 Adsorption of aniline

Aniline is one of the most common pollutants found in the wastewater stream from the pharmaceutical, petrochemicals, dyestuffs, plastics, paints, pesticides and agrochemical industries. Aniline is highly toxic and harmful to human and aquatic life as well. Due to their high toxicity, the environmental accumulation of aniline can cause potential environmental problems. Aniline is identified as a carcinogen and can convert hemoglobin into metha-hemoglobin in blood and thereby reduces the oxygen uptake and can also damage the spleen.[26] Therefore, a great attention has been paid to aniline as a potential pollutant by European Economic Community and US Environmental Protection Agency.

Aniline containing waste water is traditionally treated with photo-decomposition,[27] oxidation,[28] biodegradation,[29] and electrolysis.[30] Aniline is a chemically stable compound and thus not easily removed by degradation techniques. Therefore, there is a need for developing an efficient technology which could rapidly remove aniline from the contaminated water. Adsorption is a simple, cost-effective and efficient technique widely used for the removal of toxic organic pollutants commonly found in the industrial waste water.[31] Moreover, this adsorption technique does not produce any harmful byproducts and regeneration of both adsorbent and pollutant is possible. Though activated carbon is the most common adsorbent in the removal of organic compounds, [32] high cost and difficulty in regenerating the adsorbents make them highly limited. Therefore, it is important to find low-cost and environmentally friendly adsorbents with great adsorption capability. The adsorption potential of sulfonated mesoporous polystyrene for the removal of dissolved aniline in water was also studied.

4.3 Solid phase extraction using sulfonated mesoporous polystyrene

Materials and Methods

Sulfonated mesoporous polystyrene (IEC of 0.011 meq/g), phenol (Wako, 99% GC purity), *m*-cresol (Kanto Chemical, 98% GC purity), pyridine (Kanto Chemical, 99.5% GC purity), aniline (Kanto Chemical, 99% GC purity), ethanol (Wako, 99.5% GC purity) and Millipore water were used in our adsorption experiments.

4.3.1 Equilibrium adsorption experiment

1 wt% of organic compound stock solution (phenol, *m*-cresol, pyridine, and aniline) was prepared using Millipore water at room temperature and diluted to subsequent lower experimental concentrations. Sulfonated mesoporous polystyrene (IEC = 0.011 meq/g) was used as adsorbents in all the adsorption experiments. In a typical equilibrium adsorption experiment, 50 g/*l* of sulfonated mesoporous polystyrene was used whereas the organic compound solutions of different concentrations including 10 mg/*l* to 1000 mg/*l* were used. Prior to use as an adsorbent, the sulfonated polystyrene was added into ethanol to remove the filled air inside the pores. Then the polymer is filtered and used as the adsorbent. The adsorption reaction has been carried out at different temperatures of 30 ^{o}C to 50 ^{o}C. The sulfonated mesoporous polystyrene was added to the organic compound solution, which was continuously stirred and kept in a water bath at the temperatures mentioned as above. After 4 h, the adsorption experiment was quenched by filtering off the adsorbents from the organic compound solution.

4.3.2 Kinetics

To study the adsorption kinetics, the organic compound solution of 100 mg/*l* was used. 50 g/*l* of sulfonated polystyrene was used in each of the experiments. Prior to use as adsorbent, the sulfonated polystyrene was added into ethanol to remove the filled air in the pores. Then the polymer was filtered and used as adsorbent. The kinetics of organic compounds adsorption onto the sulfonated mesoporous polystyrene was investigated at three different temperatures, 30 ^{o}C, 40 ^{o}C and 50 ^{o}C. The adsorbent was added to organic compound solution which was continuously stirred and kept at the water bath maintained at different temperatures. At equal time interval (every 10 min), a decrease in concentration of organic compounds was monitored using UV-Vis spectroscopic measurements. The adsorption experiment was stopped no more decrease in the solution concentration was observed.

4.3.3 UV measurements

The UV spectra are recorded for all the organic compound (phenol, *m*-cresol, pyridine, and aniline) solutions before and after the adsorption experiments. The decrease in the concentrations of the solution after the adsorption was calculated by subtracting the final UV-Vis absorbance from that of the initial. The spectra measurement was carried out in a standard measuring cell (10 mm) and at room temperature. For phenol and *m*-cresol, the peak at λ_{max} 270 nm was considered while for pyridine and aniline λ_{max} 256 nm and λ_{max} 230 nm were used, respectively.

4.4 Results and discussion

4.4.1 Equilibrium adsorption isotherm

Adsorption isotherm is a plot of equilibrium adsorption q_e (mg/g) against the equilibrium concentration C_e (mg/*l*). The equilibrium adsorption isotherms of organic compounds adsorption by sulfonated mesoporous polystyrene are shown in Fig.4-1. In all cases, the adsorbate was strongly captured at relatively low temperature (30 °C). This indicates that the interaction between the adsorbate and the polymer chains is considerably reduced at high temperature, as compared with the decrease in the affinity of water with the adsorbate at that temperature. The adsorption isotherm of phenol by sulfonated mesoporous polystyrene is found to be linear which ensures the reversible physisorption. Therefore, the mesoporous polystyrene can be easily recovered and recycled at mild conditions. The adsorption isotherm of other organic compounds *m*-cresol, pyridine and aniline showed the favorable concentration regions[33] for adsorption, having the advantage of recovering the adsorbent at mild conditions or by simple washing in alcohol. The activated carbon adsorption isotherm for most of the organic compounds has wide favorable region,[34] which causes difficulty in the recovery process. The activated carbon recovery after adsorption involves harsh chemical (highly acidic or basic) or heat treatment.

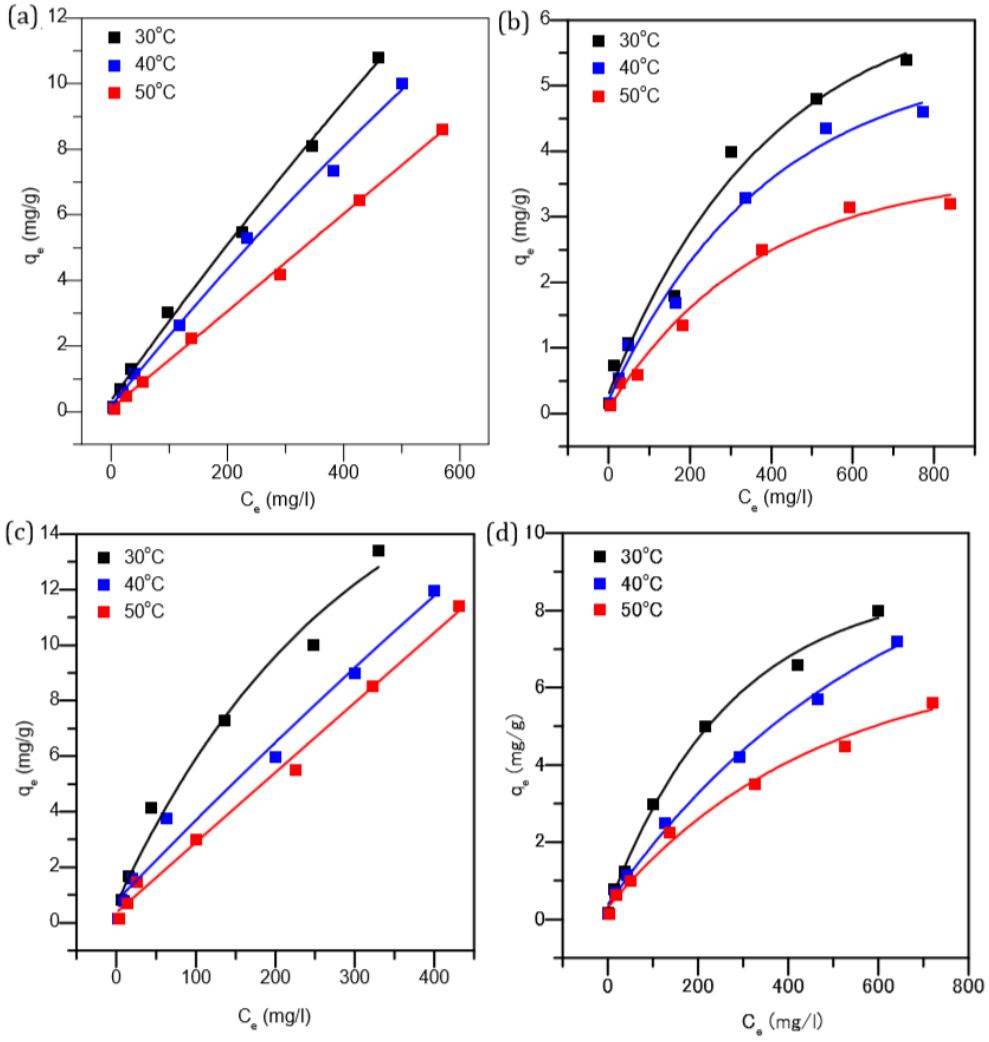

Figure 4-1. Equilibrium adsorption isotherms of sulfonated mesoporous polystyrene (a) phenol, (b) pyridine, (c) *m*-cresol and (d) aniline. The adsorption period is 4 h.

4.4.2 Freundlich adsorption isotherm

The equilibrium adsorption isotherm data were fit into the linear Freundlich equation and shown in Fig.4-2,

$$\ln q_e = \ln K_f + 1/n \ln C_e \qquad \textbf{4.4}$$

Where n and K_f are Freundlich parameters. 'K_f' represents the adsorption capacity and 'n' represents the intensity of adsorption. If the adsorption intensity n > 1, the adsorption is highly favourable. The Freundlich parameters 'K_f', 'n' and the linear correlative coefficient R^2 at different temperatures are listed in Table 5.

Table 5. Adsorption enthalpy at given equilibrium adsorption amounts and Freundlich parameters at given temperatures.

aromatic compound	q_e (mg/g)	ΔH (kJ/mol)	T (K)	Freundlich parameters		
				K_f	n	R^2
phenol	2.0	-25.9	303	0.063	1.20	0.99
	4.0	-21.2	313	0.039	1.12	0.98
	6.0	-19.6	323	0.023	1.11	0.99
	8.0	-18.5				
pyridine	1.0	-32.2	303	0.140	1.81	0.97
	1.5	-29.8	313	0.095	1.69	0.99
	2.0	-28.2	323	0.055	1.63	0.99
	2.5	-25.9				
m-cresol	2.0	-42.4	303	0.212	1.36	0.99
	4.0	-35.8	313	0.133	1.33	0.99
	6.0	-30.6	323	0.092	1.28	0.97
	8.0	-27.1				
aniline	1.0	-33.0	303	0.192	1.72	0.99
	2.0	-33.1	313	0.124	1.61	0.99
	3.0	-32.5	323	0.081	1.53	0.98
	4.0	-31.6				

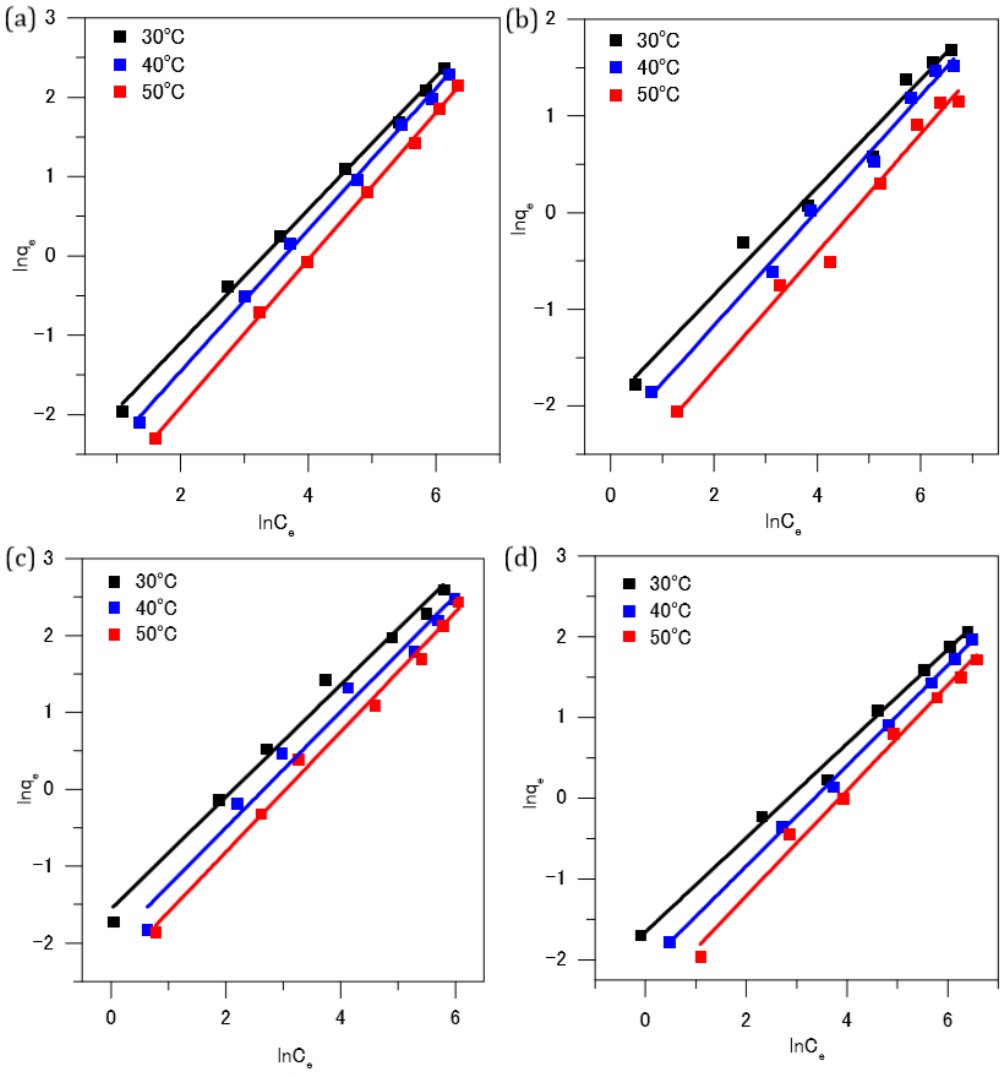

Figure 4-2. Linear Freundlich adsorption isotherms of (a) phenol, (b) pyridine, (c) *m*-cresol and (d) aniline obtained for sulfonated mesoporous polystyrene.

In all the above-mentioned organic compounds adsorption by sulfonated mesoporous polystyrene, the Freundlich adsorption parameter 'n' exceeds 1 and hence the adsorption is favourable. But the adsorption capacity (K_f) value decreases with increase in temperature indicating higher adsorption at lower temperatures.

4.4.3 Derivation of thermodynamic parameters

The isosteric heat of adsorption or adsorption enthalpy changes were estimated by fitting the adsorption data to the van't Hoff equation. From the slope of the linear plot of $\ln C_e$ against 1/T, enthalpy of adsorption (ΔH) can be calculated. The van't Hoff plots for the adsorption of organic compounds by sulfonated mesoporous polystyrene are shown in Fig.4-3.

$$\ln C_e = \left(\frac{\Delta H}{RT}\right) + \ln K_f \qquad \textbf{4.12}$$

The calculated enthalpy values at given adsorption amount of various organic compounds onto sulfonated mesoporous polystyrene are shown in Table 5. The adsorption enthalpy of organic compounds onto the surface of sulfonated mesoporous polystyrene are in the range of -18 kJ/mol to -42 kJ/mol, indicating that the adsorption is a physical process and also with the increase in the adsorbate loading on the surface, the adsorption enthalpy value decreases. The adsorption enthalpy values of all studied organic compounds demonstrate that the adsorption process is exothermic and hence the adsorption phenomenon is favourable at relatively lower temperatures.

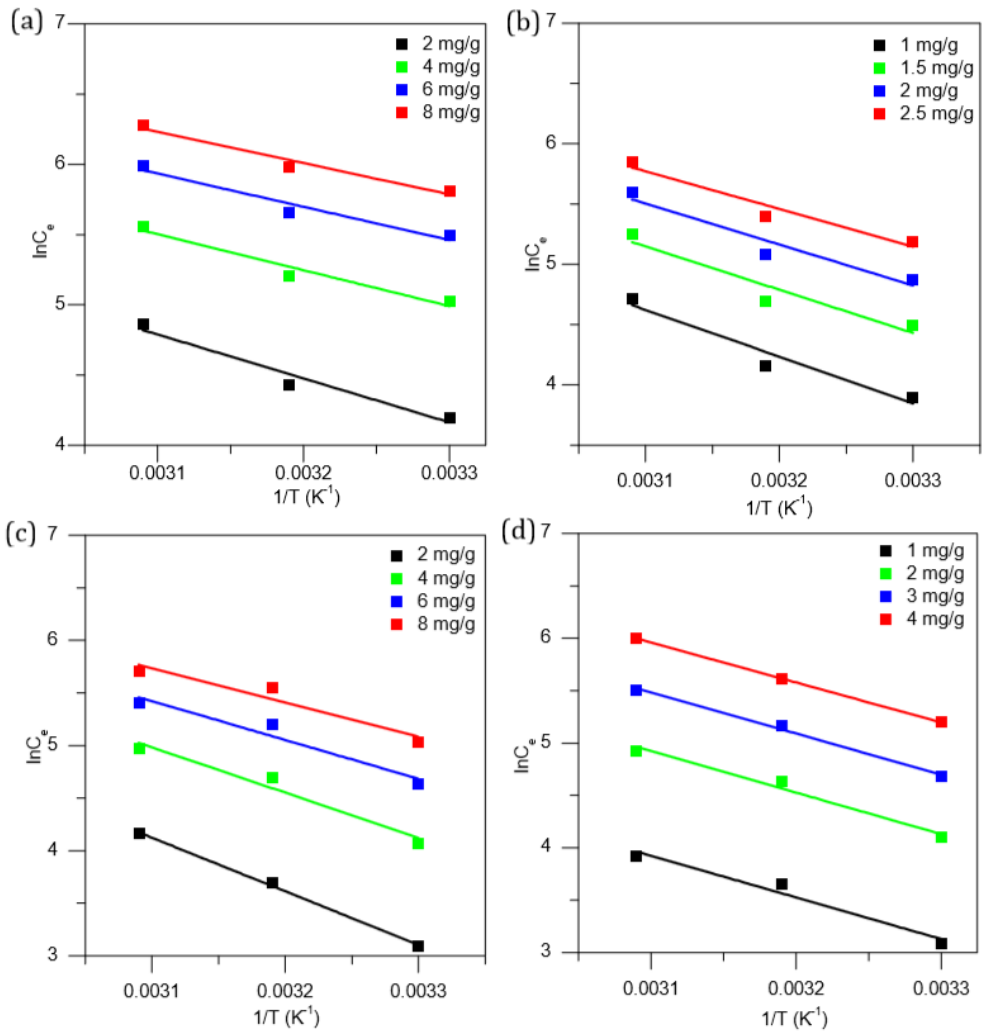

Figure 4-3. Van't Hoff plots of sulfonated mesoporous polystyrene for the adsorption of (a) phenol, (b) pyridine (c) *m*-cresol and (d) aniline.

4.4.4 Kinetic model of adsorption

Pseudo second order kinetics

The linear form of pseudo second order kinetic equation is given by,

$$\frac{t}{q_t} = \frac{1}{k_2 q_e^2} + \frac{1}{q_e} t \qquad \textbf{4.14}$$

The adsorption kinetics is basically derived from the decrease in the concentration of adsorbate with time. The adsorption kinetics of organic compounds by sulfonated mesoporous polystyrene were well fit into linear pseudo second order kinetic model with high correlation coefficients (R^2). The second order rate constants are calculated from the intercept of the plot of 't/q_t' against 't'. The second order kinetic parameters are given in Table 6, where q_{ke} is the equilibrium adsorption calculated from the slope and q_e is that obtained from the corresponding adsorption experiment.

Table 6. Second order adsorption kinetic parameters of organic compounds by sulfonated mesoporous polystyrene

Aromatic compound	*T* (K)	Rate constant, k_2 (g/mg·min)	Equilibrium adsorption (mg/g)		
			q_e	q_{ke}	R^2
phenol	303	0.081	1.30	1.42	0.99
	313	0.088	1.18	1.17	0.99
	323	0.123	0.92	1.13	0.99
pyridine	303	0.095	1.08	1.06	0.99
	313	0.176	1.04	1.01	0.99
	323	0.570	0.60	0.73	0.99
m-cresol	303	0.048	1.70	1.75	0.99
	313	0.052	1.60	1.60	0.99
	323	0.222	1.48	1.48	0.99
aniline	303	0.052	1.26	1.61	0.99
	313	0.200	1.16	1.36	0.99
	323	0.400	1.00	1.17	0.99

The linear pseudo second order kinetic plots for the adsorption of different organic compounds by sulfonated mesoporous polystyrene are given in Fig.4-4.

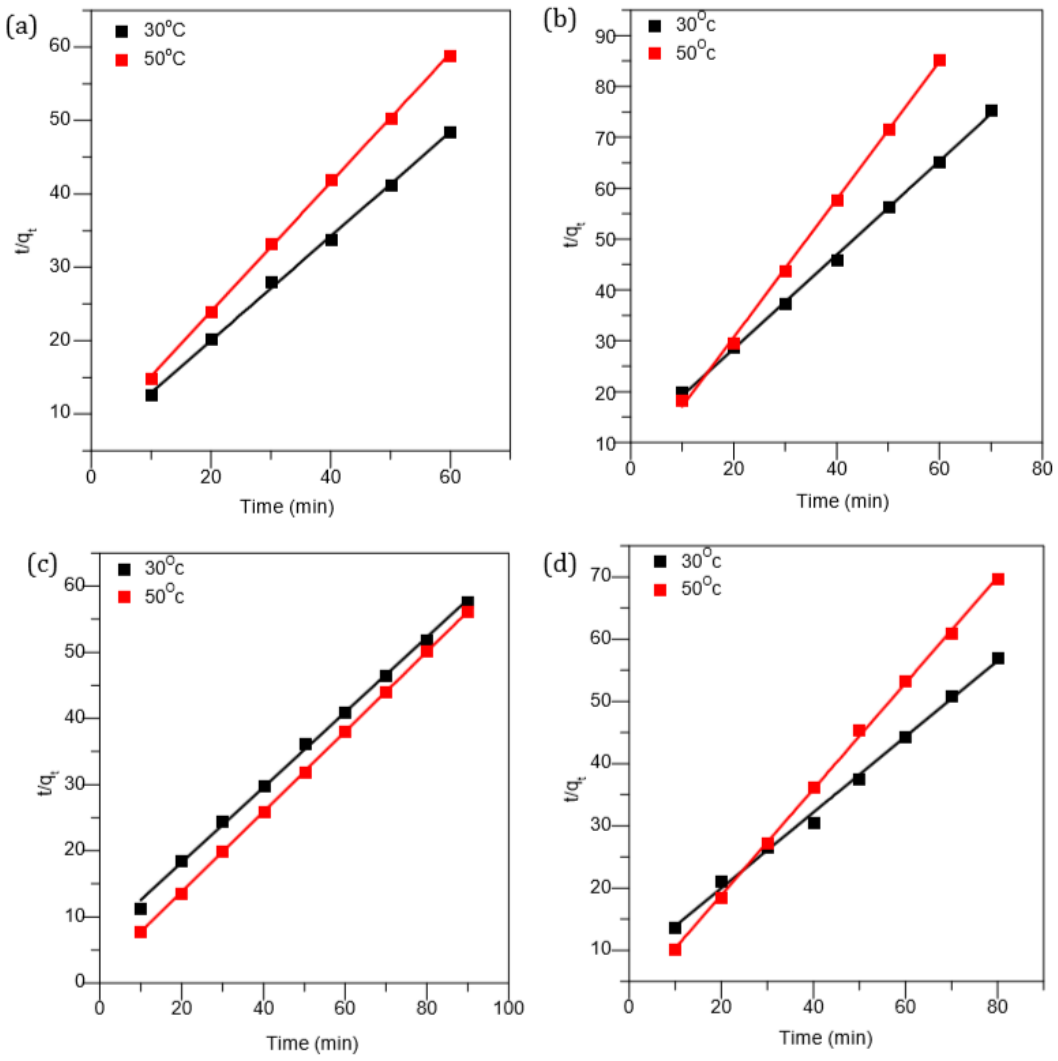

Figure 4-4. Linear pseudo-second-order kinetic plots for adsorption of (a) phenol, (b) pyridine, (c) *m*-cresol and (d) aniline.

The second order kinetics data showed that the rate constants were increased with increase in temperature of adsorption. This is because that the adsorption rate is accelerated at high temperature. But the overall adsorption amount (q_e) has inverse relationship with temperature. Also, the calculated equilibrium amount (q_{ke}) based on kinetic equations has closer agreement with the experimentally observed adsorption (q_e).

In contrast, when the q_t values (adsorption amount at time t) were analyzed using a pseudo-first order model, there were large deviations in the plot. This indicates that the adsorption process is not simple diffusion. The strong correlations in the pseudo-second order kinetics model supports that these aromatic compounds migrate via a hopping process among open adsorption sites. The second order rate constant (k_2) of phenol at 30°C was 0.081 g/mg·min, which was about twice the value observed in activated carbons.[35] Interestingly, the rate constant tends to increase suddenly with temperature. For instance, the second order rate constant (k_2) of pyridine adsorption was 0.57 g/mg·min at 50°C. This tendency is consistent with the decrease in the binding energy between the polymer chains and the organic compounds at high temperature.

In comparison with activated carbon, sulfonated mesoporous polystyrene as an adsorbent for the organic compounds from the aqueous solution shows distinct advantages. The adsorption isotherm of organic molecules like phenol and cresol by activated carbon polystyrene falls in the region of strongly favorable adsorption.[36] This is due to the excessive surface functionalities in the carbon matrix and the combined macro/micro porous structures. This strong adsorption capacity of activated carbon in turn causes the difficulty in regenerating the adsorption sites for the reuse in consecutive cycles. Moreover it requires highly acidic or basic conditions to completely recover the original adsorption sites. But the adsorption isotherm of these organic molecules by sulfonated polystyrene falls in the linear to favorable region and the adsorption sites can be rapidly regenerated by simple treatment with alcohols (e-g methanol, ethanol). Also the activated carbon exhibits higher adsorption capacity at higher temperature whereas the sulfonated polystyrene shows higher adsorption at relatively lower temperature. Therefore, the overall adsorption performance exhibited by sulfonated polystyrene is considered to be energy efficient compared to that of activated carbon. In conclusion, the rapid regeneration of adsorption sites and the overall energy efficiency of the adsorption process were makes the sulfonated mesoporous polystyrene as a distinct alternative adsorbent material.

4.5 References

[1] I. Liska, *J. Chromatogr. A*, 885, 3 (2000).

[2] (a) L. M. Ravelo-Perez, A. V. Herrera-Herrera, J. Hernandez-Borges and M. A. Rodriguez-Delgado, *J. Chromatogr. A*, 1217, 2618 (2010).

(b) F. Augusto, E. Carasek, R. G. C. Silva, S. R. Rivellino, A. D. Batista, and E. Martendal, *J. Chromatogr. A*, 1217, 2533 (2010).

(c) C. F. Poole, *Trends. Anal. Chem*, 22, 362 (2003).

(d) E. Turuial and A. Martin-Esteban, *Anal. Chim. Acta*, 668, 87 (2010).

[3] I. Liška, J. Krupčíik and P. A. Leclercq, *J. High Resolution Chromatography*, 12, 577 (1989).

[4] H. S. Frank and M. W. Evans, *J. Chem. Phys.*, 13, 507 (1945).

[5] (a) W. Huang, T. M. Young, M. A. Schlautman, H. Yu, and W. J. Weber, *J. Environ. Sci. Technol.*, 31, 1703 (1997).

(b) E. Huan and W. J. Weber, *J. Environ. Sci. Technol.*, 31, 2562 (1997).

(c) C. Thibaud-Erkey, Y. Guo, C. Erkey, and A. Akgerman, *Environ. Sci. Technol*, 30, 2127 (1996).

[6] (a) H. Freundlich, *Colloid and Capillary Chemistry*, Methuen, London, 1926.

(b) H. M. F. Freundlich, *Z. Phys. Chem*., 57, 385 (1906).

[7] Y. S. Ho and G. McKay, *Process Bicohemistry*, 34, 451 (1999).

[8] S. Lagergren, *Handlinger*, 24, 1 (1898).

[9] H. Qiu, B-C. Pan, Q-J. Zhang, W-M. Zhang and Q-X. Zhang, *Journal of Zhejiang Uni. Sci. A*, 10, 716 (2009).

[10] Phenol, *Chemical Week*, 31, 164 (2002).

[11] (a) J. S. Zogorski, S. D. Faust and J. H. Haas, *J. Colloid Interface Sci.*, 55, 329 (1976).

(b) I. Ivancev-Tumbas, B. Dalmacija, Z. Tamas and E. Karlovic, *Water Research*, 32, 1085 (1998).

(c) J. M. Dias, M. C. M. Alvim-Ferraz, M. F. Almeida, J. R. Utrilla and M. Sánchez-Polo, *J. Environ. Manage.*, 85, 833 (2007).

(d) S. H. Lin and R. S. Juang, *J. Environ. Manage.*, 90, 1336 (2009).

[12] (a) R. Wibulswas, D. A. White and R. Rautiu, *Process Safety and Environmental Protection*, 77, 88 (1999).

(b) M. Djebbar, F. Djafri, M. Bouchekara and A. Djafri, *African Journal of Pure and Applied Chemistry*, 6, 15 (2012).

[13] (a) A. Li, Q. Zhang, G. Zhang, J. Chen, Z. Fei and F. Liu, *Chemosphere*, 47, 981 (2002).

(b) A. M. Li, Q. X. Zhang, J. L. Chen, Z. H. Fei and C. Long, *J. Environ. Sci., (China)*, 14, 457 (2002).

(c) J. Huang, C. Yan and K. Huang, *J. Colloid Interface Sci.*, 332, 60 (2009).

[14] Agency for Toxic Substances and Disease Registry (ATSDR), Toxicological *Profile for Cresols.* Public Health Service, U.S. Department of Health and Human Services, Atlanta, GA. 1990.

[15] (a) U.S. Environmental Protection Agency. Integrated Risk Information System (IRIS) on 2-methylphenol. National Center for Environmental Assessment, Office of Research and Development, Washington, DC. 1999.

(b) U.S. Environmental Protection Agency. Integrated Risk Information System (IRIS) on 3-methylphenol. National Center for Environmental Assessment, Office of Research and Development, Washington, DC. 1999.

(c) U.S. Environmental Protection Agency. Integrated Risk Information System (IRIS) on 4-methylphenol. National Center for Environmental Assessment, Office of Research and Development, Washington, DC. 1999.

[16] W. Zmudzinski, *Polish. J. Environ. Stud.*, 19, 1353 (2010).

[17] B. Jaramillo-Sierra, A. Mercado-Cabrera, A. De la Piedad-Benitez et.al, *12th High-Tech Plasma Processes Conference*, 406, 012025 (2012).

[18] M. A. Shabiimam and A. K. Dikshit, *International J. Environ. Sci. Develop.*, 3, 189 (2012).

[19] D. Mohan, K .P. Singh, S. Sinha and D. Ghosh, *Carbon*, 42, 2409 (2004).

[20] S. Zhu, P. R. F. Bell and P. F. Greenfield, *Water Research*, 22, 1331 (1988).

[21] E. Sabah and M. S. Celik, *J. Colloid Interface Sci*., 251, 33 (2002).

[22] H. Bludau, H. G. Karage and W. Nissen, *Micropor. Mesopor. Mater*., 22, 297 (1998).

[23] (a) S. S. Adav, D. J. Lee and N. Q. Ren, *Water Reaserach*, 41, 2903 (2007).

(b) G. K. Sim and L. E. Sommers, *Environ. Toxicol. Chem.*, 5, 503 (1986).

[24] M. Stern, H. Elmar and O. M. Kut, *Water. Sci. Technol.*, 35, 329 (1997).

[25] H. Zhao, S. Xu, J. Zhong and X. Bao, *Catal.Today*, 93, 857 (2004).

[26] . H. Yan, X. Yang, J. Chen, C. Yin, C. Xiao and H. Chen, *J. Environ. Sci.*, 23, 1165 (2011).

[27] (a) W. Chu, W. K. Choy and T.Y. So, *J. Hazard. Mater.*, 141, 86 (2007).

(b) C. Karunakaran and S. Senthilvelan, *Sol. Energy*, 79, 505 (2005).

(c) A. Kumar and N. Mathur, *J. Colloid Interface Sci*., 300, 244 (2006).

[28] (a) N. Jagtap and V. Ramaswamy, *Appl. Clay. Sci*., 33, 89 (2006).

(b) H. T. Gomes, P. Selvam, S. E. Daburkar, J. L. Figueirdo, and J. L. Faria, *Micropor. Mesopor. Mater*., 86, 287 (2005).

[29] L. Wang, S. Barrington and J. Kim, *J. Environ. Manage.*, 83, 191 (2007).

[30] Y. Han, X. Quan, S. Chen, H. Zhao, C. Cui and Y. Zhao, *Sep. Purif. Technol.*, 50, 365 (2006).

[31] (a) W. M. Zhang, Q. J. Zhang, B. C. Pan, L. Lv, B. J. Pan, Z. W. Xu, Q. X. Zhang, X. S. Zhao, W. Du and Q. R. Zhang, *J. Colloid Interface Sci.*, 306, 216 (2006).

(b) K. Yang, W. Wu, Q. Jing and L. Zhu, *Environ. Sci. Technol.*, 42, 7931 (2008).

[32] (a) F. Villacanas, M. F. R. Pereira, J. J. M. Orafao and J. L. Figueiredo, *J. Colloid Interface Sci*., 293, 128 (2006).

(b). K. Lazlo, *Colloid Surf. A*, 265, 32 (2005).

[33] Advances in sustainable energy and environmental oriented numerical modeling, Hironi Nakajima (Ed.,) ISBN: 978-953-51-1170-2, 2013.

[34] A. E. Vasu, *E-Journal of Chemistry*, 5, 224 (2008).

[35] V. C. Srivastava, M. M. Swamy, I. D. Mall, B. Prasad and I. M. Mishra, *Colloid Surf. A*, 272, 89 (2006).

[36] (a) M. A. S. D. Barros, P. A. Arroyo and E. A. Silva, General aspects of aqueous sorption process in fixed beds in H. Nakajima (Ed). Mass transfer – *Advances in sustainable energy and environment oriented numerical modeling*, InTech, Chapter 4, 362 (2013).

(b) A. E. Vasu, *E-Journal of Chemistry*, 5, 224 (2008).

Chapter 5

Conclusions

The mesoporous polymers were successfully prepared by the nano-crystallized solvent phase separation technique. These mesoporous polymers could be obtained in the form of fibers, sheets and pellets. The mesoporous polymers were effectively modified with sulfonate groups without disrupting the meso morphology. The small number of surface sulfonate groups, with an average distance of about 5 nm (sulfonated mesoporous polystyrene), significantly improved the hydrophilicity of the mesopores, leading to rapid adsorption of water-soluble dyes and aromatic compounds in water. The mesopores in particular are suitable for rapid and efficient adsorption of large organic molecules. The adsorption intensities of small organic compounds decreased with increasing temperature, which was completely the opposite tendency to that of activated carbons. In general, the hydration energy decreases at high temperature and the binding state of the adsorbate is stabilized in relative terms. However, the energy loss of hydration seems to be smaller than the energy loss due to the spatial fluctuation of the binding sites between the polymer chains. Mesoporous polymers are expected to be applicable to the purification of oily water, since they adsorb water-soluble oil components and release the components at high temperatures.

Because of the high values of specific surface area and inter-connected porous structures, these mesoporous polymer materials exhibit a variety of separation properties. The mesoporous polysulfone membrane can be used for ultrafiltration of 5 nm gold nanoparticles with a rejection rate above 90%. These mesoporous polymers can also absorb carbon dioxide with a Henry's constant three times higher than its bulk counterpart. This thesis demonstrates the scientific grounds for the separation potential of gas and oil fields.